

MASTER

Out-of-plane stability of steel arches

Delrue, S.F.

Award date:
1998

[Link to publication](#)

Disclaimer

This document contains a student thesis (bachelor's or master's), as authored by a student at Eindhoven University of Technology. Student theses are made available in the TU/e repository upon obtaining the required degree. The grade received is not published on the document as presented in the repository. The required complexity or quality of research of student theses may vary by program, and the required minimum study period may vary in duration.

General rights

Copyright and moral rights for the publications made accessible in the public portal are retained by the authors and/or other copyright owners and it is a condition of accessing publications that users recognise and abide by the legal requirements associated with these rights.

- Users may download and print one copy of any publication from the public portal for the purpose of private study or research.
- You may not further distribute the material or use it for any profit-making activity or commercial gain

CO/98.05 Out-of-plane stability of steel arches

February 1998

Author: S. Delrue

Committee: prof. ir. H.H. Snijder (TUE CO)
dr. ir. J.C.D. Hoenderkamp (TUE CO)
ir. F.S.K. Bijlaard (TNO Bouw)
ir. H.M.G.M. Steenbergen (TNO Bouw)

PREFACE

The investigation to stability of steel arches is initiated by the committee SG/TC-8 of the Staalbouwkundig Genootschap. I want to thank this committee for offering me the possibility to work on this subject.

I also want to thank the people from TNO Building and Construction research, where I performed this study, for their interest and their help. Special thanks for Frans Bijlaard and Henri Steenbergen, who supported me during the project.

From the Eindhoven University of Technology, I want to thank my supervisors professor Snijder and dr. Hoenderkamp for keeping me on the right track.

Besides the people who supported me technically during my study, I want to thank my parents for giving me the opportunity to accomplish this study. Finally but not least I want to thank my friends who were there for reflecting my ideas or just for a cup of tea.

TABLE OF CONTENTS

SUMMARY.....	vii
SAMENVATTING.....	xi
GENERAL NOTATION.....	xv
1. INTRODUCTION.....	1
2. OUT-OF-PLANE STABILITY OF ARCHES.....	3
2.1 Review of research on stability.....	3
2.2 Codes.....	4
2.2.1 International comparison.....	4
2.2.2 DIN 18 800.....	6
3. EULER BUCKLING.....	7
3.1 Analytical models.....	7
3.1.1 The models.....	8
3.1.1.1 Timoshenko and Gere (1961).....	8
3.1.1.2 Vlasov (1961).....	9
3.1.1.3 Yoo (1982).....	9
3.1.1.4 Trahair and Papangelis (1987).....	10
3.1.1.5 Rajasekaran and Padmanabhan (1989).....	11
3.1.1.6 Yang and Kuo.....	12
3.1.2 Comparison of the models.....	12
3.1.2.1 Assumptions and limitations.....	13
3.1.2.2 Formulas.....	13
3.1.2.3 Results.....	15
3.1.3 Conclusions.....	18
3.2 Numerical models.....	19
3.2.1 Model with beam elements.....	19
3.2.1.1 The element.....	19
3.2.1.2 The model.....	20
3.2.1.3 Results.....	20
3.2.2 Model with curved shell elements.....	21
3.2.2.1 The element.....	21
3.2.2.2 The model.....	22
3.2.2.3 Results.....	22
3.3 Comparison of analytical and numerical results.....	24
4. NON-LINEAR FINITE ELEMENT ANALYSES.....	29
4.1 Physical and geometrical non-linear behaviour.....	29
4.2 Initial imperfections.....	30
4.2.1 Influence of imperfections on the stability of arches.....	30
4.2.2 Size of the imperfection.....	31
4.3 Residual stresses.....	33
4.3.1 Influence of residual stresses.....	35
4.4 Results.....	36

4.5 Ultimate load	37
5. VERIFICATION METHODS	45
5.1 Stability check for columns and beams	45
5.2 Out-of-plane stability of arches	47
5.2.1 Stability check	47
5.2.2 Check of the verification method	51
5.2.3 Combination of compression and bending	55
5.3 Comparison to other verification methods	57
5.3.1 DIN 18800	57
5.3.2 Eurocode	59
5.3.3 Comparison Proposed verification - DIN 18800	60
6. CONCLUSIONS AND RECOMMENDATIONS	63
6.1 Conclusions	63
6.1.1 Literature and Euler buckling load	63
6.1.2 Non-linear FEM analyses	63
6.1.3 Verification method	64
6.2 Recommendations	66
REFERENCES	69
APPENDICES	71
A.CODES	71
A.1 Code DIN 18800	71
A.2 Buckling curves	78
B.EULER BUCKLING LOAD	81
B.1 Calculation methods	81
B.2 Timoshenko & Gere	83
B.3 Vlasov	84
B.4 Yoo	85
B.5 Trahair & Papangelis	87
B.6 Rajasekaran & Padmanabhan	89
B.7 Yang & Kuo	91
B.8 Influence of warping	92
C. SHELL ELEMENT FEM MODEL	95
C.1 Cross section properties shell element model	95
C.2 Preliminary investigation shell element model	97
C.3 Verifying shell element	99
D. NON-LINEAR ANALYSES	101
D.1 Numerical results non-linear analyses	101
D.2 Load-displacement diagrams	102
E. DIANA FILES	109
E.1 Data file	109
E.2 Command files	112
E.3 Output files	115

SUMMARY

The increasing use of steel arches (example in figure 1) has led to a growing demand for design rules for arches. Since the Dutch codes lack a verification method to check arches, the research committee SG/TC 8 of the Staalbouwkundig Genootschap, has initiated an investigation to develop a verification method for steel arches. The first part of the investigation has been executed by Verstappen(1996). Here attention was mainly focused on in-plane stability. The second part of the investigation is described in this report and it aims at out-of-plane stability of arches.

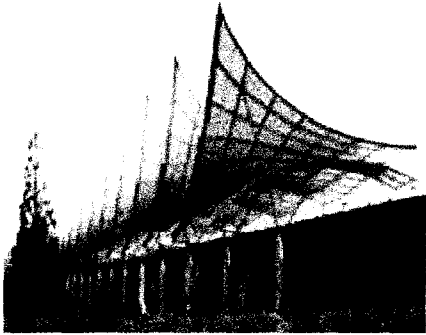


Figure 1 arch structure

Several analytical models are known in the literature, which describe the out-of-plane stability of arches. The Euler buckling load for arches subjected to uniform compression or uniform bending can be determined with these models. Six different models have been considered in this investigation. The model of Timoshenko (1961) is based on straight beam theory and neglects the influence of warping. The model of Vlasov (1961) is also based on straight beam theory but includes the warping effects. Yoo's model (1982) is the third model which is based on straight beam theory, but the calculation method is not direct. Instead of using the equilibrium equations to obtain

the Euler buckling load, the principle of virtual displacements is used. The model of Trahair (1987) is the first one which is based on curved beam theory. The models of Rajasekaran (1989) and Yang (1989) are also based on curved beam theory. The difference between the three models is due to different assumptions in the strain-displacement relations.

The results of the different models are compared to each other for a range of arches. In figure 2 the Euler buckling loads, F_E , are given for arches subjected to uniform compression and in figure 3 for arches subjected to uniform bending. Besides the analytical Euler buckling loads, numerical Euler buckling loads are given, which are obtained by a FEM analysis.

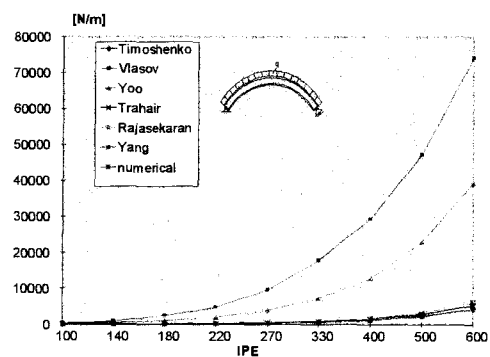


Figure 2 F_E , uniform compression

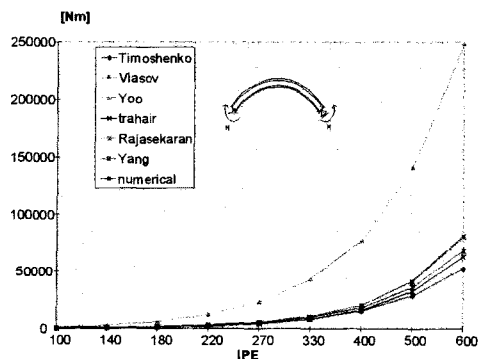


Figure 3 F_E , uniform bending

The model of Rajasekaran is used in further investigations to obtain the Euler buckling load. The results obtained by this model are reliable and the equations for the Euler buckling loads of the two loadcases concerned are rather simple.

Non-linear Finite Element Method analyses were performed to obtain more information about the out-of-plane behaviour of the arch. They included geometrical and physical non-linear behaviour.

Most of the arches investigated have a positive post-buckling behaviour, which means that the arch can carry a larger load than the buckling load. In figure 4 this is indicated by line 2. There are also arches without a positive post-buckling behaviour. Their behaviour is shown in figure 4 by line 1.

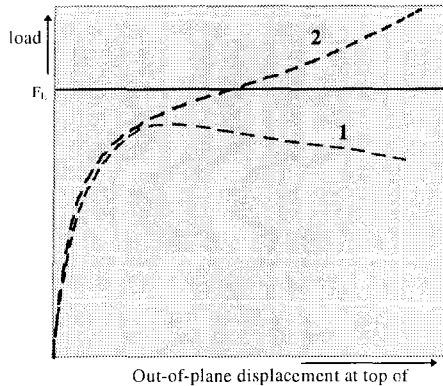


Figure 4 Load-displacement diagram

For arches without a positive post-buckling behaviour, the ultimate load is clearly defined, namely the top in the load-displacement curve: ultimate capacity. For arches with a positive post-buckling behaviour this is not the case. The arch can even resist a larger load than the Euler buckling load and deformations can be very large before the ultimate strength is reached. In this investigation a definition is suggested for the ultimate load which is valid

for arches with and without positive post-buckling behaviour.

The ultimate load can be determined by the minimum slope in the load-displacement diagram, i.e. :

$$\min \left| \frac{d(\text{load})}{d(\text{out-of-plane displacement})} \right|$$

For an arch without a positive post-buckling behaviour this is the top in the load-displacement diagram and for an arch with a positive post-buckling behaviour this is the point of contraflexure in the load-displacement diagram.

For two loadcases, uniform compression and uniform bending, a verification method is proposed. This method shows close comparison with non-linear FEM analyses.

The stability check for uniform compression is:

$$\frac{N_{c,s,d}}{\omega_{\text{arch,out}} N_{c,u,d}} \leq 1$$

with:

$N_{c,s,d}$ design value of the compressive force
 $N_{c,u,d}$ design plastic resistance to compression of the cross section
 $\omega_{\text{arch,out}}$ buckling factor for out-of-plane buckling of arches

The stability check for uniform bending is:

$$\frac{M_{y,s,max,d}}{\omega_{\text{arch,out}} M_{y,u,d}} \leq 1$$

with:

$M_{y,s,max,d}$ design value of the bending moment
 $M_{y,u,d}$ design plastic resistance to bending of the cross section
 $\omega_{\text{arch,out}}$ buckling factor for out-of-plane buckling of arches

The buckling factor for out-of-plane buckling of arches can be obtained from the column

buckling curves. Only the relative slenderness must be known, in order to obtain the buckling factor.

The relative slenderness for the two loadcases is:

$$\text{for uniform compression: } \lambda_{rel} = \sqrt{\frac{N_{c,u,d}}{F_{y,E}}}$$

$$\text{for uniform bending: } \lambda_{rel} = \sqrt{\frac{M_{c,u,d}}{M_E}}$$

in which

$N_{c,u,d}$ is the design plastic resistance to compression of the cross section

$M_{c,u,d}$ is the design plastic resistance to bending of the cross section

$F_{y,E}$ is the Euler buckling load for uniform compression based on the model by Rajasekaran

M_E is the Euler buckling load for uniform bending based on the model by Rajasekaran

$$F_{y,E} = \beta_{red} \frac{M_0}{R^2} \left(\frac{b/a(a^2 - 1)^2}{a^2 + b^2} \right)$$

$$M_E = \beta_{red} M_0 \left(-\frac{a}{b} - \frac{ab}{2} + \sqrt{\left(\frac{a}{b} + \frac{ab}{2} \right)^2 + 1 - a^2} \right)$$

with:

L, H, ℓ and R according to figure 5

$$a = \frac{L}{\pi R} \quad b = \frac{\pi M_0}{P_z L}$$

In which:

$$P_z = \frac{\pi^2 EI_z}{L^2} \quad M_0 = \sqrt{P_z \left(GJ + \frac{\pi^2 EI_w}{L^2} \right)}$$

$$\beta_{red} = 1 \quad \text{for } \frac{H h}{L \ell} \leq 0.25$$

$$= 1.05 - 0.2 \frac{H h}{L \ell} \quad \text{for } \frac{H h}{L \ell} > 0.25$$

The reduction factor β_{red} is added to the original formulae from Rajasekaran yielding Euler buckling loads that comply with numerical results.

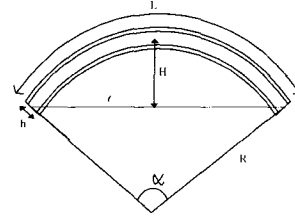
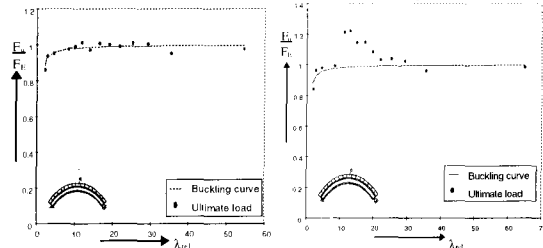


Figure 5 Parameters of the arch

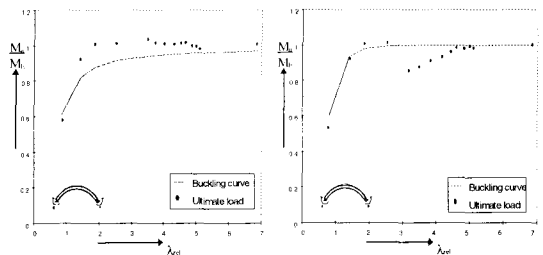
The German code DIN 18800 is the only code that includes a verification method for out-of-plane stability of arches. In figure 6 the method proposed in this study is compared to DIN 18800.

For arches subjected to uniform compression, DIN 18800 is more conservative than the proposed method. For arches subjected to uniform bending the proposed method is more conservative but DIN 18800 is not always safe. Since most arches have a positive post-buckling behaviour this is not a big problem.



a) Proposed method

b) DIN 18800



c) Proposed method

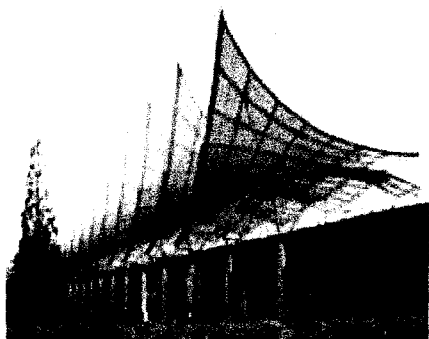
d) DIN 18800

Figure 6 Comparison of methods

It can be concluded that the proposed verification method provides a safe method to check the out-of-plane stability of arches subjected to uniform compression or uniform bending.

SAMENVATTING

De stijgende populariteit van het gebruik van bogen als constructief systeem, leidt tot een toenemende vraag naar toetsingsregels voor bogen. In afbeelding 1 is een voorbeeld van een boogconstructie te zien. Omdat er in de Nederlandse normen geen toetsingsregels voor bogen aanwezig zijn, heeft de commissie SG/TC 8, een onderzoekscommissie van het Staalbouwkundig Genootschap, een onderzoek geïnitieerd met als doel hanteerbare rekenregels voor stalen bogen te op te stellen. Het eerste deel van het onderzoek is uitgevoerd door Verstappen [1]. De aandacht in dit gedeelte is voornamelijk gericht op de stabiliteit in het vlak van de boog. Het tweede gedeelte van het onderzoek, is beschreven in dit rapport. Het beschrijft de stabiliteit uit het vlak van de boog.

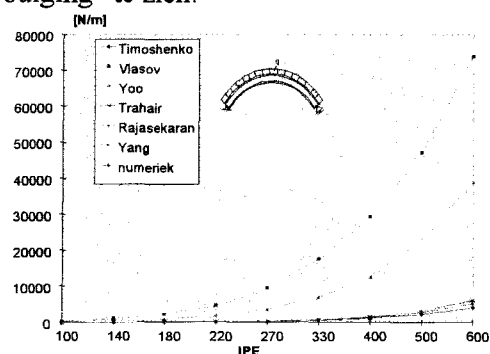


Afbeelding 1 Boogconstructie

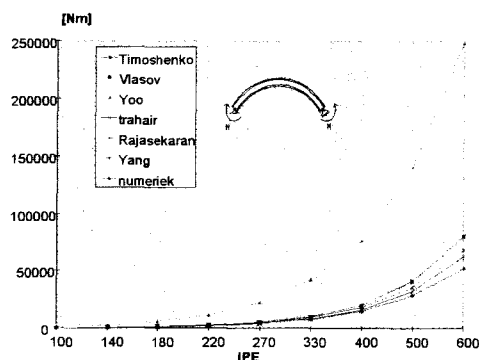
In de literatuur zijn verschillende modellen aanwezig die de stabiliteit uit het vlak van de boog beschrijven. Deze modellen zijn erop gericht de Eulerse kniklast voor bogen onder zuivere druk en onder zuivere buiging te bepalen. Zes verschillende modellen zijn in dit onderzoek beschouwd.

Het model van Timoshenko (1961) is gebaseerd op de theorie van een rechte balk en de invloed van de welving wordt niet meegenomen in dit model. Het model van Vlasov (1961) is eveneens gebaseerd op de theorie van een rechte balk maar de invloed

van de welving is wel verdisconteerd in het model. Het model van Yoo (1982) is het derde model wat gebaseerd is op de theorie van een rechte balk. De berekeningsmethode om de Eulerse kniklast te bepalen is echter niet gelijk aan de twee andere modellen. In plaats van de evenwichtsvergelijkingen te gebruiken, maakt dit model gebruik van het principe van virtuele arbeid. Het model van Trahair (1987) is het eerste model wat gebaseerd is op de theorie van een ggebogen staaf. De modellen van Rajasekaran (1989) en Yang (1989) zijn eveneens gebaseerd op deze theorie. Dat de modellen verschillende resultaten opleveren wordt veroorzaakt door de verschillend aangenomen rekverplaatsingsvergelijkingen. In afbeelding 2 is voor een reeks bogen de Eulerse kniklast voor het belastingsgeval "zuivere druk" te zien volgens de verschillende modellen. In afbeelding 3 zijn de resultaten voor het belastingsgeval "constante buiging" te zien.



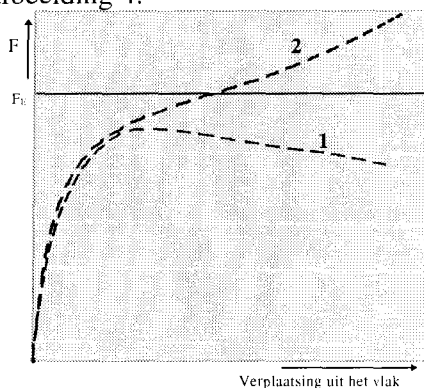
Afbeelding 2 Eulerse kniklast belastingsgeval 1



Afbeelding 3 Eulerse kniklast belastingsgeval 2

In afbeelding 2 en 3 zijn naast de analytische resultaten ook numerieke resultaten gegeven die verkregen zijn door een EEM berekening. Het blijkt dat de resultaten volgens het model van Rajasekaran betrouwbaar zijn en de vergelijkingen voor de Eulerse kniklasten zijn relatief eenvoudig. Daarom wordt dit model in het verdere onderzoek gebruikt om analytisch de Eulerse kniklast te bepalen.

Niet-lineaire eindige elementen berekeningen zijn uitgevoerd om meer informatie over het gedrag van de boog (uit het vlak) te krijgen. Bijna alle onderzochte bogen hebben een positief na-kritisch gedrag, wat betekent dat de boog een grotere belasting dan de Eulerse kniklast kan dragen. In afbeelding 4 is dit gedrag aangegeven met lijn 2. Er zijn ook bogen waarvoor de kniklast de maximale belasting is, dit is weergegeven met lijn 1 in afbeelding 4.



Afbeelding 4 belasting-verplaatsings diagram

Voor bogen die geen positief na-kritisch gedrag bezitten is het duidelijk wat de uiterste draagkracht is. Voor bogen die wel een positief na-kritisch gedrag bezitten is dat niet zo duidelijk. De boog kan in dat geval een belasting verdragen die zelfs groter is dan de Eulerse kniklast. De vervormingen die gepaard gaan met het bereiken van de uiterste sterkte kunnen echter onacceptabel groot zijn, zodat dit niet als uiterste draagkracht gezien kan worden. Daarom is in dit onderzoek een

definitie voor de uiterste draagkracht afgeleid die geldig is voor bogen met en zonder positief na-kritisch gedrag.

De uiterste draagkracht kan m.b.v. de volgende formule worden bepaald:

$$\min \left| \frac{d(\text{belasting})}{d(\text{verplaatsing uit het vlak})} \right|$$

Voor een boog zonder positief na-kritisch gedrag is dit de top in het last-verplaatsingsdiagram. Voor een boog met een positief na-kritisch gedrag is dit het buigpunt.

Voor de twee belastingsgevallen zuivere druk en zuivere buiging zijn twee toetsingsregels voorgesteld en succesvol geverifieerd met behulp van niet lineaire EEM analyses.

De toetsingsregel voor bogen onder zuivere druk luidt:

$$\frac{N_{c,s,d}}{\omega_{\text{boog}} N_{c,u,d}} \leq 1$$

met:

$N_{c,s,d}$ rekenwaarde van de normaaldrukkracht t.g.v. de belasting

$N_{c,u,d}$ rekenwaarde van de normaaldrukkracht m.b.t. de capaciteit in de uiterste grenstoestand

ω_{boog} knikfactor voor knik uit het vlak

De toetsingsregel voor bogen onder zuivere buiging luidt:

$$\frac{M_{y,s,max,d}}{\omega_{\text{boog}} M_{y,u,d}} \leq 1$$

met:

$M_{y,max,s,d}$ rekenwaarde van het buigend moment t.g.v. de belasting

$M_{y,u,d}$ rekenwaarde van het buigend moment m.b.t. de capaciteit in de uiterste grenstoestand

ω_{boog} knikfactor voor knik uit het vlak

De knikfactor voor knik uit het vlak kan verkregen worden m.b.v. de kolom-

knikcurven. Om deze te gebruiken moet de relatieve slankheid van de boog bekend zijn. De relatieve slankheid voor de twee belastingsgevallen is als volgt:

zuiver druk: $\lambda_{rel} = \sqrt{\frac{N_{c.u.d}}{F_{y,E}}}$

zuiver buiging: $\lambda_{rel} = \sqrt{\frac{M_{c.u.d}}{M_E}}$

waarin

$F_{y,E}$ is de Eulerse kniklast voor een boog onder zuivere druk, gebaseerd op het model van Rajasekaran

M_E is de Eulerse kniklast voor een boog onder zuivere buiging, gebaseerd op het model van Rajasekaran

$$F_{y,E} = \beta_{red} \frac{M_0}{R^2} \left(\frac{b/a(a^2 - 1)^2}{a^2 + b^2} \right)$$

$$M_E = \beta_{red} M_0 \left(-\frac{a}{b} - \frac{ab}{2} + \sqrt{\left(\frac{a}{b} + \frac{ab}{2} \right)^2 + 1 - a^2} \right)$$

met:

L, H, l en R volgens afbeelding 5.

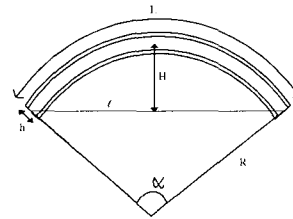
$$a = \frac{L}{\pi R} \quad b = \frac{\pi M_0}{P_z L}$$

$$P_z = \frac{\pi^2 EI_z}{L^2} \quad M_0 = \sqrt{P_z \left(GJ + \frac{\pi^2 EI_w}{L^2} \right)}$$

$$\beta_{red} = 1 \quad \text{als } \frac{H h}{L \ell} \leq 0.25$$

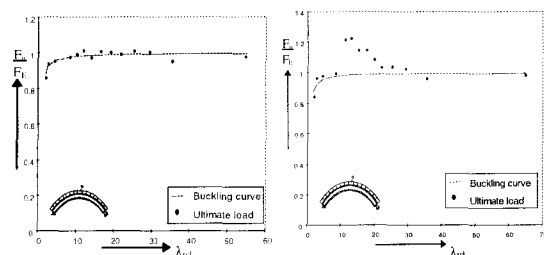
$$= 1.05 - 0.2 \frac{H h}{L \ell} \quad \text{als } \frac{H h}{L \ell} > 0.25$$

De reductiefactor β_{red} is ten opzichte van het origineel door Rajasekaran gepresenteerde werk toegevoegd om Eulerse kniklasten te verkrijgen die overeenkomen met numerieke resultaten.

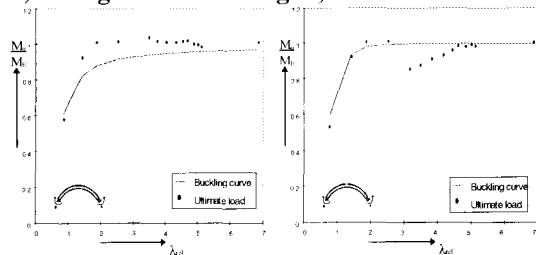


Afbeelding 5 Parameters van de boog

De Duitse norm DIN 18800 is het meest uitgebreid wat betreft toetsing van bogen. In afbeelding 6 is de voorgestelde toetsing vergeleken met die van DIN 18800. Voor bogen onder zuivere druk is DIN 18800 conservatiever dan de voorgestelde toetsing. Voor bogen onder zuivere buiging is de voorgestelde methode conservatiever dan die van DIN 18800, maar deze is niet altijd veilig. Omdat de meeste bogen een positief na-kritisch gedrag hebben hoeft dit echter niet altijd gevaar op te leveren.



a) Voorgestelde toetsing b) DIN 18800



c) Voorgestelde toetsing d) DIN 18800

Afbeelding 6 Toetsings methodes

Geconcludeerd kan worden dat de voorgestelde methode een veilige toetsing oplevert voor bogen onder zuivere druk of zuivere buiging.

GENERAL NOTATION

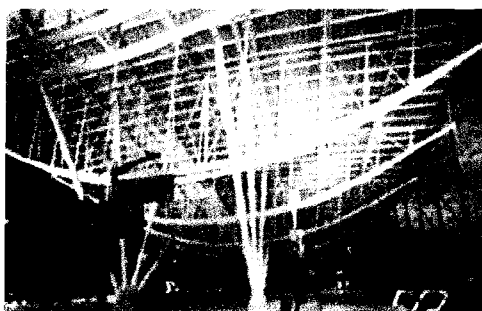
A	Cross sectional area
a	$L/\pi R$
b	$\pi M_0 / P_z L$
d	Design value (subscript)
E	Modulus of elasticity
F	Force
F_u	Ultimate load
f	Strength
G	Shear modulus of elasticity
H	Crown height of arch
h	Height of cross section
I_z	Second moment of area about the weak-axis
I_y	Second moment of area about the strong-axis
I_w	Warping section constant
J	Torsion section constant
L	Arch length
ℓ	Span of arch
l_{buc}	Buckling length
M	Moment in general
M_E	Euler buckling moment
M_0	$\sqrt{P_z (GJ + \frac{\pi^2 E I_w}{L^2})}$
$M_{y,max,s,d}$	Design value of maximum bending moment
$M_{y,u,d}$	Design plastic resistance to bending of the cross section
N	Axial force
$N_{c,s,d}$	Design value of compressive force
$N_{c,u,d}$	Design plastic resistance to compression of the cross section
P_z	$\frac{\pi^2 E I_z}{L^2}$
q	Uniformly distributed radially directed force
q_E	Euler buckling load
R	Arch radius
r	Radius of gyration
t	Thickness
u	Shear centre deflection out-of-plane
v	Shear centre deflection in-plane
W_{el}	Elastic section modulus
W_{pl}	Plastic section modulus
w	Shear centre deflection in longitudinal direction
x	Longitudinal axis through centroid
y, z	Principal centroidal axes

α	Angle
α_k	Imperfection factor
β_{red}	Reduction factor for analytical Euler buckling load
γ	Shear strain
Δ	Relative error analytical-numerical Euler buckling load
δ	Deformation
ε	Strain
λ	Slenderness
λ_{rel}	Relative slenderness
λ_0	Slenderness for a relevant buckling mode
λ_o	Load factor w.r.t. Euler buckling load
λ_s	Load factor w.r.t. plastic resistance of cross section
κ	Buckling factor DIN 18800
σ	Normal stress
τ	Shear stress
ϕ	Rotation
ψ	Imperfection parameter
ω_{buck}	Buckling factor for columns
$\omega_{arch.out}$	Buckling factor for out-of-plane buckling of arches

1. INTRODUCTION

Arch structures are more and more used in constructions. The architectural value combined with the efficient shape is the cause of their increasing popularity. Especially for structures with a large span it is efficient to use arches, because of the reduction of bending moments in the structure. In structures like coverings, roofs with a large span, bridges and art objects, arches are frequently found. Figure 1.1 shows examples of this kind of arch structures.

The increasing use of arches leads to a growing demand for a verification for arches. Since the Dutch codes lack a verification method to check arches, SG/TC 8 initiated an investigation to develop a verification method for steel arches. SG/TC 8 is a committee of the Dutch Steel Society (Staalbouwkundig Genootschap), which is active on the subject of stability of steel constructions. The first part of the investigation has been executed by Verstappen [1]. Here attention was mainly focused on the in-plane stability of steel arches. The study resulted in a proposal for the verification of the in-plane stability of circular arches. The second part of the investigation is described in this report. Attention is mainly paid to the out-of-plane stability of steel arches. The objective of this investigation is to provide a proposal for a verification method for out-of-plane stability of steel arches.



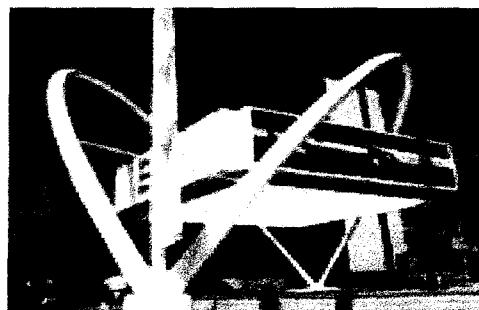
a) TGV station, Charles De Gaulle Airport, Paris



b) The Cable & Wireless College, Coventry



c) Merchants Bridge, Castlefield, Manchester



d) Old Street Roundabout, London

Figure 1.1 Arch structures

This report has been arranged as follows.

Chapter two starts with a short review of research on the subject stability and a review of provisions in international codes concerning arches.

Chapter three deals with the Euler buckling load, which is an useful tool to study the out-of-plane stability of arches. First some analytical models are considered and compared to each other. Next the Euler buckling load is determined numerically. The chapter finishes with a comparison between the analytical and numerical models.

In chapter four the "real" behaviour of arches is simulated with non-linear Finite Element Method analyses. The information obtained from these analyses is used in chapter five to determine a verification method for the out-of-plane stability of arches. Additional FEM analyses are performed to check the proposed verification.

Chapter six contains the general conclusions and the recommendations of this research.

2. OUT-OF-PLANE STABILITY OF ARCHES

The stability of arches is limited by different types of buckling. An important type is out-of-plane buckling. The cross-section of the arch is in this case submitted to a rotation and a translation. For the out-of-plane buckling of straight beams a distinction is made between flexural-torsional buckling and lateral-torsional buckling. Buckling of a column under compression is called flexural-torsional buckling and buckling of a beam under bending is called lateral-torsional buckling (see Figure 2.1). Here two different cases are concerned, with each their own behaviour. An arch on the other hand behaves under compression and under bending in the same way; a deformation out-of-plane and a rotation around the longitudinal axis. Nevertheless the terms flexural-torsional buckling and lateral-torsional buckling are used for arches in literature. To avoid confusion, in this investigation the term out-of-plane buckling is used, whether the arch is under compression, bending or a combination of the two.

2.1 Review of research on stability

Research on stability started in 1759 when Euler presented an analytical method to predict the buckling load of a slender column. His theory was fundamental and is still the basis of modern stability analysis. Another important step forward in the theory of torsional buckling was made by Saint-Venant. In 1855 he investigated the twisting response of members subjected to uniform torsion. In the beginning of the 20th century, Timoshenko was the one who extended this work with respect to the effects of warping torsion.

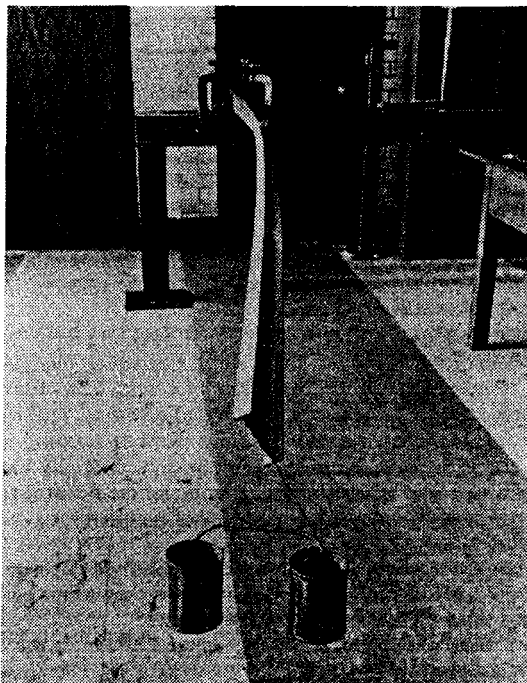


Figure 2.1 Lateral-torsional buckling

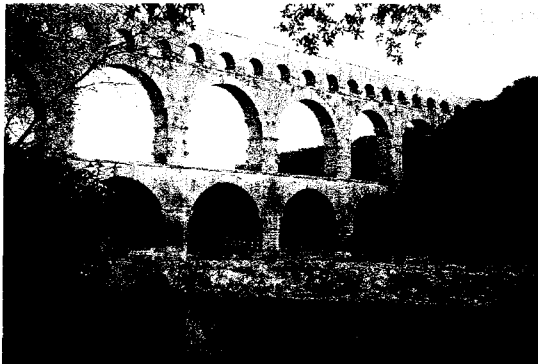
Many researchers studied the topic of flexural-torsional buckling and lateral-torsional buckling. Especially the 1960s show an increase in published work. This is mainly caused by the introduction of the computer. Extensive calculations by hand were no longer necessary. One was no longer limited to isolated members, but the influence of different restraints and the continuity with other members could be investigated. Later, with the introduction of the Finite Element Method in combination with increased computer performance, nearly every situation could be analysed. The new publications are mainly extensions of previously accepted analytical theories, based on differential equations or the energy equation of buckling.

One of these extensions is the out-of-plane buckling of arches. In the 1960s, Timoshenko and Vlasov were among the first who paid attention to this stability problem. In the 1980s some investigators came with an improvement of the earlier model.

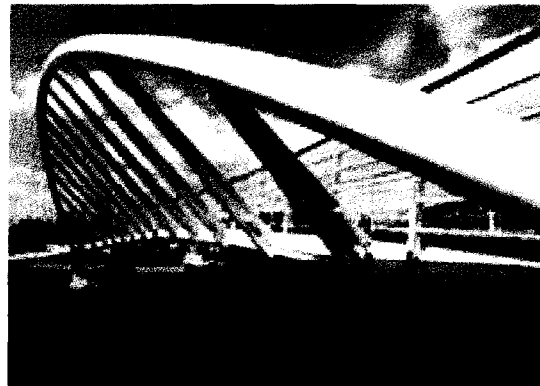
The existence of the numerous extensions on the buckling theory gives not always a better understanding of the subject. Not all published theories are commonly accepted and some contradict each other. In the 1980s an attempt was made to develop a general theory on flexural-torsional and lateral-torsional buckling. For straight beams this worked out, but for arches fundamentally different models on out-of-plane stability still exist.

2.2 Codes

In the previous section, attention was paid to the theoretical side of the out-of-plane stability of arches. But what happens in practice? We know that the Romans already made arches, without ever having heard of the term out-of-plane buckling. Their arches were very wide and stocky, so it is obvious they had no stability problems (see Figure 2.2a). When we look at the arches in the Gothic period, the slenderness already increased significantly. Nowadays architects go for the ultimate, by making the arch as slender as possible (see Figure 2.2b). It is no longer obvious that the arch will not buckle, so attention must be paid to its stability. Questions arise about how this is done and about the availability of codes concerning this kind of instability.



a) Roman aqueduct



b) Merchants Bridge, Castlefield, Manchester

Figure 2.2 Arch structures

2.2.1 International comparison

In 1991 a study of over 100 specifications and codes on stability design of metal structures was made[2]. One of the topics addressed by this study is the stability of arches. Code provisions were studied, for four geographical regions. Afterwards the codes were compared with each other and some comment was given.

The four regions with their specifications are:

- East Europe [editor: Kollar]

In the Czech and former East-German codes, an effective buckling length is used to describe out-of-plane buckling. In this effective buckling length, two factors are used to introduce different features of an arch. The first one considers the behaviour of the load during buckling. The second one considers the variation of the moment of inertia and the rise to span ratio of the arch. Other codes in this region give no provisions for out-of-plane buckling of arches.

- Asia [editor: Kuranishi]

In Japan, the specification for out-of-plane buckling in the JRA 89, is related to the allowable axial compressive stress in the following way:

$$\frac{H}{A_g} < 0.85\sigma_{ca}$$

in which:

H is the horizontal thrust (axial compression in a member) of the arch rib

A_g is the mean value of cross sectional area of a single arch member along its length

σ_{ca} is the allowable axial compressive stress

- North America [editor: Vinnakota]

The AASHTO 89, Standard Specifications for Highway Bridges, does not cover lateral buckling of individual ribs, or spatial stability of the system. The majority of arch bridges constructed in the USA are composed of box section ribs, widely spaced and braced by lateral members.

Therefore, in general lateral stability is not considered to be critical. Studies confirming this assumption are not available. Also other codes in North America do not cover the topic stability of arches.

- West Europe [editor: Kuranishi]

Germany is the only country in West Europe with specifications for arches. The buckling strength is verified by the column strength formula in DIN 18 800. The used slenderness parameter represents the features of the arches. Specifications are given for parabolic and circular arches, for braced and unbraced arches.

Due to the complexity of out-of-plane buckling, it is very difficult to cover all aspects of system stability of arches in terms of code provisions. In Table 2.1, a comparison is made between the codes for the four before mentioned regions. A review is given of the aspects which are included in the codes.

Table 2.1 shows that of the investigated codes, DIN 18 800 Part 2 (1986) provides the most complete description for the out-of-plane stability of arches. It gives provisions which can deal with a wide range of variables. It provides values mainly according to the results of an elastic analysis and effective length concept. The specifications of other countries seem to be too conservative and do not reflect the results obtained in recent research.

Table 2.1 Comparison of codes w.r.t out-of-plane stability of arches

Region	East-Europe			Asia	North America	West Europe
Country	Czechoslovakia	Hungary	former DDR	Japan	USA	Germany
Code	CSN 73 1401 84	MSZ 15024/1 85	TGL 13503/01 82	JRA 89	AASHTO 89	DIN 18 800 Part2 86
1a Application of column strength formula	X	X		X		X
1b Effective buckling length	X	X		X		X
1c Effect of the inclination of hangers or posts during buckling	X	X		X		X
1d Effect of bracing systems						X
1e Effect of end portal frames						X
2a Effect of load combination						X

2.2.2 DIN 18 800

As mentioned before, the German code DIN 18 800 is the most extensive code on out-of-plane stability of arches. Therefore this code is looked upon more closely.

The verifications for out-of-plane stability of arches in this code, are all based on the verification of the stability of columns. The same unity check as for columns is used to verify the stability of

arches: $\frac{N}{\kappa N_{pl,d}} \leq 1$

By introducing an adapted slenderness, the features of the arch are taken into account. The effect of variation of the shape, the load and the restraints of the arch are included in it. From the slenderness, the buckling factor κ can be determined. For the extensive verification the reader is referred to appendix A.1. Below, arches with their characteristics are given, for which verifications are present in DIN 18 800. The numbers refer to the corresponding articles in the code.

- Article 6.1.2 Arches under compression
 - Article 6.1.2.1 Arches without bracing

Two methods are given to determine the slenderness of an arch. One for a parabolic arch and one for a circular arch.
 - Article 6.1.2.2 Arches with braces and end frame
- Article 6.2.2 Arches under compression and bending
 - Article 6.2.2.1 General
 - Article 6.2.2.2 Arches loaded in the crown of the arch, with invariable rectangular or I-shaped cross section.
 - Article 6.2.2.3 Circular arch with I-shaped cross section and pin-ended supports
- Article 6.3 Spatial loaded arches

No stability check is given, it is just mentioned how to determine the load carrying capacity according to the elastic theory and how to introduce imperfections.

3. EULER BUCKLING

One of the characteristics of an arch, is the first order elastic out-of-plane buckling load. This is a critical loading for a perfect arch, with elastic behaviour and without the influence of deformations. In practice, an arch is never perfect and does not deform fully elastically. Therefore it will not collapse at this load. This load however, is a useful tool to study the out-of-plane stability of an arch. The term Euler buckling load is used in this report for the first order elastic buckling load. In the literature different terms are found for this load. Elastic critical load, bifurcation point, eigenvalue and buckling load are also used to describe the first order elastic buckling load.

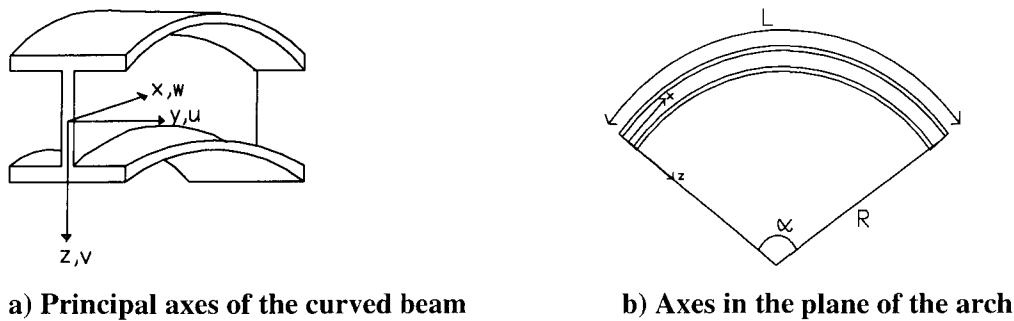
In this chapter two calculation methods will be considered to determine the Euler buckling load of an arch. In paragraph 3.1 some analytical methods are discussed. In paragraph 3.2, a numerical method to determine the Euler buckling load for an arch is given. Finally the results of the two calculation methods are compared in paragraph 3.3.

3.1 Analytical models

In this paragraph, the theories developed by several researchers will be discussed. In spite of the same approach to the problem, performing an eigenvalue analysis, they found different solutions. To make a better comparison afterwards between the different theories, the models will be compared to each other, based on a standard arch.

All researchers used their own co-ordinate system, which is confusing for a proper comparison. For this investigation a standard co-ordinate system is defined. In Figure 3.1a, the directions of the local axes of the standard arch that is used in this investigation, are shown. The standard arch is a part of a circle and has a double symmetric cross section. The dimensions are defined by the radius R and the length L as given in Figure 3.1b. The boundary conditions are defined as pin-ended for one support, which means: the ends are able to rotate freely around the principal axes and the translations are fixed in three directions. The other support has the same conditions with one exception: the translation in radial direction is not fixed, to obtain uniform compression and uniform bending in the arch. To prevent the arch from turning on its side, an extra boundary condition is created: a restraint against rotation around the tangential axis of the arch.

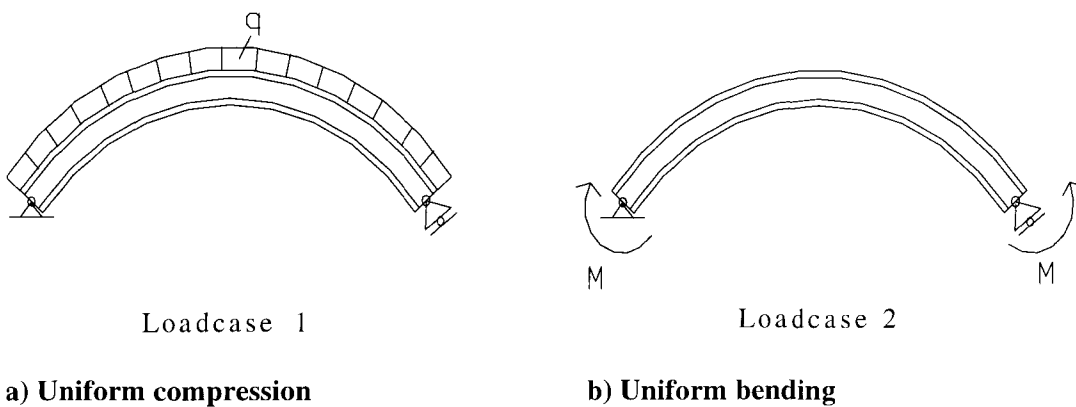
The Euler buckling load is determined for two different loadcases. The first one consists of a load q , which is uniformly distributed along the centre line of the arch and radial directed. This results in a case of uniform compression in the arch (see Figure 3.2a). The second case is uniform bending along the length of the arch, two equal end moments are applied around the y -axis (see Figure 3.2b).



a) Principal axes of the curved beam

b) Axes in the plane of the arch

Figure 3.1 Axes of the standard arch



Loadcase 1

Loadcase 2

a) Uniform compression

b) Uniform bending

Figure 3.2 Two loadcases

3.1.1 The models

3.1.1.1 Timoshenko and Gere (1961)

Timoshenko and Gere[3] were among the first who investigated the stability of curved beams. They investigated a circular arch with rectangular cross section. By solving the equilibrium for a straight beam directly, they obtained the equilibrium equations. These equations were adapted for a curved beam by replacing the equations for the curvatures and twist of a straight beam for the ones of a curved beam. For more details the reader is referred to appendix B.2.

Timoshenko did not take into account the influence of warping. For closed rectangular cross sections, which he used, this influence is negligible. Therefore this neglect does not have a large effect on the results of his investigation. The disadvantage of this model is the limited applicability.

Euler buckling load for curved beams under uniform compression

$$q_E = \frac{EI_z \left(\frac{\pi^2 R^2}{L^2} - 1 \right)^2}{R^3 \left(\frac{\pi^2 R^2}{L^2} + \frac{EI_z}{GJ} \right)}$$

Euler buckling load for curved beams under uniform bending

$$M_E = \frac{EI_z + GJ}{2R} + \sqrt{\left(\frac{EI_z - GJ}{2R}\right)^2 + \frac{EI_z GJ \pi^2}{L^2}}$$

3.1.1.2 Vlasov (1961)

Like Timoshenko, Vlasov [4] used straight beam theory as starting-point to derive the equilibrium equations for curved beams. He extended the model in such a way, that his model is also valid for double symmetric I-sections. For this kind of cross sections, warping is no longer negligible. Vlasov took this into account, which can explain the presence of the rigidity of warping in the solution. A drawback of this model is again its limitation. Only the Euler buckling loads of double symmetric cross sections can be calculated with this model. See appendix B.3 for the derivation.

Euler buckling load for curved beams under uniform compression

$$q_E = \frac{M_0}{R^2} \left(\frac{1}{2ab} + \frac{abR^2}{2r^2} \pm \sqrt{\left(\frac{1}{2ab} + \frac{abR^2}{2r^2} \right)^2 - \frac{R^2}{r^2} (1 - a^2)} \right)$$

Euler buckling load for curved beams under uniform bending

$$M_E = M_0 \left(\frac{ab}{2} + \frac{a}{2b} \pm \sqrt{\left(\frac{ab}{2} + \frac{a}{2b} \right)^2 + (1 - a^2)} \right)$$

$$\text{with: } a = \frac{L}{\pi R} \quad b = \frac{\pi M_0}{P_z L} \quad P_z = \frac{\pi^2 EI_z}{L^2} \quad M_0 = \sqrt{P_z \left(GJ + \frac{\pi^2 EI_w}{L^2} \right)}$$

3.1.1.3 Yoo (1982)

Like Timoshenko and Vlasov, Yoo also uses an analogy between straight and curved beams (see [5, 6]). Instead of solving the equilibrium equations directly, Yoo starts with the total potential energy. The curvatures and twist for a curved beam are substituted in straight beam energy. The equilibrium equations are obtained by differentiating the total energy twice. To solve these equations a displacement field is assumed for the out-of-plane displacement and the rotation. See appendix B.4 for the equations. As Yoo did not make any assumption concerning the cross section in advance, critical loads of asymmetric cross sections can be calculated with his model.

Euler buckling load for curved beams under uniform compression

$$q_E = \frac{-B \pm \sqrt{B^2 - 4AC}}{2AR}$$

with:

$$A = -r^2 (1 - a^2) - \frac{a^4 R^2}{4} \quad B = P_z r^2 (a^2 - 1)^2 + P_0 r^2 (a^2 - 1) \quad C = M_0^2 (a^2 - 1)^2$$

Euler buckling load for curved beams under uniform bending

$$M_E = M_0 (ab - a^3b \pm (1 - a^2) \sqrt{a^2b^2 + 1})$$

As mentioned before, Yoo started with the total potential energy for a straight beam and substituted the curvatures and twist for a curved beam. For example the first derivative of the twist ϕ' is replaced by $(\phi' - \frac{u}{R})$. In the total potential energy equation, the term $(u')^2$ occurs related to the normal force P. Yoo has no substitute for the first derivative of the out-of-plane displacement u' , therefore he rewrites $(u')^2$ to uu'' . By doing so he introduces an error. To study the influence of this substitution, Yoo's model is adapted to model Yoo*. The term $(u')^2$ in this model is used and not substituted by the term of a curved beam. The moment in the total potential energy is not related to u' , so the critical moment for both models is the same. The critical q-load for the adapted model is given below, for the derivation see appendix B.4.

Euler buckling load for curved beams under uniform compression

$$q_E^* = \frac{-B \pm \sqrt{B^2 - 4AC}}{2AR}$$

with:

$$A = 1 \quad B = -P_\phi - P_z \left(a \frac{4R^2}{r^2} + (a^2 - 1)^2 \right) \quad C = \frac{M_0^2}{r^2} (a^2 - 1)^2$$

3.1.1.4 Trahair and Papangelis (1987)

The validity of Vlasov's and Yoo's theories has been criticised by Trahair and Papangelis, due to the use of straight beam theory [7,8,9,10,11]. Trahair and Papangelis investigated the problem of curved beams without using the straight-beam theory. They used the potential-energy approach for curved beams.

First non-linear expressions for the axial and shear strains are derived for a curved beam. These expressions are substituted in the second variation of the total potential energy to get the buckling equations. To solve these equations, displacement fields for the out-of-plane translation and the rotation around the axis of the arch, are assumed. This results in two differential equations with two variables, which are related to each other. The Euler buckling loads for buckling under uniform bending or compression can be obtained from these equations. See appendix B.5 for the equations.

Euler buckling load for curved beams under uniform compression

$$q_E = \frac{P_z}{R} ab \left(\left(ab + \frac{1}{ab} \right) - \frac{\left(b + \frac{1}{b} \right)^2}{\frac{a}{b} + \frac{b}{a}} \right)$$

Euler buckling load for curved beams under uniform bending

$$M_E = M_0 \left(-ab + \frac{a^3b}{2} - \frac{a}{2b} + \sqrt{\left(-ab + \frac{a^3b}{2} - \frac{a}{2b} \right)^2 + (1-a^2)^2} \right)$$

3.1.1.5 Rajasekaran and Padmanabhan (1989)

Rajasekaran and Padmanabhan use more or less the same approach as Trahair [12]. However, instead of deriving the equation for the total potential energy, they work with the principle of virtual displacement.

Trahair only assumed that the deformations in the plane have no influence on the out-of-plane stability and neglected these terms in the total potential energy. Rajasekaran and Padmanabhan did not neglect these terms. They showed with the four differential equations, obtained by executing the principle of virtual displacement, that the assumption of Trahair was right for the two loadcases of uniform bending and uniform compression. See appendix B.6 for these equations.

In spite of using the same theory, the models of Trahair and Rajasekaran do not correspond for the arch under uniform bending. Different assumptions in strain-displacement equations are the cause of the difference.

Euler buckling load for curved beams under uniform compression

$$q_E = \frac{M_0}{R^2} \left(\frac{1}{2abR} \left(1 + \frac{a^2L^2}{\pi^2r^2} \right) + \frac{abR}{2r^2} \left(1 + \frac{r^2}{R^2} \right) \pm \sqrt{\left(\frac{1}{2ab} \left(1 + \frac{a^2L^2}{\pi^2r^2} \right) + \frac{abR^2}{2r^2} \left(1 + \frac{r^2}{R^2} \right) \right)^2 - \frac{1}{r^2} (a^2 - 1)^2} \right)$$

Euler buckling load for curved beams under uniform bending

$$M_E = M_0 \left(-\frac{a}{2b} - \frac{ab}{2} \pm \sqrt{\left(\frac{a}{2b} + \frac{ab}{a} \right)^2 - a^2 + 1} \right)$$

The just mentioned Euler buckling equations are given in the work of Rajasekaran and Padmanabhan [12]. The equilibrium equations of which these solutions are derived are also given. In these equations no terms related to the radius of gyration is present. The radius of gyration is introduced afterwards to compare the result to other models. When the Euler buckling q-load is calculated from the equations in [12] another solution is found. This is the same solution as the result of Trahair. See appendix B.6. This solution is also used to make a comparison with the other models. The name of this modified model is Rajasekaran*.

Euler buckling load for curved beams under uniform compression

$$q^*_E = \frac{M_0}{R^2} \left(\frac{b(a^2 - 1)^2}{a^3 + ab^2} \right)$$

3.1.1.6 Yang and Kuo

Yang and Kuo studied the existing theories and adapted them according to their point of view [13, 14, 15]. Like Rajasekaran and Padmanabhan, their model is derived with the principle of virtual displacements. The difference between the two theories lies in a different assumed strain-displacement relation. See appendix B.7.

It is to be expected that the results are very close to the ones of Rajasekaran and Padmanabhan.

Euler buckling load for curved beams under uniform compression

$$q_E = \frac{1}{R} \left(\frac{-B \pm \sqrt{B^2 - 4C}}{2} \right)$$

$$\text{with: } B = P_z \left((a^2 - 1)^2 + a^4 \frac{R^2}{r^2} \right) + \frac{GJ}{r^2} + EI_w \frac{\pi}{L} (1 - a^2)^2 \left(1 + \frac{R^2}{r^2} \right)$$

$$C = \frac{P_z GJ}{r^2} (a^2 - 1)^2 + EI_w \left(P_z + \frac{GJ}{R^2} \right) \frac{\pi^2}{L^2 r^2} (1 - a^2)^2$$

Euler buckling load for curved beams under uniform bending

$$M_E = \frac{-B \pm \sqrt{B^2 - 4AC}}{2A}$$

$$\text{with: } A = 1 - \frac{r^2}{R^2}$$

$$B = P_z R \left(a^2 - \frac{r^2}{R^2} (a^2 - 1) \right) + \frac{GJ}{R} + \frac{EI_w}{R^3 a^2} (1 - a^2) \left(1 - \frac{r^2}{R^2} \right)$$

$$C = \left(\frac{P_z EI_w}{R^2 a^2} + P_z GJ + \frac{GJ EI_w}{R^4 a^2} \right) (a^2 - 1)$$

3.1.2 Comparison of the models

The analytical models discussed in this chapter, have different assumptions and limitations. These differences lead to different Euler buckling loads for an arch under uniform compression or bending. In the past investigators made comparisons between the models. The different co-ordinate system and boundary conditions made this a complex task. The standard arch with the assumed co-ordinate system, introduced in this chapter, gives the possibility to compare, besides the results (Euler buckling loads), also the formulas.

In this paragraph the models are compared to each other in the next three ways.

With respect to:

- assumptions and limitations
- resulting formulas
- Euler buckling loads.

Concluding remarks, based on the different comparisons, will finish the paragraph.

3.1.2.1 Assumptions and limitations

The features of the different analytical models are shown in Table 3.1. During the years, the model generally improved. The calculation method changed from direct into indirect. The applied theory is adapted specially for curved beams and the cross section restrictions disappear slowly. These changes point to a continuous improvement of the model.

Table 3.1 Assumptions and limitations

Researcher(s)	year	theory	calculation method	effect of warping	cross section
Timoshenko & Gere	1961	straight beam	direct	not included	closed, double symmetric
Vlasov	1961	straight beam	direct	included	double symmetric I cross section
Yoo	1982	straight beam	energy method	included	non-symmetric cross sections
Trahair & Papangelis	1987	curved beam	energy method	included	non-symmetric cross sections
Rajasekaran & Padmanabhan	1989	curved beam	virtual displacement	included	non-symmetric cross sections
Yang & Kuo	1989	curved beam	virtual displacement	included	non-symmetric cross sections

3.1.2.2 Formulas

Timoshenko and Vlasov use the same calculation method, solving the equilibrium equations directly. The execution however is different. Timoshenko defines the curvatures and twist for a curved beam and substitutes them into the constitutive equations. Vlasov uses curvatures and twist for a straight beam and introduces the influence of the curved beam in the equilibrium equations. See appendix B.2 and B.3. There are two differences between the resulting equilibrium equations. First Vlasov introduces a warping rigidity in contrast to Timoshenko, secondly the terms of the equations are not corresponding.

The other researchers used the energy method or the principle of virtual displacement. Both methods can be divided into two parts. One part represents the strain energy while the other part represents the potential energy.

Strain energy

For the strain energy the strain-displacement relations are required. See appendices B.4-B.7 for the linear axial strain and shear strain equations. Besides small differences, the strain-displacement relations of all models correspond to the following equations.

$$\varepsilon_x = \frac{R}{R-z} \left[(w' - \frac{v}{R}) - y (u'' + \frac{\phi}{R}) - z (v'' + \frac{w'}{R}) + \alpha_w (\phi'' - \frac{u''}{R}) \right]$$

$$\gamma = 2t \left(\phi' - \frac{u'}{R} \right)$$

Yoo uses in his model for the third term between the brackets the term $-z (v'' + \frac{w'}{R})$ in the equation of ε_x . For out-of-plane stability, this term is irrelevant and disappears out of the differential equation (in-plane deformations have no influence on the out-of-plane stability). Therefore, the results are not influenced by the different term.

Rajasekaran and Padmanabhan use for $-y (u'' + \frac{\phi}{R})$ only $-y u''$ in their model. This can lead to

different results, because the influence of the curvature is not taken into account.

Finally Yang and Kuo find $-\alpha_w$ instead of $+\alpha_w$, in their relation. This has no influence on the result for out-of-plane buckling, because ε^2 is used.

Potential energy

The second part of the energy, the potential energy, is different for every model.

$$\text{Yoo:} \quad \frac{1}{2} P \left[u \left(u'' + \frac{\phi}{R} \right) + r^2 \left(\phi' - \frac{u'}{R} \right)^2 \right] + M \left[u'' \phi + \frac{\phi^2}{R} \right]$$

$$\text{Trahair:} \quad \frac{1}{2} P \left[(u')^2 + r_y^2 (\phi')^2 + r_z^2 \left(\phi' - \frac{u'}{R} \right)^2 \right] + M \left[u'' \phi + \frac{\phi^2}{2R} \right]$$

$$\text{Rajasekaran:} \quad \frac{1}{2} P [(u')^2] + M \left[u'' \phi + \frac{\phi^2}{2R} + \frac{(u')^2}{2R} \right]$$

$$\text{Yang:} \quad \frac{1}{2} P \left[(u')^2 + r^2 \left(\phi' - \frac{u'}{R} \right)^2 \right] + M \left[u' \phi' + \frac{\phi^2}{2R} + \frac{(u')^2}{2R} - \frac{r^2}{2R} \left(\phi' - \frac{u'}{R} \right)^2 \right]$$

First of all, the terms related to the normal force P are considered.

Yoo used the straight beam theory and introduced the twist and curvatures for curved beams in this theory. The substitution of the term $(u')^2$ is executed in two steps. Instead of using the term $(u')^2$ Yoo replaced it by $u u''$ which is substituted by $u \left(u'' + \frac{\phi}{R} \right)$, see appendix B.4. The difference of the first term between brackets is explained by this.

Other differences for the part of P are all related to the radii of gyration. Rajasekaran already neglects these terms in the formulation of the principle of virtual displacements. In the total energy of Trahair the terms related to the radii of gyration are still present but are later neglected. Therefore the Euler buckling load of an arch under uniform compression according the model of Trahair is the same as for the model of Rajasekaran. In appendix B.6 this is shown.

The results according the model of Yang are probably corresponding the models of Trahair and Rajasekaran, because the term with r^2 is negligible as Trahair demonstrated.

The sum of the terms that will influence the critical moment M are all different. The first two terms are the same, only Yoo misses a factor $\frac{1}{2}$. This is again the result of replacing the first derivative of the curvature by an other term. Trahair has no terms with u' , compared to Rajasekaran and Yang. Rajasekaran ignores again the term with the radius of gyration, compared to Yang and the model of Yang has a different first term compared to all others.

3.1.2.3 Results

In Figure 3.3 and Figure 3.4, the Euler buckling loads of the different models are shown for a circular arch with different features. For the two loadcases, two different sections are calculated, combined with two different geometries resulting in 8 figures. The models marked with a star represent an adaptation of the original model. For explanation see paragraph 3.1.1 of this chapter.

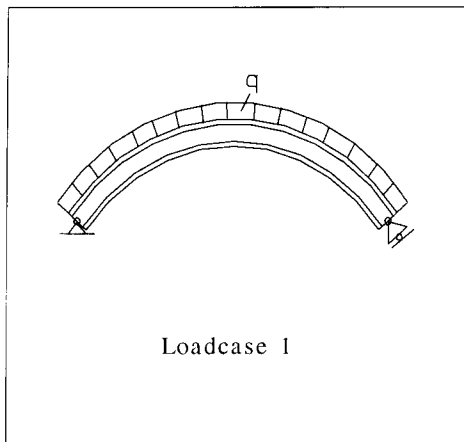
Some remarks based on these figures are given below

For the Euler buckling load loadcase 1: (Figure 3.3)

- The models of Vlasov and Yoo give very high results, especially with an arch length of 10 m.
- The other models give good corresponding results.
- Timoshenko's model gives a remarkable low result for the arch with IPE500 R=7m and L=3.5m.

For the Euler buckling load loadcase 2: (Figure 3.4)

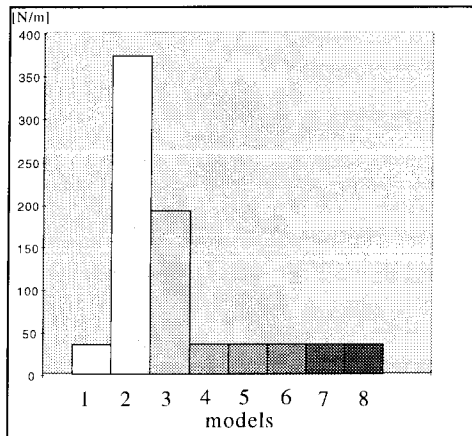
- The load of Yoo is for the four different cases remarkably higher than the other loads. For the arches with a larger arch length, the discrepancy is the largest.
- In general Timoshenko gives a load which is lower, especially for the last case (IPE500, Radius 7m, Length 3.5m).
- Trahair gives for all cases a Euler buckling load which is lower than the models of Rajasekaran and Yang, especially for the more slender arches (IPE100).
- The models of Vlasov, Rajasekaran and Yang give good corresponding results



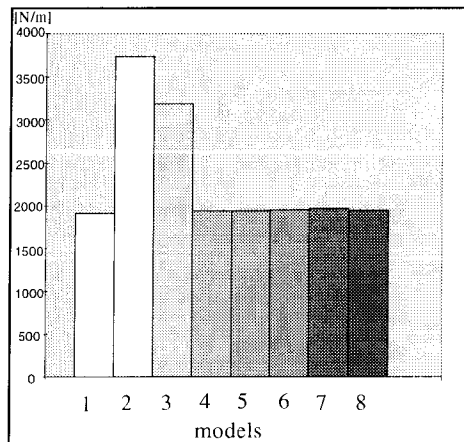
a) Basic arch

1	Timoshenko
2	Vlasov
3	Yoo
4	Trahair
5	Rajasekaran
6	Yang
7	Rajasekaran*
8	Yoo*

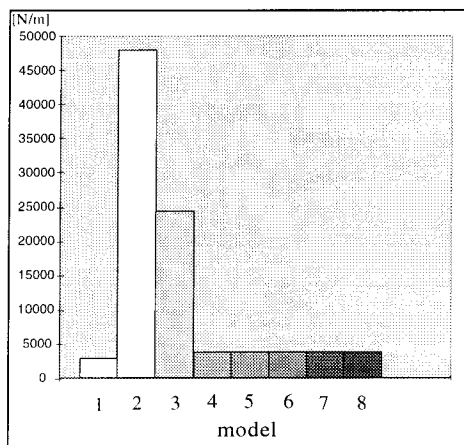
b) Legend



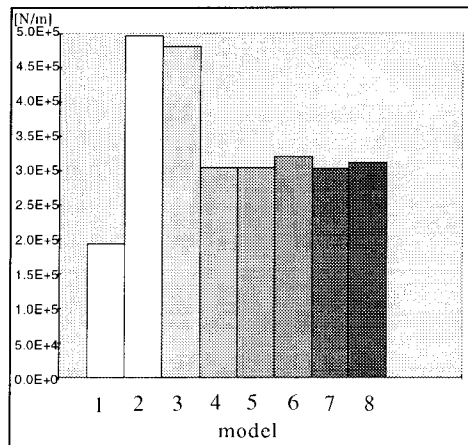
c) cross section IPE100
arch length: 10 m radius: 7 m



d) cross section IPE100
arch length: 3.5 m radius: 7 m

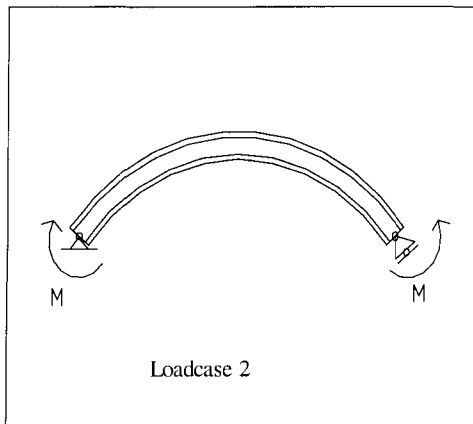


e) cross section IPE500
arch length: 10 m radius: 7 m



f) cross section IPE500
arch length: 3.5 m radius: 7 m

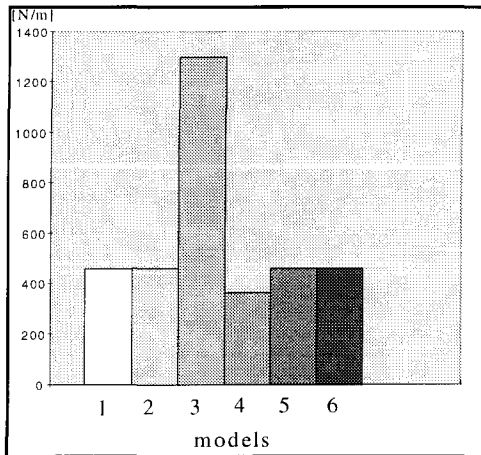
Figure 3.3 Euler buckling loads of the basic arch under uniform compression



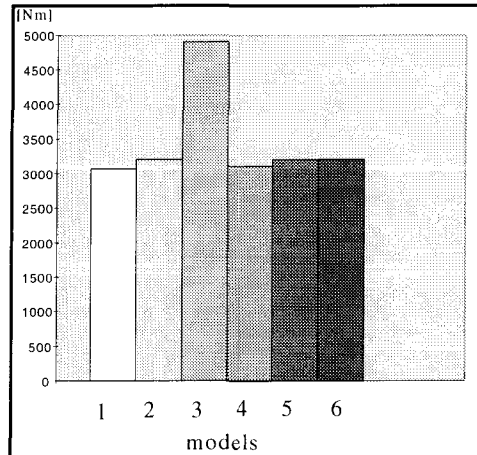
a) Basic arch



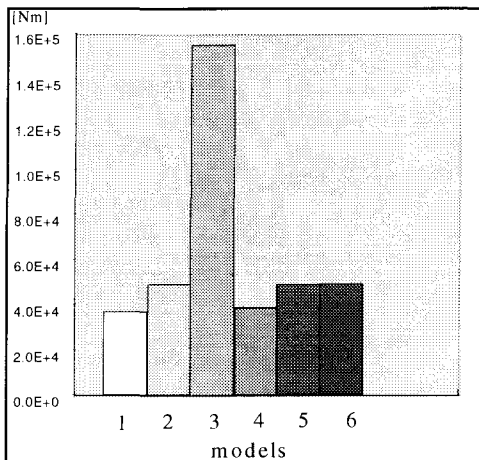
b) Legend



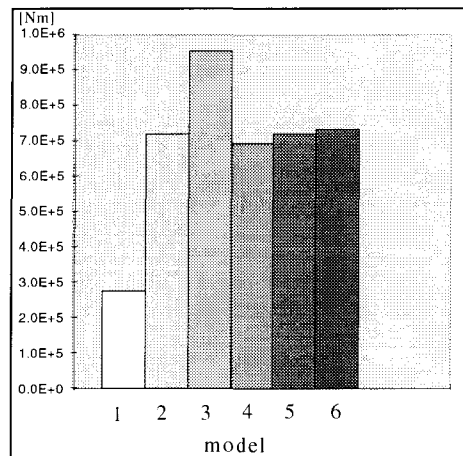
c) cross section IPE100
arch length: 10 m radius: 7 m



d) cross section IPE100
arch length: 3.5 m radius: 7 m



e) cross section IPE500
arch length: 10 m radius: 7 m



f) cross section IPE500
arch length: 3.5 m radius: 7 m

Figure 3.4 Euler buckling loads of the basic arch under uniform bending

3.1.3 Conclusions

Timoshenko and Vlasov used both the same calculation method (direct) and theory (straight beam theory), even so their results do not correspond very well. Due to their calculation method it is very hard to point out the difference in the formulas. The results however tell a lot about the methods. The results of Timoshenko are of the same order of magnitude as the other results. Sometimes the Euler buckling load is slightly lower but this can be explained by the neglect of the warping effect. Especially the stocky arches give a lower result, which confirm the just mentioned explanation, because stocky arches are more sensitive for warping (see appendix B.8). The model of Vlasov gives for the first loadcase extremely high results. A possible explanation can be found in the use of the straight beam theory. An arch with a shorter arch length resembles a straight beam better, this is shown in Figure 3.5. As can be seen in Figure 3.3 Vlasov's results correspond more to the other results for an arch with a shorter length.

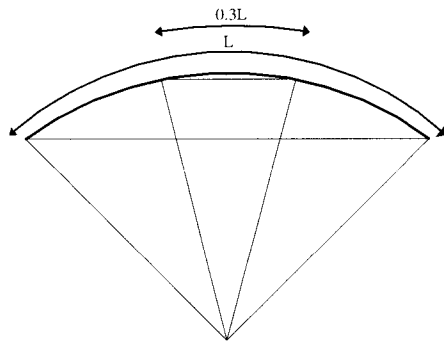


Figure 3.5 Arch with same radius and varying length

The model of Yoo may be regarded as a transition to the latest models. He still uses straight beam theory but already uses a virtual displacement method. The high results nevertheless are more an obstacle than a link between two methods concerning out-of-plane stability of arches. His substitution of $(u')^2$ into uu'' is not successful. The model Yoo* in which this substitution is omitted, indicates this. The model gives namely results in the same order of magnitude as the other models do. Concluding from this, Yoo's original model is not reliable.

The models of Trahair, Rajasekaran and Yang remain. They are based on the same theory (curved beam) and all use more or less the same calculation method. The formulas correspond also quite well. Trahair neglects a term related to the bending moment which results in small Euler buckling loads for the loadcase uniform bending. The second difference concerns the terms related to the radius of gyration, they are not in all models the same. In the model of Rajasekaran they are absent. The model of Trahair contains these terms but they are neglected afterwards. In the model of Yang, the terms are not neglected. The results of the three models however are very similar.

3.2 Numerical models

In paragraph 3.1, Euler buckling loads of different arches are obtained by using different analytical models. This is carried out for two loadcases: uniform compression and uniform bending. In this paragraph the Euler buckling load is determined numerically with the general purpose Finite Element Method DIANA. Two different models for FEM calculations are discussed: one model with beam elements and one model with shell elements. The objective of performing numerical buckling calculations is to verify the analytical models.

3.2.1 Model with beam elements

3.2.1.1 The element

This investigation is focused on out-of-plane stability. To describe the out-of-plane displacements of an arch, beam elements with six degrees of freedom for each node are needed. Element L12BE is such an element. See Figure 3.6. It is a two-node, three-dimensional class-I beam element. This means that it has as basic variables: three translations u_x , u_y and u_z and three rotations ϕ_x , ϕ_y and ϕ_z in the nodes. Class-I points to a classical beam. This means that shear deformations are not taken into account and that it is assumed that the cross sections remain plane and perpendicular to the slope of the beam axis. This can be seen as Bernoulli's theory holds.

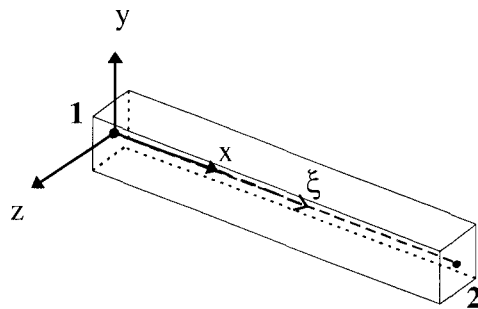


Figure 3.6 L12BE beam element

The expected displacement fields of the arch are sinus-shaped and are well described with a couple of these elements. The L12BE element does not take into account the influence of warping, because this element has no warping rigidity. When the arch has the possibility to warp at its supports, the Euler buckling load determined by DIANA is too small. As in most FEM programs, in DIANA an element is absent, which takes into account the influence of warping. Some programs do have a beam element that takes the warping-effect into account, but these are only straight beam elements. The warping moment in this element is developed along the beam-axis. When two beam elements are coupled at an angle the warping moment is set to zero in the node. To model an arch, straight

elements have to be connected at an angle. The consequence is that for every element the warping moment is put back to zero. This does not reflect the real warping behaviour and is therefore not appropriate to use.

When we use beam elements to create a FEM model of an arch, the aspect of warping is neglected. Therefore, the results of the DIANA calculations can only be compared to the results of Timoshenko's model; he also neglects the warping rigidity in his model.

3.2.1.2 The model

Exactly the same arch as used for the analytical models, has to be used in the numerical model. This means the same shape of arch, the same section and similar boundary conditions. The shape of the arch can be defined exactly. The same section is obtained by attaching the right rigidities to the beam element. The boundary conditions are the one for a pin-ended supported arch. Special attention must be paid to the bending moment and compression force that appear in the arch. In the analytical models, uniform bending and uniform compression are assumed. To obtain this in the arch, one of the supports must be able to displace in radial direction of the arch (see Figure 3.7). When this is not the case, an extra force is introduced at the supports, which affects the uniform bending and the uniform compression in the arch.

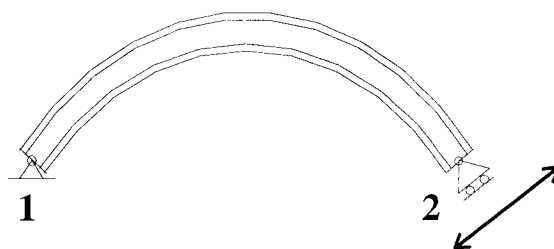


Figure 3.7 Free translation in radial direction at support 2

3.2.1.3 Results

The arch with uniform bending gives a very high Euler buckling load. This load is not the Euler buckling load for flexural-torsional buckling of the arch, but just for lateral buckling. With this beam element second order terms due to bending moments are not taken into account, which it makes it not appropriate to describe torsional buckling. Therefore, no Euler buckling load for the loadcase uniform bending is found.

The Euler buckling load of the arch under uniform compression, agrees with the Euler buckling load of Timoshenko's model. This is illustrated in Table 3.2. From these results the conclusion can be drawn that for arches, not sensitive to warping, the numerical model with beam elements give good results.

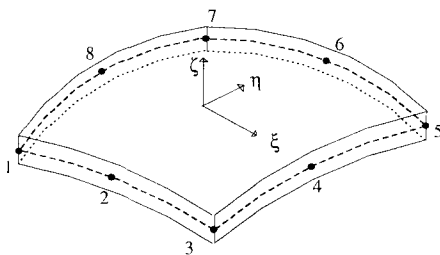
Table 3.2 Euler buckling loads, numerical and according to Timoshenko

cross section	$q_{critical}$	Timoshenko
IPE100	35.4 N/m	35.3 N/m
IPE140	75.7 N/m	75.6 N/m
IPE180	151 N/m	151 N/m
IPE220	289 N/m	289 N/m
IPE240	414 N/m	414 N/m
IPE270	515 N/m	515 N/m
IPE330	913 N/m	912 N/m
IPE400	1660 N/m	1660 N/m
IPE450	2150 N/m	2150 N/m
IPE500	2870 N/m	2870 N/m
IPE600	5250 N/m	5250 N/m

3.2.2 Model with curved shell elements

3.2.2.1 The element

To make a model in which warping effect is not neglected, curved shell elements can be used. The curved-shell element CQ40S is chosen to model the arch. See Figure 3.8. This isoparametric element has eight nodes, which have five degrees of freedom each: three translations and two rotations. The rotation in the plane of the element is prevented. The element is based on two shell hypotheses. The first one is that normals remain straight, but not necessarily normal to the reference surface. The second hypothesis assumes that the normal stress component in the normal direction of the shell is forced to zero.

**Figure 3.8 CQ40S element**

With the use of shell elements, the influence of warping can be described but another problem is introduced. The rigidities of a section can not simply be attached to the elements like for the beam elements. By using shell elements, a section is created with its own rigidities and dimensions,

depending on the element dimensions. A solution for this problem is not found in adapting the numerical model to the analytical model, but the other way around.

The rigidities of the numerical model can be calculated from the cross section created with the shell elements. These values can also be used in the analytical models and a comparison can be made between the two models. See appendix C.1 for determination of the rigidities.

3.2.2.2 The model

Again shape, section and boundary conditions must be the same as in the analytic model. The shape of the arch depends on the position of the elements. It is possible to model a circular arch with the right dimensions. The section is not the same as used in the analytical models, but the rigidities of the numerical model are introduced in the analytical model. The boundary conditions are obtained by placing the next supports: the mid-node of the cross section at one support has prescribed translations in three directions and the other support has only two prescribed translations like in the beam model. The rotation around the beam axis is prevented in the supports by prescribing the translations in the out-of-plane direction of six nodes. See Figure 3.9 for the boundary conditions.

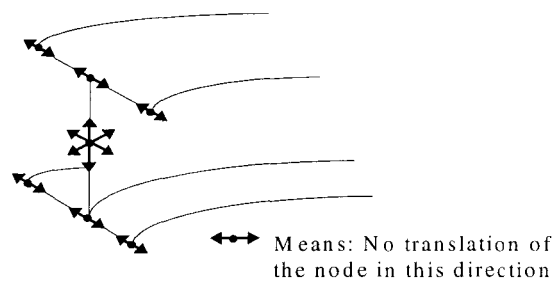


Figure 3.9 Boundary conditions

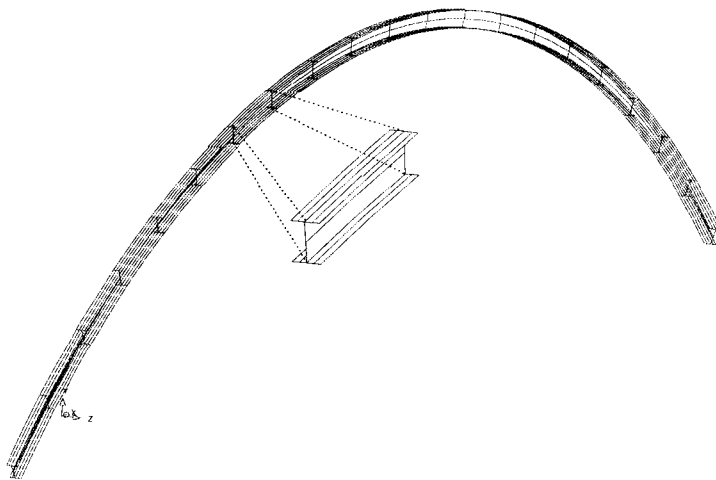
The arch is divided in twenty equidistant parts over its length. Each part consists of ten elements, which is shown in Figure 3.10. These are enough elements to describe the out-of-plane stability; in appendix C.2 the results are given of the investigation to the influence of the number of modelled elements on the results. At the supports beam elements are added to prevent the web and flange from deforming. The beam elements are placed on the edges of the shell elements at the ends of the arch. If these beam elements were not modelled, the Euler buckling load found by DIANA could not be compared to the ones found analytically. The local deformations at the supports affect the Euler buckling load and this does not happen in the analytical model.

3.2.2.3 Results

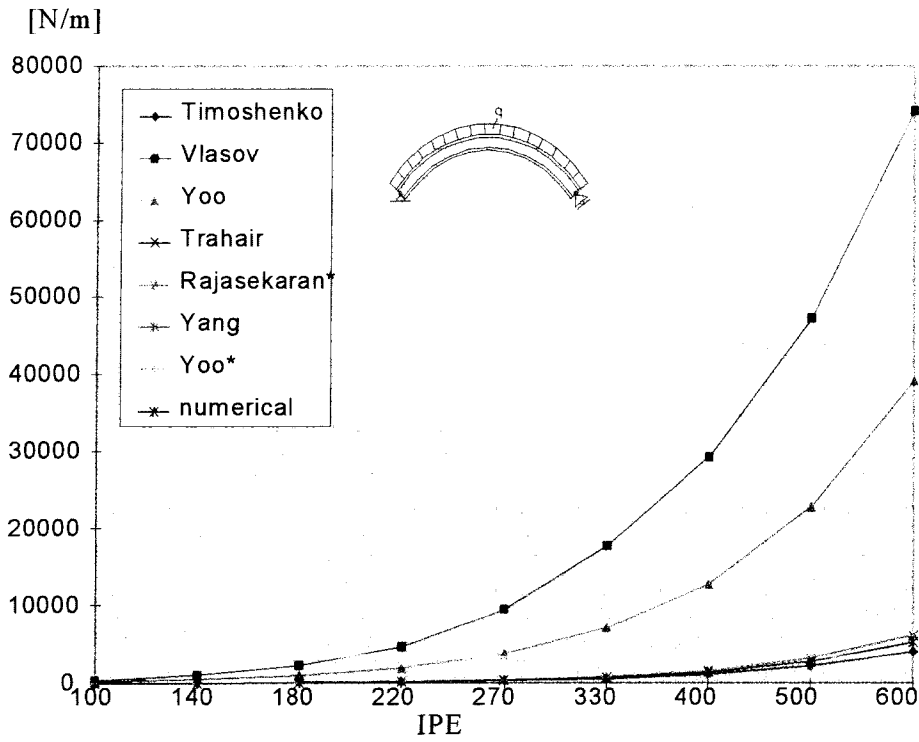
In Table 3.3 the Euler buckling loads are given for the two loadcases. The model with the shell elements takes the effect of warping into account. So these results can be compared to all analytical results except Timoshenko's model.

Table 3.3 Euler buckling loads

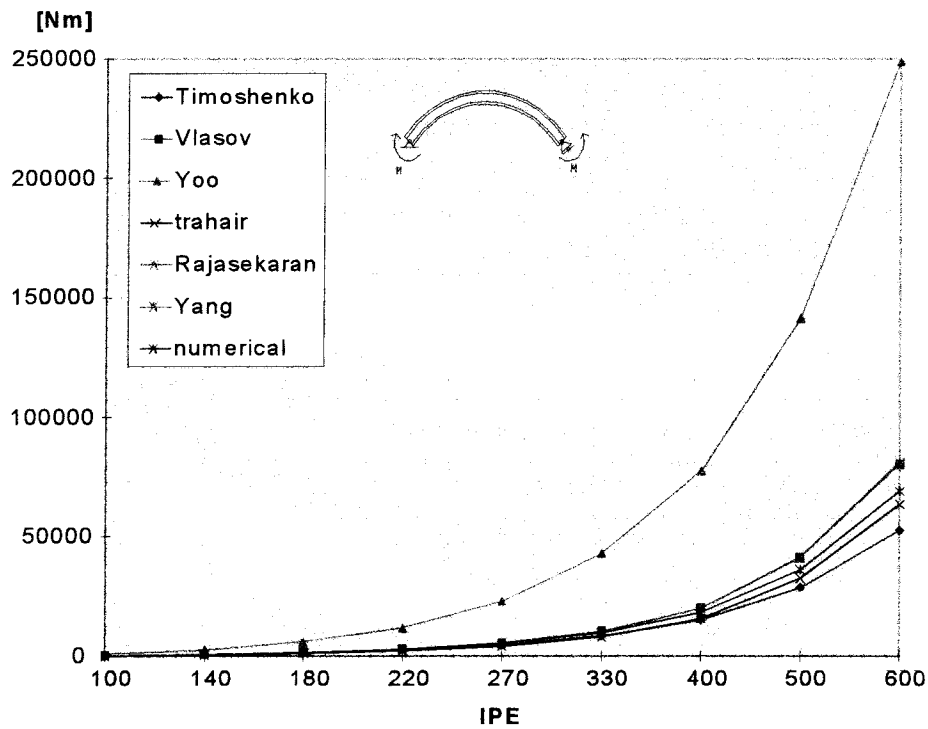
cross section	$Q_{critical}$	$M_{critical}$
IPE100* ¹	27.0 N/m	347 Nm
IPE140*	64.0 N/m	823 Nm
IPE180*	127 N/m	1636 Nm
IPE220*	238 N/m	3055 Nm
IPE270*	424 N/m	5456 Nm
IPE330*	771 N/m	9921 Nm
IPE400*	1437 N/m	18540 Nm
IPE500*	2813 N/m	36340 Nm
IPE600*	5313 N/m	69140 Nm

**Figure 3.10 Model with curved shell elements**

¹ IPE100* refers to a section with shell elements, which resembles as good as possible an IPE100.



a) Uniform compression



b) Uniform bending

Figure 3.12 Analytical and numerical Euler buckling loads (radius 7m, arch length 10m)

3.3 Comparison of analytical and numerical results

To determine the Euler buckling load of an arch under uniform compression or uniform bending, two different methods are used until now. The first one is analytical, by solving the differential equations. The second one is numerical, determining the Euler buckling load with the finite element method DIANA. To see whether the results of the two calculation methods correspond, a comparison has been made. The results are given in Figure 3.12. For the loadcase uniform compression (Figure 3.12a) the results of the model of Vlasov and Yoo are much greater than the numerical results. The results of the other models are all close to the numerical results. The model of Timoshenko is the only model with lower results than the numerical results. For the loadcase uniform bending (Figure 3.12b) Yoo's results are again different from the other ones. This time not only the model of Timoshenko gives lower results than the numerical results but also the model of Trahair.

For further investigation one model should be chosen to work with. The models of Yoo and Vlasov are dropped because their results can not be trusted. The model of Timoshenko is also not a good option because it neglects the warping influence which leads to conservative results. The three remaining models, Trahair, Rajasekaran and Yang, give very corresponding results. When the equations for the Euler buckling load are compared to each other, it is obvious that the equations of Yang are less surveyable than the other equations. There the equations shall be used for a verification it is important to keep them as simple as possible. The models of Trahair and Rajasekaran remain.

In Figure 3.11 the relative differences are given between the numerical and these analytical models. It is striking that for the loadcase uniform compression the differences are greater for arches with a larger profile for both models and for the loadcase uniform bending not. The model of Trahair gives lower results than the numerical one and for larger sections the difference is smaller. It looks like that the model of Trahair contains two differences with an opposite effect. The first one is an underestimation for all sections and the second one is a (smaller) overestimation for larger profiles. The model of Rajasekaran shows a more consistent result, for this reason this model is chosen for in further investigations.

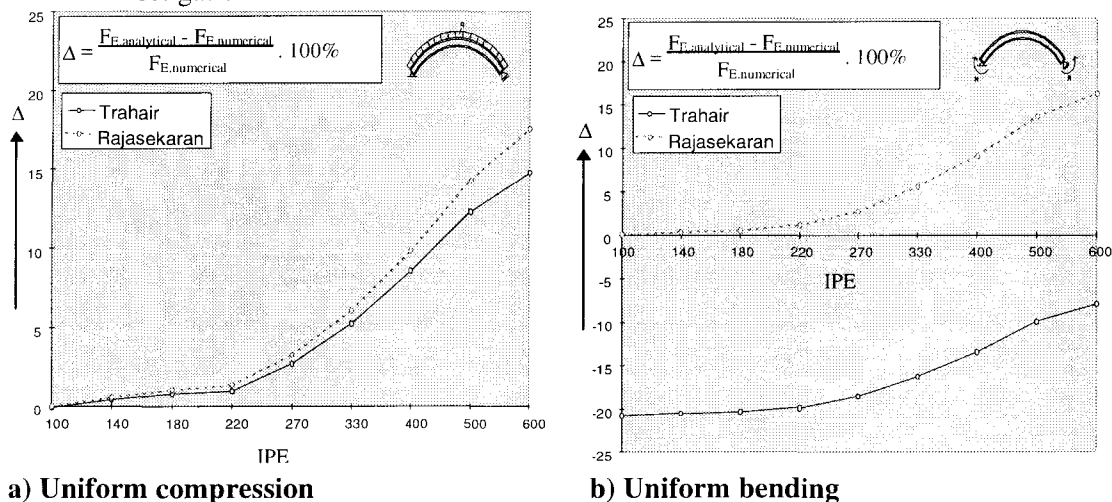


Figure 3.11 Percentage error in Euler buckling load

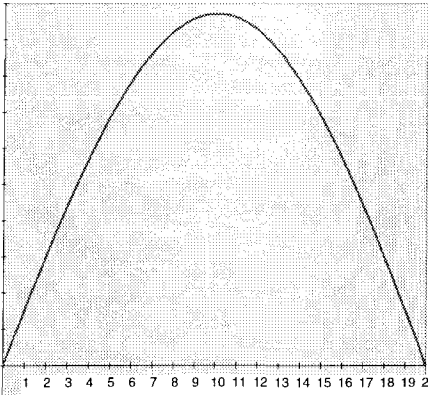
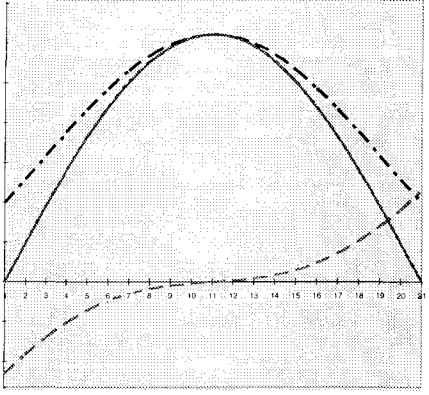
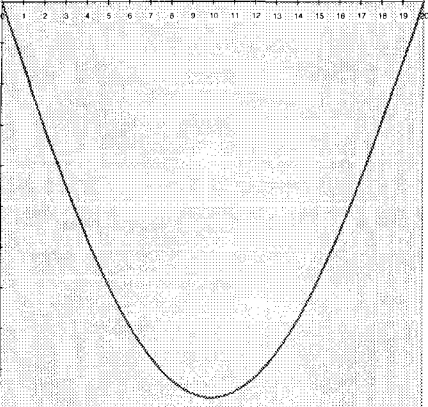
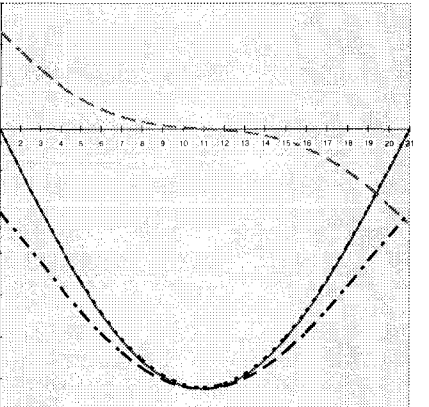
The differences between the analytical model of Rajasekaran and the numerical model are small for arches with a small cross section but for larger cross sections the differences are greater. There must be a reason for this increasing difference between analytical and numerical model. The modelled arches in both methods are exactly the same, therefore the cause of the differences in results must be sought in the calculation method. A possible cause can be the assumed displacement-field in the analytical model. To solve the differential equations of the analytical method, two displacement-fields are assumed. One for the out-of-plane translation and one for the rotation around the axis of the arch. Both displacement-fields are assumed to have a sinus-shape and are just an approximation of the real displacement-fields. When they differ too much from reality, this can be the cause for a discrepancy between analytical and numerical results. To investigate this, the displacements of the numerical model are compared to the sinus shape assumed in the analytical model. Table 3.4 shows graphs for the two cases: uniform compression and uniform bending.

The local out-of-plane displacements are given for the nodes in the neutral axis of the cross section. For both loadcases the displacements hardly differ with the sinus-shape. The local rotation around the x-axis is obtained from the rotation around the global x-axis and global z-axis. As Table 3.4 shows, the resulting local x-rotation is also a sinus-shape.

To assume a sinus-shape for the displacement fields seems a good assumption. The cause of the differences in analytical and numerical results is not found in the displacement fields.

For larger cross sections the difference is significantly greater than for smaller profiles. More stocky arches are more sensible for the influence of warping, this is shown in appendix B.8. No direct cause is found, but this points to a different interpretation of the warping effect in the two models. It is also remarkable that the results of Timoshenko's model and the model with beam elements correspond quite well; both models with no warping effect. This also points to difficulties in the modelling of the warping effect. It can be concluded that both the analytical and the numerical model give reliable results. Only the effect of warping seems not to be interpreted in the same way in the two methods.

Table 3.4 displacement-fields DIANA

IPE500	Displacement in local Z direction	Rotations in global X and Y direction and local X direction
uniform pressure (load-case 1)	 <p data-bbox="399 1008 526 1075"> — DIANA sinus </p>	 <p data-bbox="941 985 1157 1086"> - - - drx - . - drz — rotation local sinus </p>
uniform bending (load-case 2)	 <p data-bbox="399 1635 526 1702"> — DIANA sinus </p>	 <p data-bbox="941 1635 1157 1736"> - - - drx - . - drz — rotation local sinus </p>

4. NON-LINEAR FINITE ELEMENT ANALYSES

In the previous chapter, attention was paid to the Euler buckling load of an arch. This buckling load represents the critical load of a perfect arch, which is obtained by performing a first order elastic analysis. In practice, an arch will not buckle at this load due to simplification in the analysis of the arch. Non-linear FEM analyses are performed in this chapter to find out more precisely how arches behave under uniform bending and uniform compression. With these calculations the real behaviour of an arch is simulated as good as possible. Non-linear analyses include both **physical non-linear** and **geometrical non-linear** behaviour. The arch is also given an **initial imperfection** and **residual stresses**.

The model used for the non-linear analyses is the same model as used to determine the Euler buckling load. For details see paragraph 3.2.2 and appendix C.

Non-linear behaviour, imperfections and residual stresses are discussed in this chapter; not only these aspects themselves but also their influence on the arch behaviour. Next, the results of non-linear analyses are given and the chapter finishes with a definition of the ultimate load.

4.1 Physical and geometrical non-linear behaviour

Physical non-linear behaviour

Three relations between stress and strain are given in Figure 4.1. The relation in Figure 4.1a is used in a physical linear analysis. The relation between stress and strain is always linear and there is no limitation in this model. In reality, the material shows this behaviour only in the beginning of the loading. At a certain value it starts to yield and deformations increase at an increasing rate. Another effect is strain hardening of the material, which occurs after yielding. Successively, linear behaviour, yielding and hardening are presented in Figure 4.1b. This stress-strain relationship comes closest to the real physical behaviour. A schematic bi-linear model of the behaviour used in the non-linear analysis is shown in Figure 4.1c.

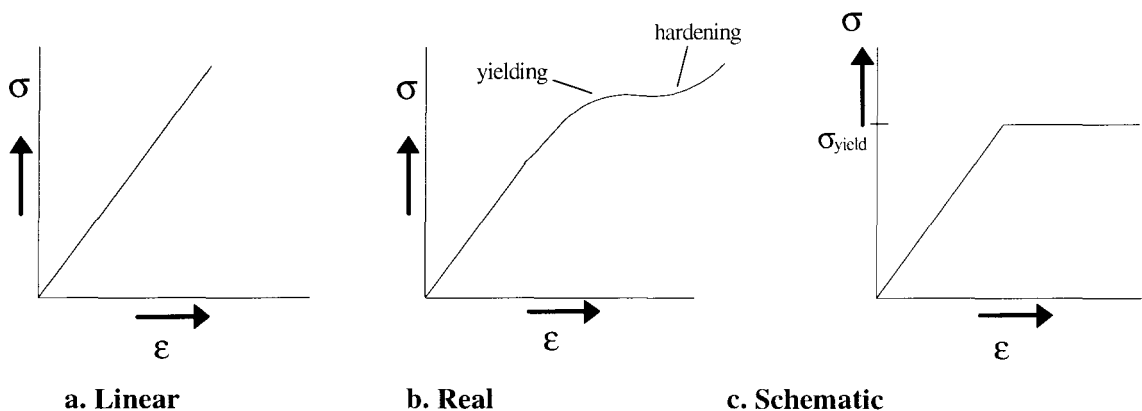


Figure 4.1 stress-strain relation

An arch will deform infinitely with a physical behaviour as in Figure 4.1a. With the behaviour of Figure 4.1c, a plastic hinge is developed when all points in a cross-section yield. When enough plastic hinges are present, the arch will “collapse”. Depending on the iteration method used in the FEM model the calculation will stop at this point or the load will decrease.

Geometrical non-linear behaviour

When geometrical linear behaviour is assumed, the effect of deformations on the stress distribution in the system, is not taken into account. Only for calculations with small deformations, this is a useful model, because small deformations hardly influence the load distribution in the structure. When the deformations are relatively large, the equilibrium should be set up for the deformed shape. Before an arch buckles out-of-its plane the deformations are rather large. These deformations cause an increase of the stresses in the cross section, which again lead to an increase of the deformations. This second order effect causes a reduction of the load that an arch can resist.

4.2 Initial imperfections

4.2.1 Influence of imperfections on the stability of arches

When an arch is manufactured, imperfections are inevitable. In-plane imperfections of the arch, are not important for the out-of-plane stability, as long as they remain small. The imperfections that are important for out-of-plane stability, are the initial displacement out-of-plane and the initial rotation around the plane of the arch. See Figure 4.2. These imperfections facilitate the beginning of the deformation.

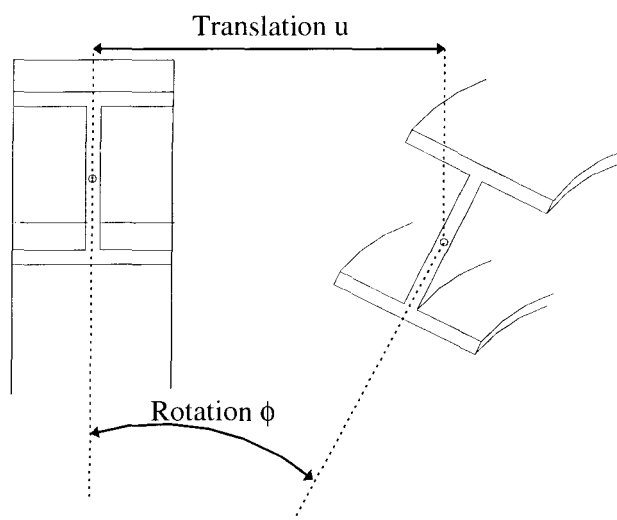


Figure 4.2 Out-of-plane translation and rotation around the longitudinal axis

The influence of the imperfection on the behaviour of the arch can be shown in a load-displacement diagram. Two possible load-displacement diagrams are given for an arch in Figure 4.3. When a perfect arch is loaded, it does not deflect until a certain load. At this value, the buckling load, the arch suddenly deforms largely. This phenomenon is called bifurcation. The original load-

displacement path becomes unstable and the arch will snap to a different path. Figure 4.3a and Figure 4.3b both show a different post-buckling behaviour. For Figure 4.3a counts, when deformations increase without load increasing, the buckling load has been reached. When positive post-buckling is taken into account (as in For Figure 4.3b) the stiffness of the structure will increase with increasing load application thereby reaching a higher load than the buckling load.

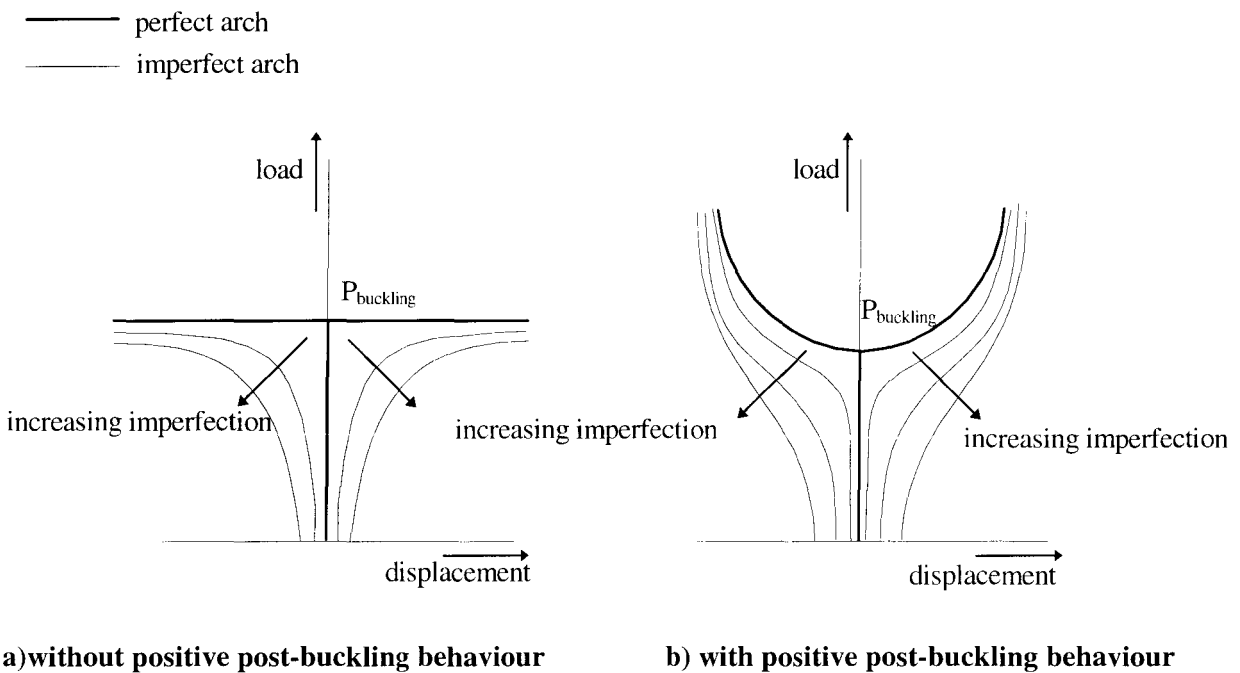


Figure 4.3 Load-displacement diagrams

An imperfect arch will not deform as suddenly as a perfect arch. The deformations grow as the load increases. When the load approaches the critical load, the deformations grow with an increasing rate. This is shown in Figure 4.3. It also shows that the larger the initial imperfection the more the load-deflection path differs with the path of the perfect structure.

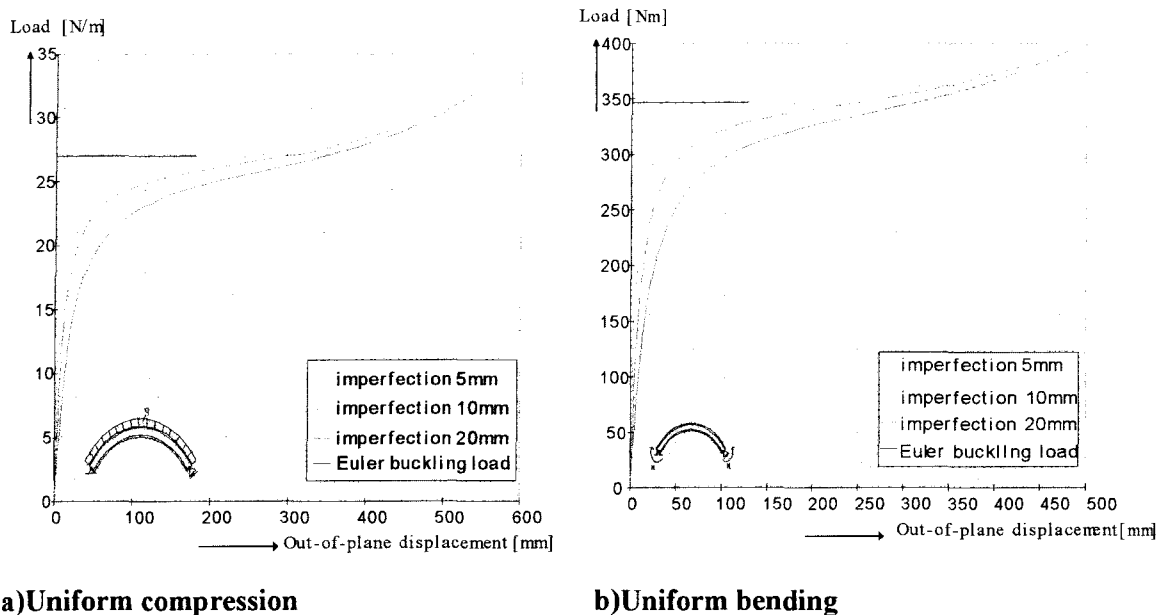
In Figure 4.4 load-displacement diagrams are given for an arch under uniform compression respectively uniform bending. The post-buckling behaviour is positive for both loadcases, because the arch can resist a higher load than the Euler buckling load. The following can be concluded with respect to the influence of the imperfection on the behaviour of the arch: It is clearly shown that the larger the initial imperfection, the more the load-displacement diagram differs from the path of a perfect arch.

4.2.2 Size of the imperfection

When non-linear FEM analyses are performed, a certain imperfection should be given to the arch. To determine a reasonable size for the imperfection, the causes of the imperfections are addressed.

Two possible causes are:

- member imperfection, caused during production
- sway imperfection, caused during assembly



a) Uniform compression

b) Uniform bending

Figure 4.4 Influence of imperfections on the load-displacement diagram

Codes of practice do not provide rules for imperfections of arches. When an arch is considered as a sway frame, the rules for frames can be used as a starting point. An analogy between imperfections of frames and imperfections of arches can be seen in Figure 4.5.

In NEN 6771 10.2.5 rules about imperfections of frames are given. Here two options are presented to introduce imperfections:

- Applying a sway imperfection to the arch combined with residual stresses
- Applying an adjusted sway imperfection to the arch

With the second option, the residual stresses are taken into account by means of an adjusted imperfection. The residual stresses for an arch are not the same as for a frame. So the second option for a frame is not usable for an arch.

For a frame, the sway imperfection is based on practical experience. It is reasonable to assume that an arch can be produced and assembled with the same accuracy as a frame. In that case the sway imperfections can be calculated in the same way.

The sway imperfection ψ can be obtained with the following equation: $\psi = \psi_0 k_1 k_2 \geq \frac{1}{400}$

with: $\psi_0 = \frac{1}{250}$

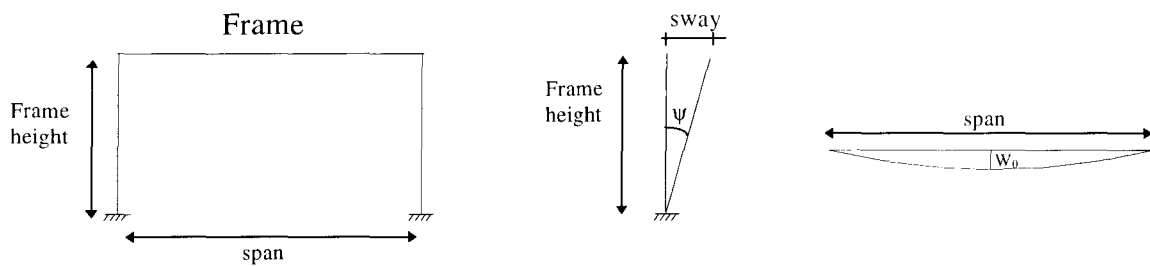
$$k_1 = \sqrt{0.2 + \frac{1}{n_s}} \leq 1 \quad \text{and} \quad k_2 = \sqrt{0.5 + \frac{1}{n_k}} \leq 1$$

n_s is the number of floors of the structure

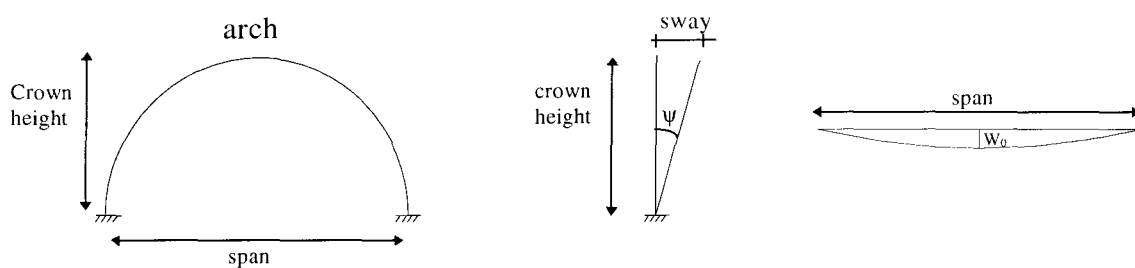
n_k is the number of loaded columns with at least 50% of the average normal force.

For a simple arch, k_1 and k_2 are both equal to 1. This results in an initial imperfection of:

$$\psi = \psi_0 = \frac{1}{250} \geq \frac{1}{400}$$



a) Sway imperfection and member imperfection, frame



b) Sway imperfection and member imperfection, arch

Figure 4.5 Analogy between frame and arch

It is possible, for an arch, that the size of the member imperfection is larger than the sway imperfection. This is because the member imperfection is related to the span of the arch, instead of the crown height of the arch. See Figure 4.5. For this reason both imperfections are determined and the largest one is applied.

Like for a beam, member imperfection is held to $\frac{1}{1000}$ of the span.

In the FEM calculations, the initial imperfection is applied with the help of an Euler analysis. With this calculation the buckling shape of the arch is determined. Afterwards the maximum deformation is scaled to the initial imperfection required.

4.3 Residual stresses

After production, residual stresses remain in the cross-section of the arch. Due to the existence of these stresses, the arch can carry a smaller load than expected. The yield stress is reached at a smaller load, so plasticity is sooner developed and the arch will collapse under a smaller load. For physical non-linear analyses, the size and the distribution of the residual stresses in the cross-section should be known.

In NEN 6771 prescriptions are given about the size and the distribution of residual stresses in a hot-rolled I-section. To produce an arch, a beam with an I-section is bent, which affects the residual stresses.

So the residual stresses which should be introduced in arch analyses are not the same as for straight beams.

To obtain an arch, a straight beam is bent till it deforms plastically. The stresses in the cross-section in this phase are shown in Figure 4.6a. In the next phase, the arch is unloaded, this happens elastically. Figure 4.6b gives the stresses in the cross-section for this process. Figure 4.6c gives stresses after manufacturing of the arch.

The same bending moment, which is applied to the beam to produce an arch, is removed in the second phase.

With this information σ_{res} can be determined and next the residual stresses.

$$\text{Phase a:} \quad M = W_{pl} f_y$$

$$\text{Phase b:} \quad M = W_{el} \sigma_{res} \Rightarrow \sigma_{res} = \frac{W_{pl}}{W_{el}} f_y$$

For example for the standard arch with IPE100* this is:

$$\begin{aligned} W_{pl} &= 38678 \text{ mm}^3 \\ W_{el} &= 35640 \text{ mm}^3 \text{ and} \\ f_y &= 235 \text{ N/mm}^2 \end{aligned} \quad \Rightarrow \quad \sigma_{res} = 255 \text{ N/mm}^2$$

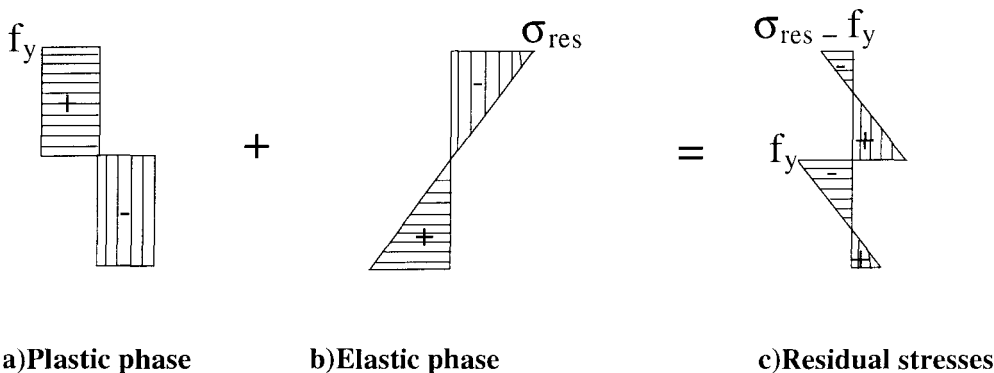


Figure 4.6 Stresses in cross-section

The residual stresses in Figure 4.6c are introduced in the web of the I-section in the FEM model. This is done by applying the stresses in the nodes of the elements. See Figure 4.7. The interpolation of the stresses between the nodes is linear. Which corresponds with Figure 4.6c. The residual stresses in the flanges are constant and have the value of the stress in the top respectively the bottom of the web.

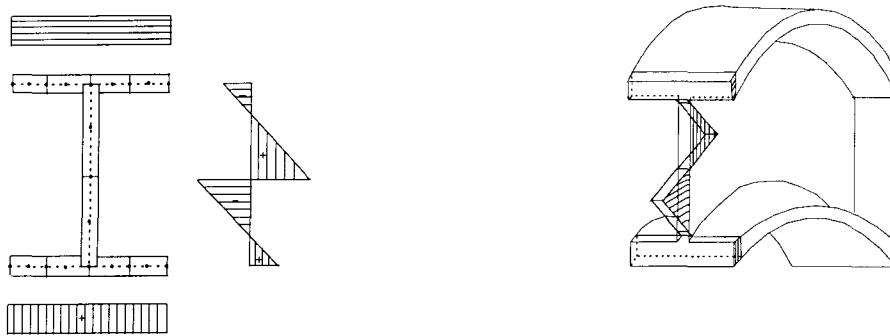


Figure 4.7 Residual stresses in FEM model

4.3.1 Influence of residual stresses

In Figure 4.8 a plot is given of two load-displacement lines for an arch under uniform compression. One line represents an arch with residual stresses and the other line represents an arch without residual stresses. The difference between the two lines is very small. When the arch deforms elastically, no difference can be distinguished between the two lines. Just for the part where plasticity occurs in the arch, the deformations of the arch with residual stresses are larger.

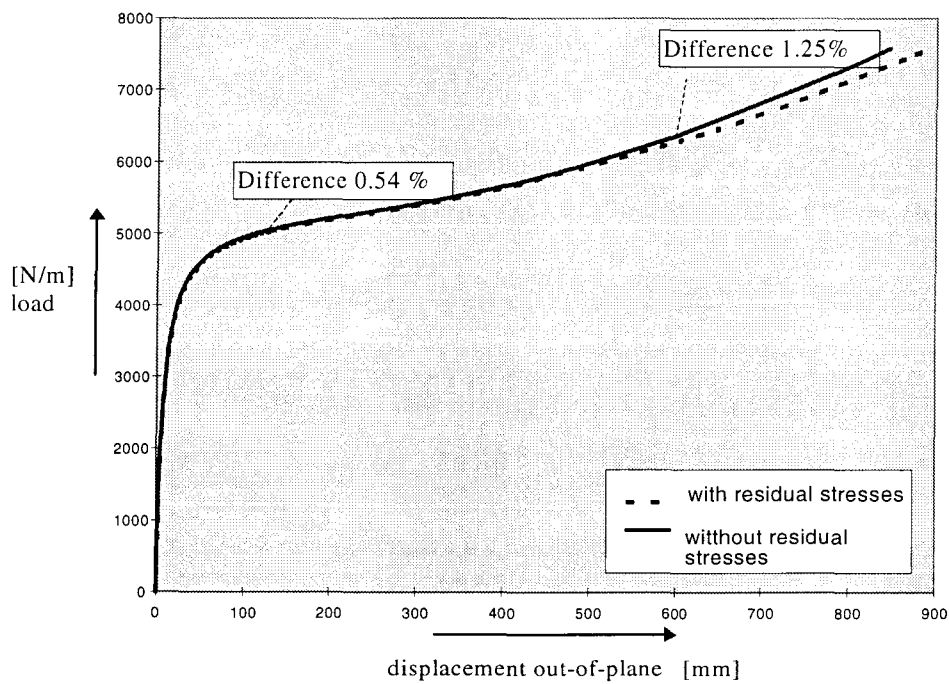


Figure 4.8 Influence of residual stresses on load-displacement curve

4.4 Results

In Figure 4.9, two general load-displacement diagrams are given. The first one describes the out-of-plane displacement at the top of an arch, with a positive post-buckling behaviour and the second one without a positive post-buckling behaviour. Both behaviours are found for arches which buckle out-of-their planes. Slender arches deform as shown in Figure 4.9a, stocky arches as shown in Figure 4.9b. The more slender the arch, the more the load increases after the point of contraflexure.

The arches which have been studied are presented in appendix D. The cross-section, arclength and radius of the arch are varied, to investigate arches with different characteristics. The load-displacement diagrams are also given in appendix D as well as some numerical data.

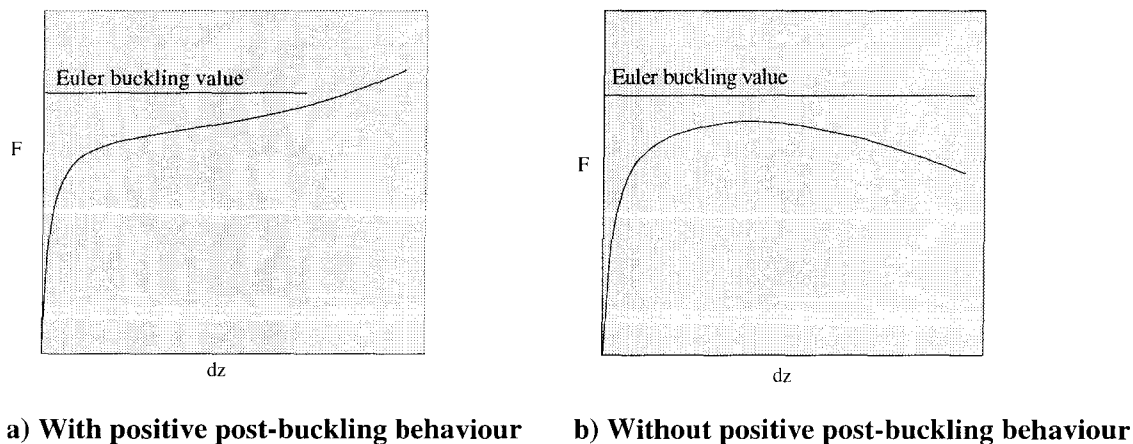


Figure 4.9 Load-displacement diagrams

Whether an arch has a positive post-buckling behaviour or not, depends on the geometry and the cross section of the arch. A slender arch deforms largely before it reaches the Euler buckling load. Due to these large deformations, the force transmission in the arch is affected, which may result in a positive post-buckling behaviour. Another item is the out-of-plane strength of the arch. When the arch stands no longer in its original plane, the load does not act any longer along the weak axis. See Figure 4.10. In this situation, the strength about the strong axis contributes also to the out-of-plane strength of the arch. These two effects are responsible for the positive post-buckling behaviour.

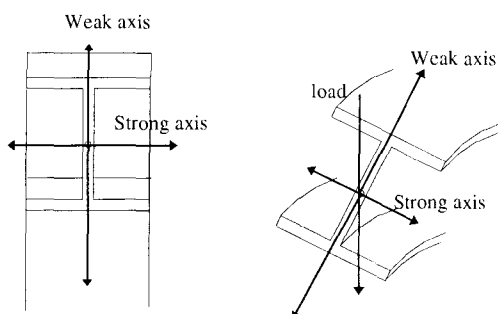


Figure 4.10 Rotation of the axes

4.5 Ultimate load

The purpose of performing a non-linear FEM analysis is to find the ultimate load carrying capacity of an arch. When the shape of the load-displacement diagram corresponds to line 1 in Figure 4.11, it is clear that the top of the curve indicates the ultimate load. At this load the arch loses its stability. But most arches do not normally have such a load-displacement diagram. Due to positive post-buckling behaviour, the curve often has the shape of line 2 in Figure 4.11. Here, the ultimate load is not easy to determine. The arch does not lose its stability and failure of the arch occurs for very large deformations. What is in this case the ultimate load?

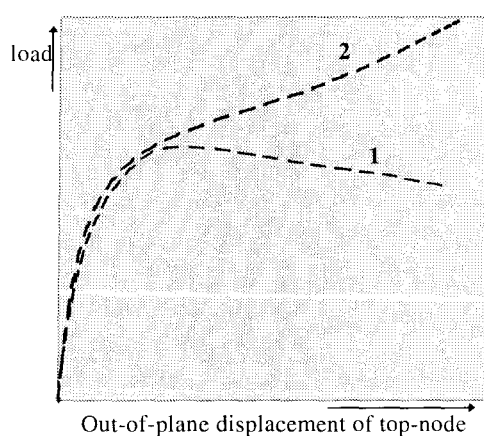


Figure 4.11 Possible load-displacement curves

In Eurocode 1 a general description of the ultimate limit state is given:

The ultimate limit state concerns in almost all cases the first passage of a limit state that is equivalent with failure.

According to Eurocode 1, the ultimate limit state includes:

- loss of equilibrium of the structure or a part of the structure, considered as a rigid body;
- attainment of the maximum resistance capacity of sections, members or connections by rupture or **excessive deformations**;
- transformation of the structure or part of it in a mechanism;
- instability of the structure or a part of it;
- sudden change of the assumed structural system to a new system (e.g. snap through).

Arches with a high slenderness can deform excessively before they collapse as shown in Figure 4.12 for an arch under uniform compression. The deformations are so large that the top of the arch nearly reaches ground level. It is difficult to determine the ultimate load for this type of failure. There is no clear point of loading from where deformations grow excessively. Therefore five options for the ultimate load are suggested and evaluated in this paragraph.

Five options for the ultimate load:

- I. ultimate strength;
- II. critical buckling load;
- III. intersection point of two linear parts;
- IV. point of contraflexure or top in load-displacement diagram;
- V. maximum deformation.

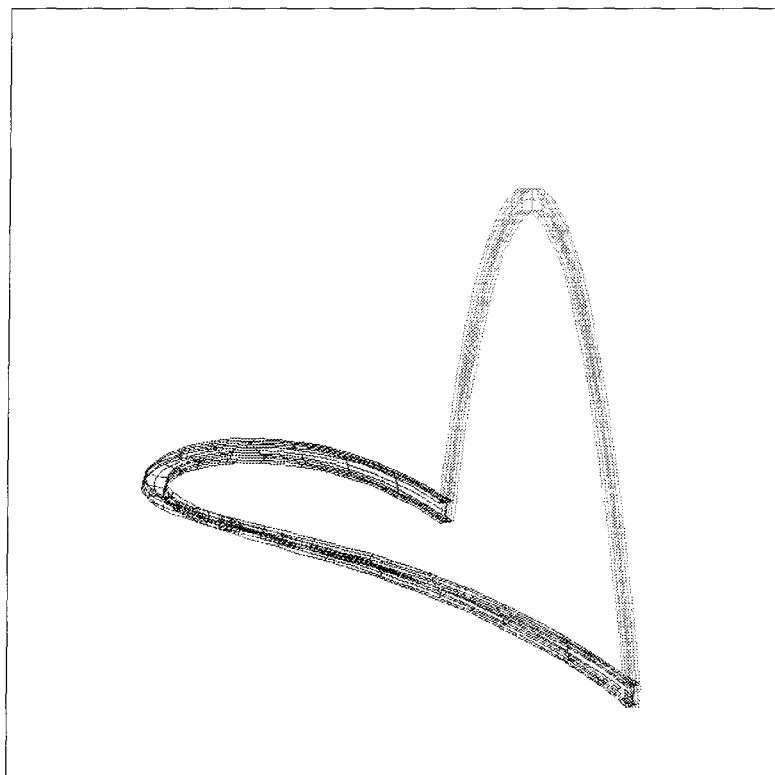


Figure 4.12 Extremely deformed arch

I. Ultimate strength

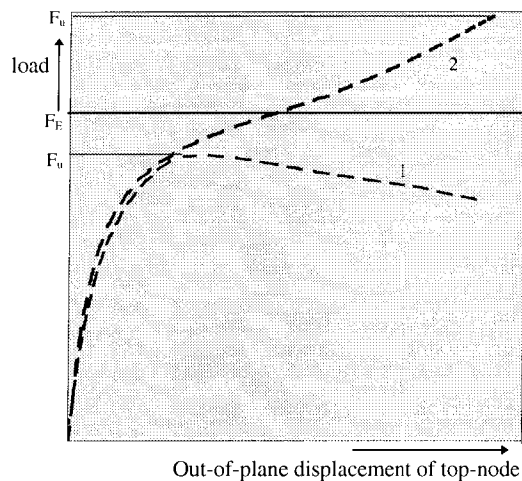


Figure 4.13 Ultimate load according option I

The ultimate strength corresponds with the load which causes real collapse of the arch. Slender arches have a positive post-buckling behaviour, which leads to a very high ultimate strength. In Figure 4.13 this is shown by line 2. For stocky arches no positive post-buckling behaviour occurs. These arches will buckle at much lower loads, which is shown by line 1 in Figure 4.13. The deformations in combination with the ultimate strength, can be extremely large for slender arches as can be seen in Figure 4.12. These large deformations are the reason why the ultimate strength is not a good option for the ultimate load of an arch.

II. Euler buckling load

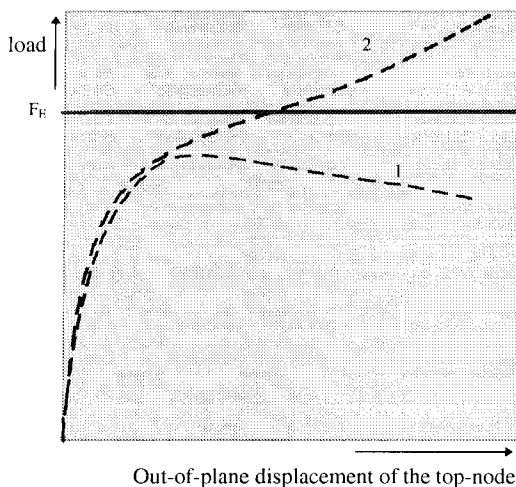


Figure 4.14 Ultimate load according option II

The second option for the ultimate load is the Euler buckling load. Compared to the ultimate strength, the deformations are mostly smaller at the Euler buckling load. Using the Euler buckling load, is a possible way to restrict the deformations. This option has nevertheless a drawback. For arches without a positive post-buckling behaviour, the Euler buckling load is higher than the ultimate strength. When the Euler buckling load is used as ultimate load for such arches it can lead to unsafe situations. See Figure 4.14. So the Euler buckling load is not a good option. Either it will lead to an unsafe situation or the ultimate load can not be determined in the same way for arches with or without a positive post-buckling behaviour.

III. Intersection point of two linear parts

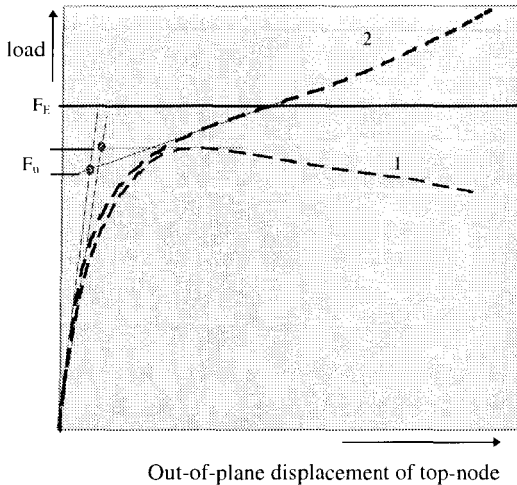


Figure 4.15 Ultimate load according option III

To restrict the deformations even more, a third option is proposed for the ultimate load. The intersection of the line that represents the linear deformation and the tangent of the load-displacement line in the point of contraflexure respectively the top. As can be seen in Figure 4.15 the deformations for this option are small compared to the deformations of the other options. Both for slender and stocky arches the same method can be used to determine the ultimate load. It should be noted that for this option the ultimate load for the arch with a positive post-buckling behaviour is smaller than for the arch without a positive post-buckling behaviour.

IV. Contraflexure point or top in load-displacement diagram

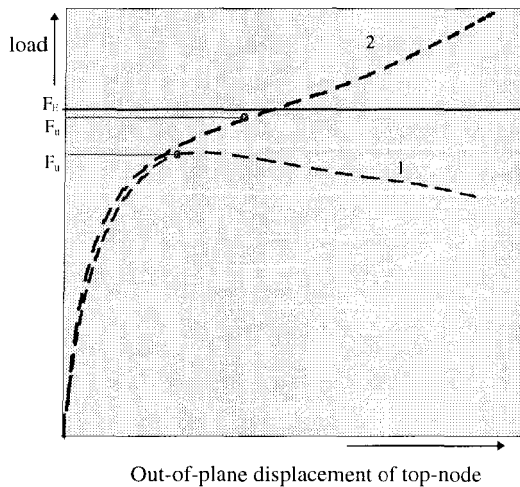


Figure 4.16 Ultimate load according option IV

The fourth option is using the point of contraflexure or the top in the load-displacement diagram, as ultimate load. A more mathematical definition of this point is:

$$\min \left| \frac{d(\text{load})}{d(\text{displ. top-node})} \right|$$
 . See Figure 4.16.

The ultimate load can be determined in the same way for slender and stocky arches. For slender arches the derivative of the load-displacement diagram has a minimum in the point of contra-flexure. For stocky arches the derivative of the load-displacement diagram has an absolute minimum of zero, the top of the diagram.

For this option of the ultimate load, the displacements are in control and for both types

of arches, it leads to safe situations. Another advantage of this option is that the arch gets another behaviour starting in the point of contra-flexure: influence of the stiffness of the strong-axis starts. So the point of contra-flexure has also a physical meaning. Also, the resulting load-displacement diagrams reflect real behaviour: for slender arches larger displacements and a greater load are allowed than for stocky arches.

V. Maximum deformation

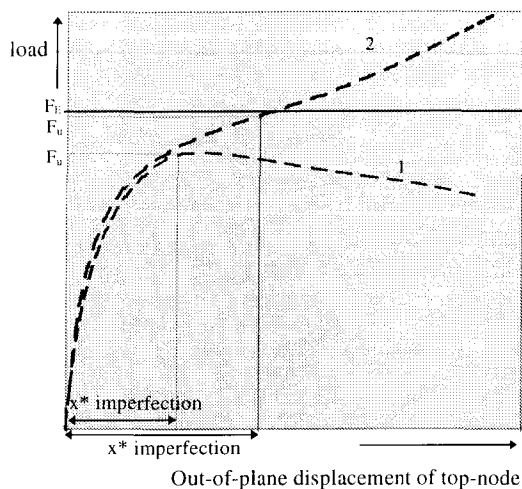


Figure 4.17 Ultimate load according option V

The final option for the ultimate load is related to the deformation of the arch. When the out-of-plane deformation is directly connected to the ultimate load, the deformation can be controlled. See Figure 4.17. But how should the maximum allowable deformation be determined? When the maximum out-of-plane displacement is related to the imperfection, the maximum displacement is indirectly connected to the dimensions of the arch. To obtain a similar ultimate load for stocky and slender arches, the deformation for the ultimate load of a stocky arch should be the directive for the maximum deformation. For two stocky arches the displacement of the top-node is determined for the ultimate load. (See Table 4.1) The factor with which the initial imperfection is multiplied to get

the top-node displacement is given in the last column. When these factors are plotted in a diagram against slenderness, a trendline could be drawn through these points, see Figure 4.18.

For a large slenderness the factor, $\frac{\text{maximum displacement}}{\text{initial imperfection}}$ is extremely high when this trendline is used as a measure for the maximum displacement. Related to the slenderness it is not possible to determine a factor for the maximum displacement. It is also impossible to take one of the factors of the calculated arches. For more stocky arches this will lead to an unsafe situation and for more slender arches, the permitted displacement is relatively small.

Therefore, it is impossible to give a good guide for the maximum displacement and the option to use the load reached for a maximum deformation as ultimate load, is not a good option.

Table 4.1 Multiplication factor

slenderness	initial imperfection	displacement of top-node	factor
1.12	1.25 mm	3.75 mm	3.00
2.72	2.49 mm	30 mm	12.05

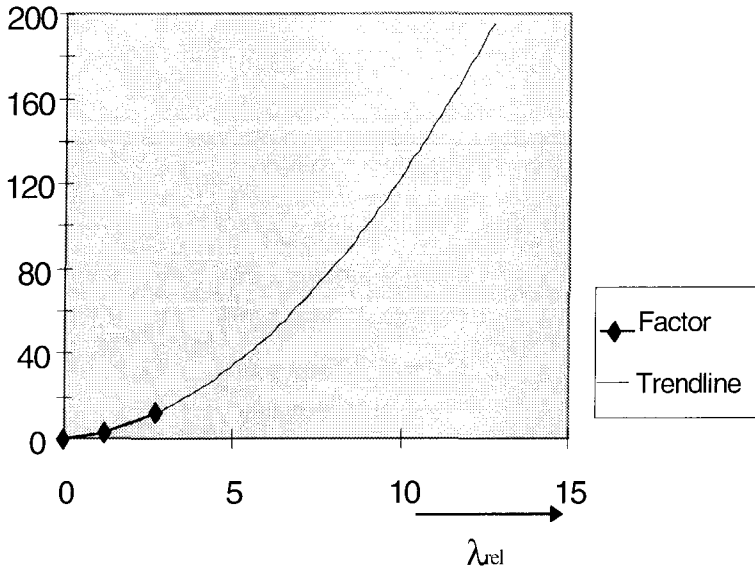


Figure 4.18 Multiplication factors with trendline

It can be stated that only two applicable options for the ultimate load are left. These two options are:

- option III, intersection point of two linear parts;
- option IV, point of contraflexure/top in the load-displacement diagram.

These two options are looked at more closely.

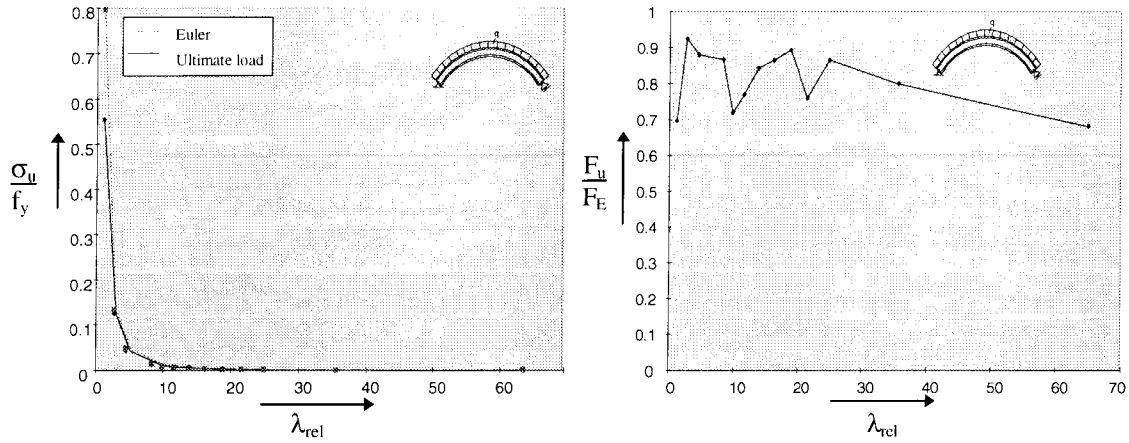
Option III, intersection point of two linear parts

To get an idea of the course of the ultimate load according to this option, results are plotted in a diagram together with the Euler hyperbola. On the y-axis in Figure 4.19a the ultimate load divided by the area of the cross-section, is shown related to the yield strength (σ_{cv}/f_y). On the x-axis the relative slenderness is given.

The relative slenderness λ_{rel} is defined as $\sqrt{\frac{N_{pl,d}}{N_{Euler}}}$.

In Figure 4.19a ultimate loads and the Euler hyperbola are plotted for a range of arches with a different slenderness. The course of the two curves is very similar, especially for a large slenderness. Only for stocky arches the difference between the hyperbola and the ultimate loads is significant. To see the difference more clearly, the ultimate loads are divided by the Euler values and are printed in Figure 4.19b. The line fluctuates significantly. The fluctuations can be explained by the difficulty in defining the beginning and ending of the two linear parts. In Figure 4.15 it can be seen that it is not obvious where the lines should be drawn for a slender arch.

This is a drawback of this option for the ultimate load; the ultimate load is not clearly defined.



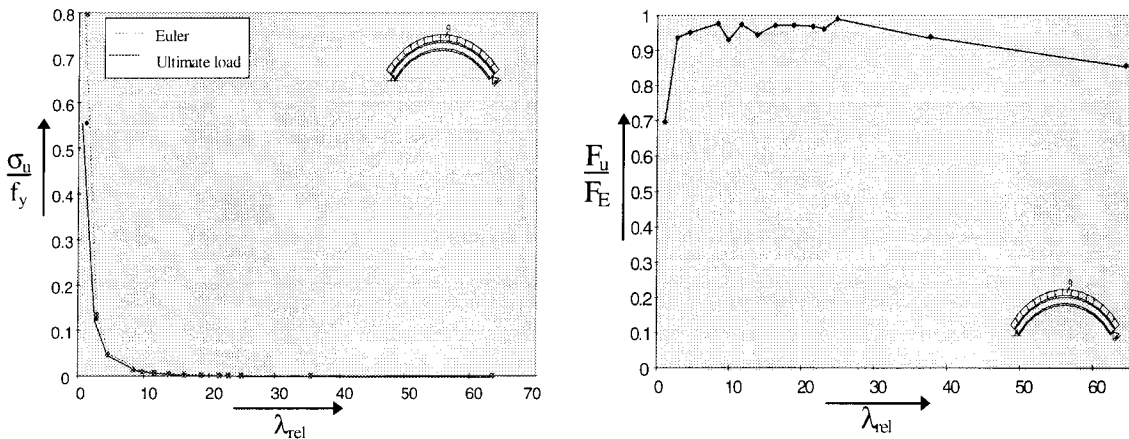
a) Ultimate load and Euler hyperbola

b) Relative ultimate load

Figure 4.19 Ultimate load (option III) as function of relative slenderness

Option IV point of contraflexure/top of load-displacement diagram

For the ultimate load defined as point of contraflexure or top in the load-displacement diagram, the same diagrams are given: in Figure 4.20a the dimensionless ultimate loads and the Euler hyperbola are shown and in Figure 4.20b the relative ultimate loads are given. Figure 4.20a resembles Figure 4.19a. The ultimate loads almost coincide with the Euler hyperbola, only for arches with a small slenderness the loads do differ. The relative ultimate loads in Figure 4.20b show fewer fluctuations than the relative ultimate loads in Figure 4.19b. The two arches with the smallest slenderness do not have a positive post-buckling behaviour and their ultimate load is smaller than the Euler load. The first part of the diagram can be explained by this. The remaining ten arches have a ultimate load very close to the Euler load, which is expected because the point of contraflexure is close to the Euler buckling load.



a) Ultimate load and Euler hyperbola

b) Relative ultimate load

Figure 4.20 Ultimate load (option IV) as a function of relative slenderness

Comparison between option III and option IV:

- The curves for the ultimate load over a wide slenderness range is similar for both the options.
- The fluctuations in option IV are smaller than in option III.
- Option IV is better defined than option III.
- Option IV has a physical meaning and option III does not have a physical meaning.

The point of contraflexure or top is the best option for the ultimate load because these points are clearly defined and have a physical meaning.

5. VERIFICATION METHODS

The purpose of this research is to provide a verification method with which a certain safety is obtained against out-of-plane buckling of arches. This safety is reached when the design load is smaller than the design strength of the arch. The introduction of material factors and load factors leads to the required safety. It is not desirable to perform a non-linear DIANA analysis, to determine the ultimate strength, each time an arch has to be verified. A first order linear calculation should be sufficient. The Euler buckling load is a result of such a calculation and is rather easy to determine. If the relationship between the ultimate load and the Euler buckling load is known, a verification can be determined, which is practical in use.

The objective is to make the verification correspond with the existing codes. Therefore this chapter starts with a discussion on the verification of buckling of columns and beams. After this, a verification for out-of-plane buckling of arches is proposed, which is checked with non-linear DIANA analyses. The chapter finishes with a comparison between the proposed verification method and other methods for out-of-plane buckling of arches.

5.1 Stability check for columns and beams

Three main cases are distinguished for the verification of stability of columns and beams: columns under compression, beams under bending and beam-columns under compression combined with bending. For all verification methods, the base is the same: the design load is compared to the capacity of the cross section and a buckling factor is introduced to take into account the effects of residual stresses, imperfections and second order behaviour.

Stability check for columns under uniform compression according to NEN 6770 art.12.1.1:

$$\frac{N_{c.s.d}}{\omega_{buc} N_{c.u.d}} \leq 1$$

$N_{c.s.d}$ is the design value of the compressive force

$N_{c.u.d}$ is the design plastic resistance of the cross section

ω_{buc} is the buckling factor, which describes the relationship between the buckling capacity and the design plastic resistance of the cross section.

Stability check for beams under uniform bending according to NEN 6770 art. 12.2.2:

$$\frac{M_{y,max.s.d}}{\omega_{kip} M_{y.u.d}} \leq 1$$

$M_{y,max.s.d}$ is the design value of the maximum bending moment

$M_{y.u.d}$ is the design plastic resistance moment of the cross section

ω_{kip} is the buckling factor for lateral torsional buckling, which describes the relationship between the buckling capacity and the design plastic resistance of the cross section.

Verification of beam-columns under a compressive force and a bending moment according to NEN 6770 art. 12.3.1.2:

$$1.1 \frac{N_{c.s.d}}{\omega_{buc} N_{c.u.d}} + 1.1 \frac{M_{y,max.s.d}}{\omega_{kip} M_{y,u.d}} \leq 1$$

The buckling factor represents the relation between the buckling capacity and the design plastic resistance of the cross section. This relation is based on numerous buckling tests on columns. With the Perry-Robertson Formula this relation can also be determined analytically and presented in a formula. If the relative slenderness and the column section are known, the buckling factor can be calculated with the following equation:

$$\omega_{buc} = \frac{1 + \alpha_k (\lambda_{rel} - \lambda_0) + \lambda_{rel}^2}{2\lambda_{rel}^2} - \frac{1}{2\lambda_{rel}^2} \sqrt{(1 + \alpha_k (\lambda_{rel} - \lambda_0) + \lambda_{rel}^2)^2 - 4\lambda_{rel}^2}$$

λ_{rel} is the relative slenderness of the column

λ_0 is a slenderness factor

α_k is a factor depending on the type of the column section

The relationship between buckling capacity and the design plastic resistance of the cross section can also be presented graphically by so-called buckling curves, which are given in appendix A.2. The value of λ_0 is constant and for α_k four values are available depending on the type and size of the cross-section and of instability with respect to the weak or strong axis of the cross-section.

The buckling factor is given as a function of the relative slenderness. The relative slenderness is defined as:

$$\lambda_{rel} = \sqrt{\frac{N_{pl,d}}{F_{y,E}}} = \sqrt{\frac{l_{buc}^2 f_{y,d} A}{\pi^2 EI}} = \frac{l_{y,buc}}{i_y \pi} \sqrt{\frac{E_d}{f_{y,d}}}$$

The relative slenderness depends on the length and boundary conditions of the column ($l_{y,buc}$), the cross-section (i_y) and material characteristics (E_d and $f_{y,d}$).

For more details about the verification for column stability, reference is made to NEN 6770 and NEN 6771. The verification in NEN 6771 is not based on a buckling factor, but on an imperfection parameter in which effects of residual stresses and initial imperfections have been taken into account.

5.2 Out-of-plane stability of arches

5.2.1 Stability check

In this investigation on out-of-plane buckling of arches, two load cases are considered: uniform compression and uniform bending. For both loadcases a stability check is required. The basis of the checking equations for columns can also be used for arches. An essential part in the stability check is the buckling factor, which describes the relationship between the buckling capacity and the design plastic resistance of the cross section. This buckling factor has to be determined for arches.

Previous research on in-plane buckling of arches [1] has shown that the buckling curves for columns are also applicable for in-plane buckling of arches. This leads to the conclusion that the influence of residual stresses and imperfections on the in-plane strength of arches is of the same order of magnitude as for columns. With this in mind, the applicability of the column buckling curves for out-of-plane strength of arches, will be checked.

The column buckling curves represent the buckling factors as a function of the relative slenderness of the column. For arches a relative slenderness can be defined in the same way as for columns,

using the definition $\lambda_{rel} = \sqrt{\frac{N_{pl,d}}{F_{y,E}}}$.

The relative slenderness of a column can be rewritten into a form in which only geometry and material factors are present. In the case of arches such a simplification is not possible and not necessary.

To determine the relative slenderness of an arch the Euler buckling load must be known. In chapter 3 two methods are presented to obtain this load: analytical and numerical.

The analytical method provides in a simple way a good approach of the Euler buckling load, which is very useful for the verification method. The non-linear analysis with which the verification method is checked, is based on the same model as the model with which the numerical Euler buckling load is determined. When an analytical model is used for the verification the analytical Euler buckling load may not be larger than the numerical Euler buckling load.

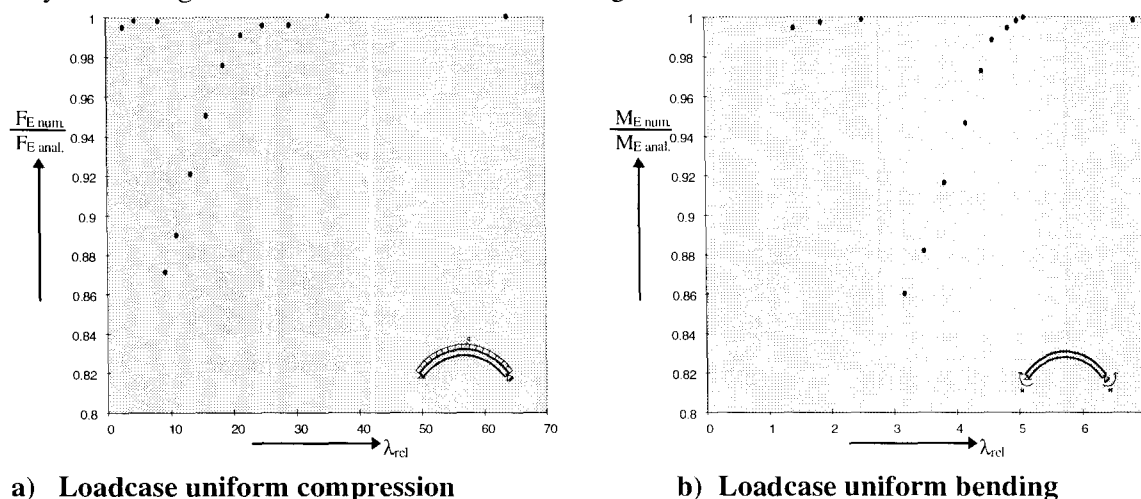
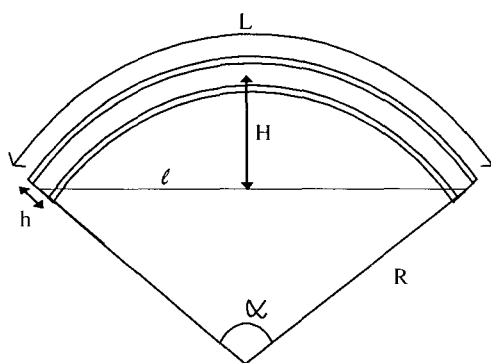


Figure 5.1 Ratio of numerical and analytical Euler buckling loads

The analytical model of Rajasekaran turned out to be the most appropriate to use as explained in chapter 3. The Euler buckling load of this model is however not always smaller than the numerical Euler buckling load. Therefore a reduction factor β_{red} is introduced to reduce the analytical load to the numerical load.

In Figure 5.1 the ratio of the results of two calculation methods is given. The data of the arch with the smallest slenderness is not used in this figure, because it is sensitive for snap-through buckling and behaves therefore differently. The difference between the two calculation methods depends not on the relative slenderness as can be seen in Figure 5.1, but rather on the depth of the cross section. When the depth of cross section is higher the difference between the two methods is larger. The length of the arch has less influence. Based on these observations a term is found which can describe the difference between the two calculation methods.



The term $\frac{H h}{L l}$ describes this relation well.

With:

- H is the crown-height of the arch
- h is the depth of section
- L is the length of the arch
- l is the span of arch

In Figure 5.2 is indicated what the different parameters are.

Figure 5.2 Parameters

In Figure 5.3 the ratio's of the numerical Euler buckling load and the analytical Euler buckling load are given related to $\frac{H h}{L l}$. Together with these values, a line is given which represents the reduction factor. The reduction factor is defined as:

$$\beta_{\text{red}} = \begin{cases} 1 & \text{if } \frac{H h}{L l} \leq 0.25 \\ 1.05 - 0.2 \frac{H h}{L l} & \text{if } \frac{H h}{L l} > 0.25 \end{cases}$$

The analytical Euler buckling load should be multiplied by β_{red} to obtain a safe approach of the Euler buckling load of an arch.

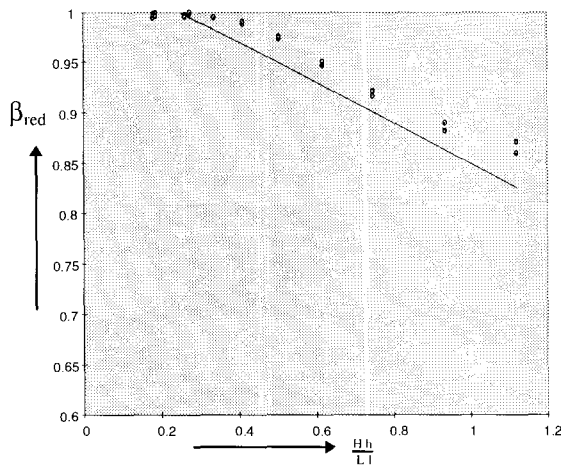


Figure 5.3 Reduction factor

Two checking equations for the out-of-plane stability of arches are proposed in this paragraph. One concerns out-of-plane buckling of circular arches under uniform compression. The other concerns out-of-plane buckling of circular arches under uniform bending.

The stability check for arches subjected to uniform compression:

$$\frac{N_{c.s.d}}{\omega_{arch.out} N_{c.u.d}} \leq 1$$

- $N_{c.s.d}$ design value of the compressive force
- $N_{c.u.d}$ design plastic resistance to compression of the cross section
- $\omega_{arch.out}$ buckling factor for out-of-plane buckling of arches

The stability check for arches subjected to uniform bending:

$$\frac{M_{y.s.max.d}}{\omega_{arch.out} M_{y.u.d}} \leq 1$$

- $M_{y.s.max.d}$ design value of the bending moment
- $M_{y.u.d}$ design plastic resistance to bending of the cross section
- $\omega_{arch.out}$ buckling factor for out-of-plane buckling of arches

The buckling factor for out-of-plane buckling of arches can be obtained from the diagrams given in appendix [A.2]. For rolled sections and circular hollow sections, buckling curve a shall be used. The choice of these curves is based on the use of the curves for columns.

The relative slenderness must be known, in order to obtain the buckling factor.

For arches under uniform compression, the relative slenderness is given by: $\lambda_{rel} = \sqrt{\frac{N_{c,u,d}}{F_{y,E}}}$

For arches under uniform bending, the relative slenderness is given by: $\lambda_{rel} = \sqrt{\frac{M_{c,u,d}}{M_E}}$

in which

$N_{c,u,d}$ is the design plastic resistance to compression of the cross section

$M_{c,u,d}$ is the design plastic resistance to bending of the cross section

$F_{y,E}$ is the Euler buckling load for uniform compression based on the model of Rajasekaran [12]

M_E is the Euler buckling load for uniform bending based on the model of Rajasekaran[12]

$$F_{y,E} = \beta_{red} \frac{M_0}{R^2} \left(\frac{b/a(a^2 - 1)^2}{a^2 + b^2} \right)$$

$$M_E = \beta_{red} M_0 \left(-\frac{a}{b} - \frac{ab}{2} + \sqrt{\left(\frac{a}{b} + \frac{ab}{2} \right)^2 + 1 - a^2} \right)$$

with:

L, H, l and R according to Figure 5.4

$$a = \frac{L}{\pi R} \quad b = \frac{\pi M_0}{P_z L}$$

$$P_z = \frac{\pi^2 EI_z}{L^2} \quad M_0 = \sqrt{P_z \left(GJ + \frac{\pi^2 EI_w}{L^2} \right)}$$

$$\beta_{red} = 1 \quad \text{if } \frac{H h}{L l} \leq 0.25$$

$$= 1.05 - 0.2 \frac{H h}{L l} \quad \text{if } \frac{H h}{L l} > 0.25$$

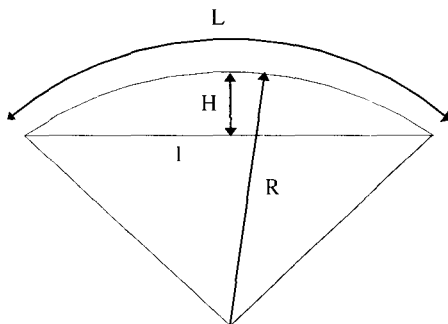


Figure 5.4 Parameters of the arch

5.2.2 Check of the verification method

In this paragraph, the proposed verification method for out-of-plane buckling of arches is verified. For a range of arches, the ultimate load has been determined and compared to the load which is allowed by the stability check. Arches with various cross sections and geometries were considered. For each arch the ultimate load is determined by a non-linear DIANA analysis. For details about the arches and the determination of the ultimate load see appendix D. All investigated arches consist of an IPE-section and buckle out-of-plane: buckling curve **a** shall be used to determine the buckling factor.

In Figure 5.5 and Figure 5.6 the buckling curve and the ultimate loads are given for the two loadcases. In these figures the numerical Euler buckling load is used to obtain the relative slenderness. In Figure 5.7 and Figure 5.8, again the buckling curve and ultimate loads are given but in these figures the relative slenderness is obtained with the analytical Euler buckling load. The differences between the figures based on the numerical Euler buckling load and the figures based on the analytical Euler buckling load are very small. The analytical Euler buckling load is a safe approach of the numerical model, so the results are also on the safe side.

The ultimate load obtained from FEM analyses correspond very well with the buckling curve. For the loadcase uniform compression all ultimate loads lie on the buckling curve and for the loadcase uniform bending the ultimate loads are on the safe side of the buckling curve. From these figures can be concluded that the proposed verification method for out-of-plane stability of arches seems to be well usable.

The same arches are used for the determination of the ultimate load in Figure 5.5 and Figure 5.6. The relative slenderness of an arch subjected to loadcase 1 or to loadcase 2 is very different as can be seen in these figures. The relative slenderness of arches subjected to loadcase 1, varies from 1.14 to 65. For the same arches, but now subjected to loadcase 2, the relative slenderness varies from 0.8 to 6.8. The relative slenderness of an arch depends not only on geometry and boundary conditions but also on the load distribution. It is important to keep in mind that a comparison of arches based on the relative slenderness is only useful for the same loadcase.

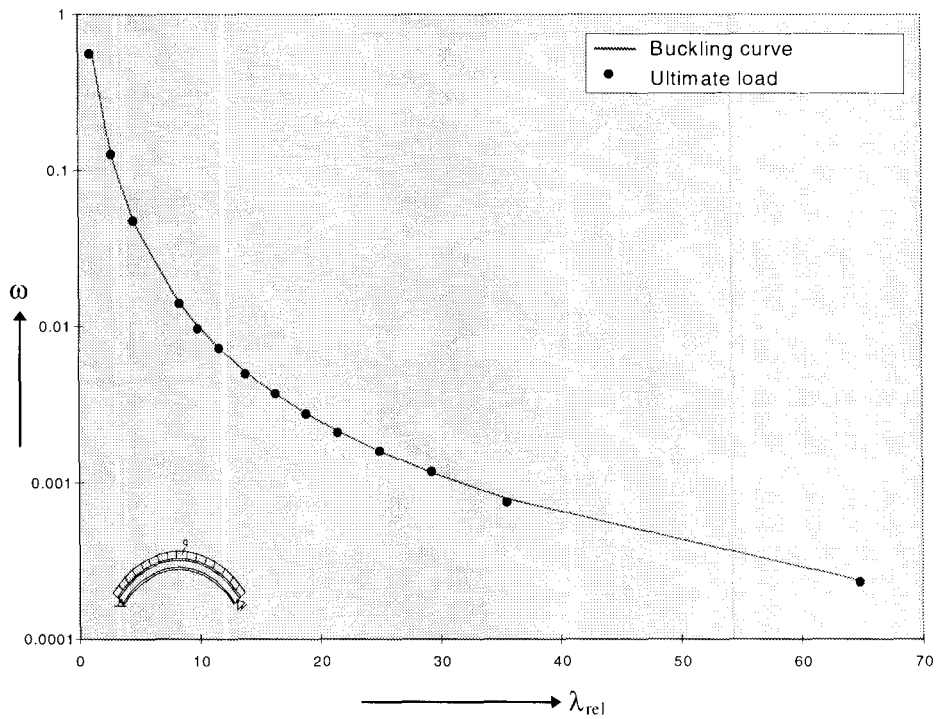


Figure 5.5 Check of verification method with numerical Euler buckling load for uniform compression

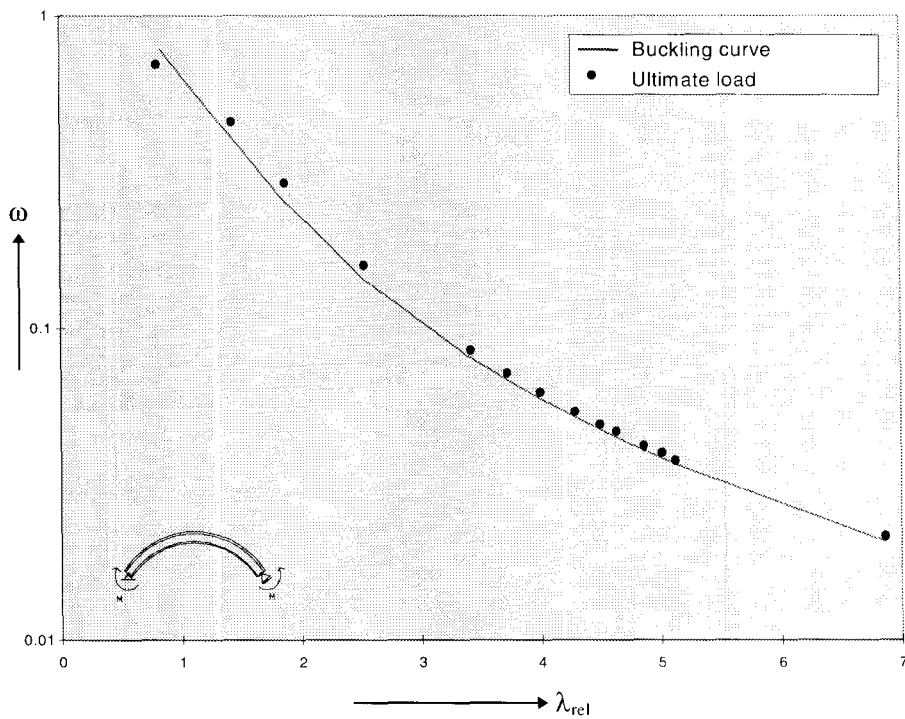


Figure 5.6 Check of verification method with numerical Euler buckling load for uniform bending

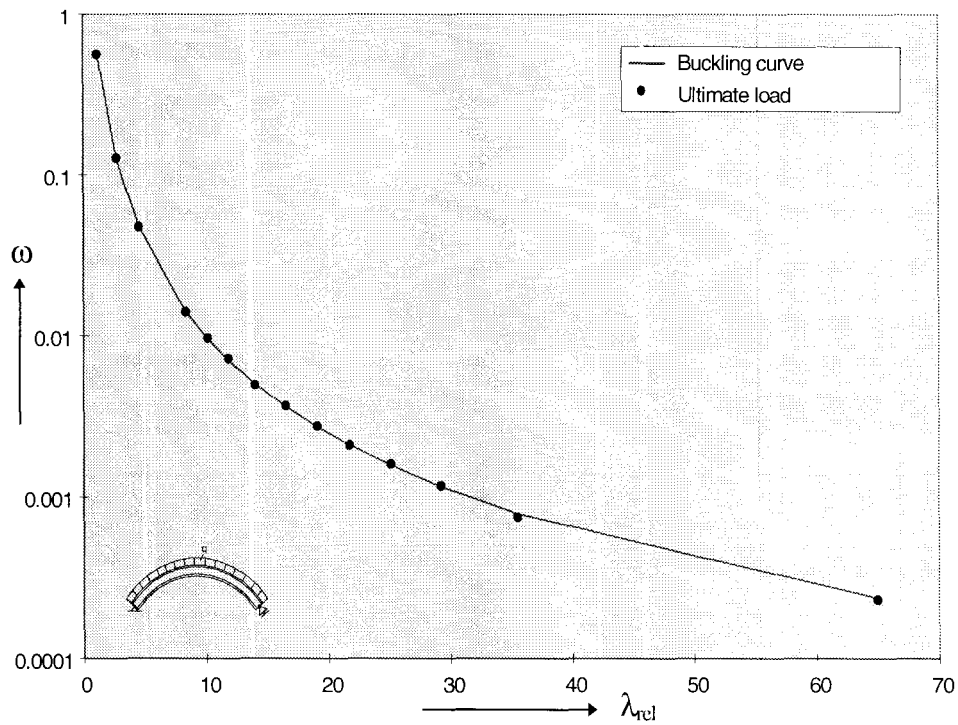


Figure 5.7 Check of verification method with analytical Euler buckling load for uniform compression

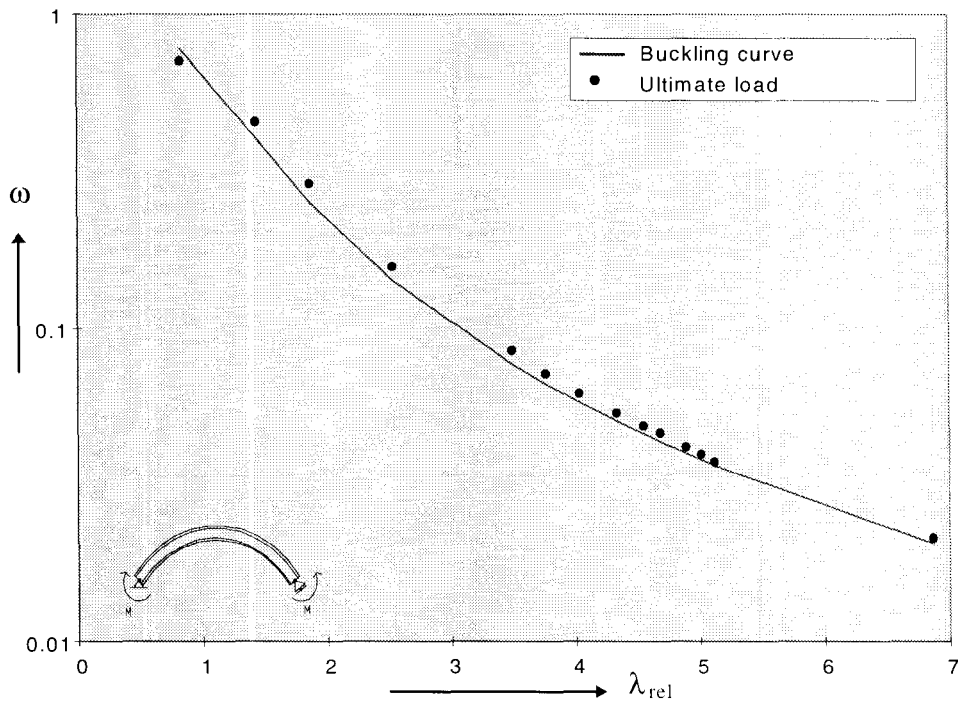


Figure 5.8 Check of verification method with analytical Euler buckling load for uniform bending

For arches without a positive post-buckling behaviour it is very important that the ultimate load is larger than the maximal allowed load by the stability check. When this is not the case the arch will collapse. For an arch with a positive post-buckling behaviour this is less critical. The arch will deform more when the load is larger than the ultimate load, but will not collapse. In Figure 5.9b an example is given of an arch with a positive post-buckling behaviour and an ultimate load which is slightly smaller than the maximum load allowed by the stability check. It is clear that this causes no problems.

Three arches of the investigated range do not have a positive post-buckling behaviour. In Figure 5.9a an example is given of such an arch for which the buckling curve gives a good prediction of the ultimate load. (See appendix D.2 for the load-displacement diagrams with load levels of the other arches.) The arches which do not have a positive post-buckling behaviour are stocky arches. The transition from arches without to arches with a positive post-buckling behaviour is for loadcase 1 about a relative slenderness of 4, and for loadcase 2 about 2.

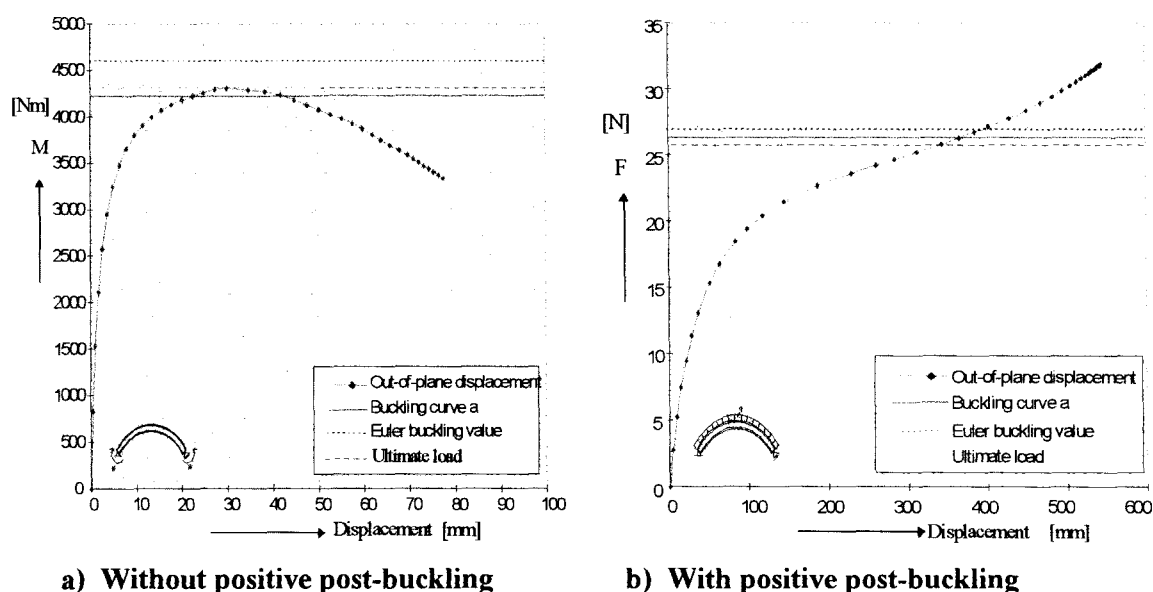


Figure 5.9 Load-displacement diagrams

Only the arch with the smallest relative slenderness can not be verified with the proposed verification method. This arch has no positive post-buckling behaviour and the ultimate load is smaller than the maximum allowed load by the stability check. This arch however is very flat and the deformations out-of-plane are of the same order of magnitude as the in-plane deformations. This points to an interim phase between out-of-plane buckling and snap-through buckling. Snap-through buckling is another type of buckling to which a flat arch is sensitive and requires an additional verification method.

5.2.3 Combination of compression and bending

In practice it hardly occurs that an arch is subjected to uniform compression or uniform bending. The two checking equations previously proposed in this chapter can be seen as a basis for the verification of other loadcases. In this subparagraph a possible approach is given how to determine a verification method for arches under uniform compression and uniform bending.

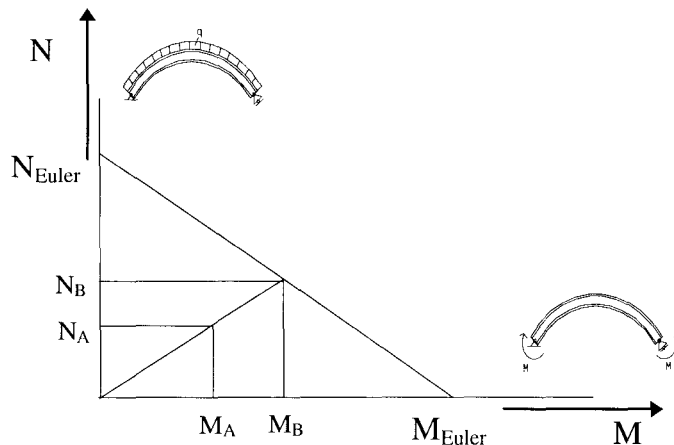


Figure 5.10 Combination of uniform compression and uniform bending

In the analytical equations for the out-of-plane stability of arches (appendix B) it can be seen that the compression force and the bending moment can be linearly combined. This is shown in Figure 5.10. The verification method for arches subjected to uniform compression and to uniform bending is in principal the same as for arches subjected to uniform compression. A difficulty is that the stability check is related to the design plastic resistance of the cross section. For a combination of uniform compression and uniform bending, the two load types have each their own plastic resistance. The introduction of load factors solves this problem.

1. λ_s is the load factor with which the design load has to be multiplied to use the full plastic resistance of the cross section.
2. λ_0 is the load factor with which the design load has to be multiplied to obtain the load which belongs to the Euler level.
3. $\lambda = \sqrt{\frac{\lambda_s}{\lambda_0}}$ is the relative slenderness of the arch

With the just defined relative slenderness a buckling factor ω can be obtained. This buckling factor represents the relationship between the buckling capacity and the design plastic resistance of the cross section ($\omega = \lambda_d / \lambda_s$).

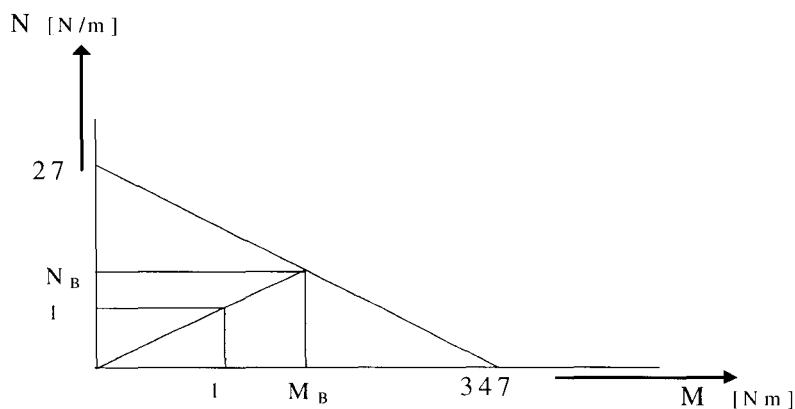
The load factor, λ_d , is the factor with which the design load has to be multiplied to achieve out-of-plane buckling. In other words the stability check is $\lambda_d \geq 1$.

In Table 5.1 the verification method is compared to the verification of the stability of columns. In the first column the verification of columns is presented. The second column contains an adaptation of the first column to a verification with load factors. The third column contains the proposed verification for arches subjected to uniform compression and uniform bending.

Table 5.1 Comparison of verification for columns and arches

Column	Column*	Arch
$N_{pl,d}$	$\lambda_s = \frac{N_{pl,d}}{N_{s,d}}$	$\lambda_s = \frac{f_y}{\sigma_{s,d}}$ with $\sigma_{s,d} = \frac{N_{s,d}}{A} + \frac{M_{s,d}}{W_{pl,d}}$
N_{Euler}	$\lambda_0 = \frac{N_{Euler}}{N_{s,d}}$	$\lambda_0 = \frac{M_B}{M_A} = \frac{N_B}{N_A}$
$\lambda_{rel} = \sqrt{\frac{N_{pl,d}}{N_{Euler}}}$	$\lambda = \sqrt{\frac{\lambda_s}{\lambda_0}}$	$\lambda = \sqrt{\frac{\lambda_s}{\lambda_0}}$
$f(\lambda_{rel}) = \omega$	$f(\lambda) = \omega$	$f(\lambda) = \omega$
$\frac{N_{s,d}}{\omega N_{pl,d}} \leq 1$	$\frac{\sigma_{s,d}}{\omega f_y} \leq 1$	$\frac{\sigma_{s,d}}{\omega f_y} \leq 1 \quad (= \lambda_d \geq 1)$

In this investigation this verification method is not checked with FEM analyses. One example will follow to present the method.

Example :**Figure 5.11 Euler buckling level**

The arch used in this example has as profile IPE100*, a radius of 7 meter and a length of 10 m. (the standard arch).

Load: $N = 1 \text{ N/m} = 1 * 7 \text{ N}$ and $M = 1 \text{ Nm} = 1000 \text{ Nmm}$

- λ_s : $\sigma = 7 / 1014 + 1000 / 40464.8 = 0.0316 \text{ N/mm}^2$
 $\lambda_s = 235 / 0.0316 = 7432.9$

- λ_0 : $N = M$ (see Figure 5.11)
 $N = 27 - 27/347 M$ intersection point: $M=N=25.05$
 $\lambda_0 = 25.05/1 = 25.05$
- λ : $\lambda = \sqrt{\frac{\lambda_s}{\lambda_0}} = 17.225$
- ω : buckling curve a: $\omega = 3.33212 \cdot 10^{-3}$
- λ_d : $\lambda_d = 3.33212 \cdot 10^{-3} * 7432.9 = 24.767$

According to the verification, the buckling capacity of the arch is $N = 24.767$ N/m combined with $M = 24.767$ Nm. A non-linear FEM analysis gives as ultimate load (point of contraflexure) for the arch subjected to compression and bending with a ratio 1 to 1, 25.33 (25.33 N/m and 25.33 Nm). The stability check is for this example safe.

5.3 Comparison to other verification methods

In this section a comparison is made between the proposed verification method and the existing verification method in the German code DIN 18800. The proposed method will also be compared to the verification of steel bridges in the European prestandard, Eurocode 3 part 2.

5.3.1 DIN 18800

The German code DIN 18800 contains a verification method for out-of-plane buckling of circular arches. In this code the model of Timoshenko[3] is the basis for obtaining a critical load. Timoshenko's model is just appropriate for arches with closed cross sections. In this critical value the influence of warping is neglected, which results in a conservative verification for arches with a cross section sensitive to warping. For more details about the DIN 18800, the reader is referred to appendix A.1.

According to DIN 18800, verification for a circular arch subjected to uniform compression should be carried out as:

$$\frac{N}{\kappa N_{pl,d}} \leq 1$$

The relative slenderness should be determined to obtain the factor κ , the buckling factor. The relation between κ and the relative slenderness can be found in appendix A.1.

$$\lambda_k = \sqrt{\frac{N_{pl}}{N_{Ki,Kr}}} \quad \text{with } N_{Ki,Kr} = \frac{EI_z}{R^2} \frac{(\pi^2 - \alpha^2)^2}{\alpha^2(\pi^2 + \alpha^2 K)} \quad K = \frac{EI_z}{GI_t}$$

If in the equation for $N_{ki,Kr}$, α is substituted with $\frac{L}{R}$, exactly the same equation as the solution of Timoshenko's model is obtained.

The DIN 18800 has no stability check especially for an arch subjected to uniform bending. For a combination of compression and bending, the next stability check is present:

$$\frac{N}{\kappa_z N_{pl,d}} + \frac{M_y}{\kappa_m M_{pl,u,d}} k_y \leq 1$$

For an arch only subjected to uniform bending this can be reduced to:

$$\frac{M_y}{\kappa_m M_{pl,u,d}} \leq 1 \quad (\kappa_y = 1, \text{ see appendix A.1})$$

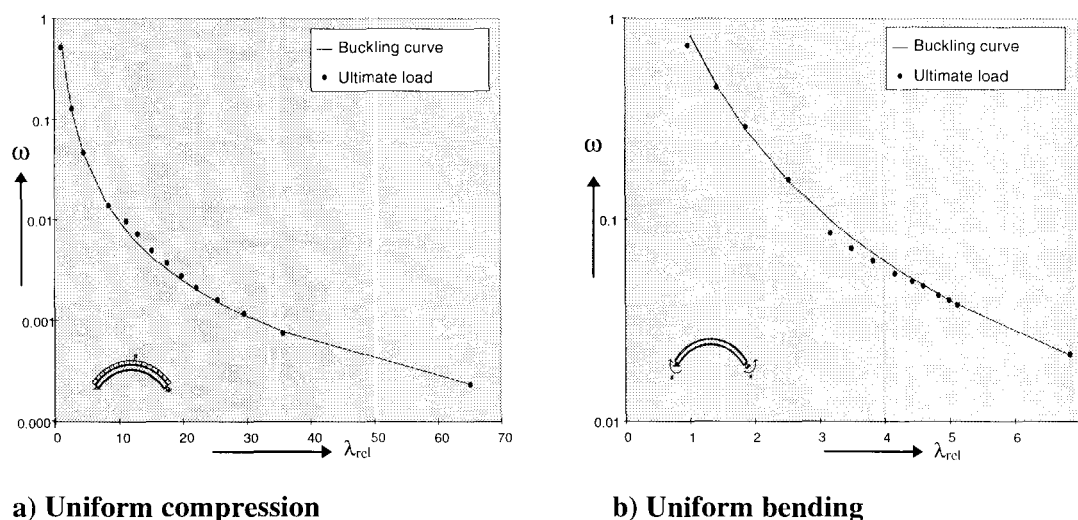
Again a relative slenderness should be determined to obtain the factor κ_m (see appendix A.1 how to determine κ_m).

$$\lambda_m = \sqrt{\frac{M_{pl,y}}{M_{ki,y}}} \quad \text{with} \quad M_{ki,y} = -\frac{EI_z + C}{2R} \pm \sqrt{\left(\frac{EI_z - C}{2R}\right)^2 + \frac{EI_z C \pi^2}{R^2 \alpha^2}} \quad \text{and} \quad C = \frac{EI_\omega \pi^2}{R^2 \alpha^2} + GJ$$

The critical bending moment $M_{ki,y}$ resembles also the critical bending moment of Timoshenko, but here an extra term, for warping is included.

The ultimate loads from the DIANA analyses are compared to the verification according to DIN 18800. In Figure 5.12a, the line represents the buckling curve and the points are the DIANA results. For the load case uniform compression, most of the DIANA results are slightly above the buckling curve. This can be explained by the neglect of warping in Timoshenko's model. The estimated Euler buckling load is small, which results in a conservative verification. On the other hand for the load case of uniform bending, the influence of warping is not neglected, which leads to DIANA results lower than the verification, see Figure 5.12b. As shown before, for most arches this is not a problem, due to positive post-buckling behaviour. Only the three arches with the smallest relative slenderness do not have this behaviour. So for these arches it is important that the DIANA results are on the safe side of the buckling curve. For the arches under uniform compression this is the case, but the ultimate load of the second arch under uniform bending is lower than the load allowed by the stability check. For this arch DIN 18800 appears to be just on the unsafe side. The load allowed by DIN is 1.5% higher than the ultimate load of the arch. This difference is very small.

From the comparison of the Din 18800 and the FEM results can be concluded that the verification method for out-of-plane stability of arches in DIN 18800 is a safe method.



a) Uniform compression

b) Uniform bending

Figure 5.12 Verification according DIN 18800

5.3.2 Eurocode

The European prestandard, Eurocode 3, part 2 handles steel bridges. In this part a brief description is given on how to determine the critical buckling force of free standing arches for out-of-plane buckling.

In general this is written as $N_{cr} = \left(\frac{\pi}{\beta l}\right)^2 EI_z$.

The factor β for a free standing circular arch with radial loading is given as: $\beta = R \alpha \frac{\sqrt{\pi^2 + \alpha^2 K}}{l(\pi^2 - \alpha^2)}$

The factor β substituted in N_{cr} results in: $N_{cr} = \frac{\pi^2 (\pi^2 - \alpha^2)^2 EI_z}{R^2 \alpha^2 (\pi^2 + \alpha^2 K)}$

Substituting α for $\frac{L}{R}$ this becomes $N_{cr} = \frac{\pi^2 \left(\frac{\pi^2 R^2}{L^2} - 1\right)^2 EI_z}{R^2 \left(\frac{\pi^2 R^2}{L^2} + K\right)} = \pi^2 N_{cr \text{ Timoshenko}}$

It seems that for the critical buckling force a factor π^2 too much is introduced.

In the prestandard no verification method is present. When a verification method is determined in the same way as the proposed verification method with the critical force, $\pi^2 N_{cr \text{ Timoshenko}}$, the method would be very unsafe. In Figure 5.13 the results are given for this assumed verification based on the prestandard of the Eurocode. The ultimate loads are much lower than the load allowed by the stability check. Even for arches with a positive post-buckling behaviour this leads to unsafe situations. In Figure 5.13 for example, the deformations and the load allowed by the assumed verification of arch number four (appendix D) is given. From this figure it is clear that the assumed verification based on the critical load of the Eurocode prestandard can be very unconservative.

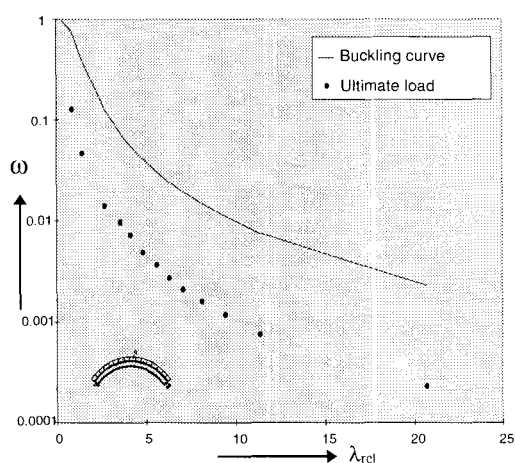


Figure 5.13 Verification based on the critical load of the Eurocode

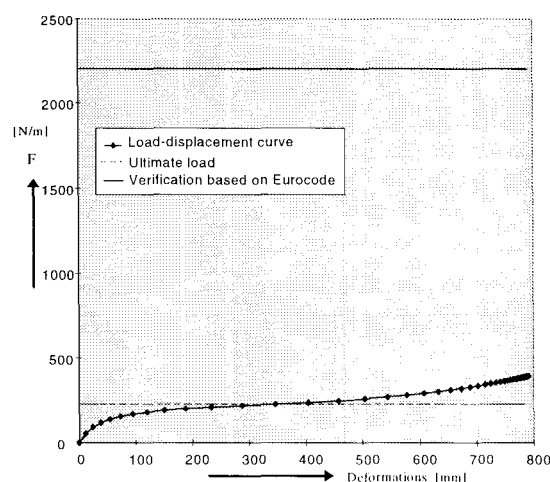


Figure 5.14 Load-displacement diagram and maximum load ac. verification based on N_{kr} of the Eurocode.

Summarised:

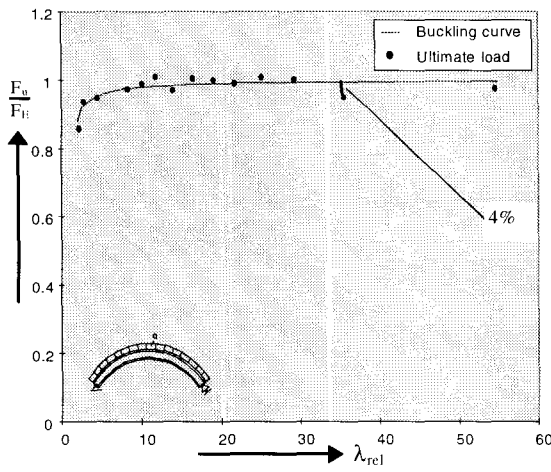
- The critical out-of-plane buckling load for arches subjected to uniform compression in the prestandard of EC3, differs a factor π^2 with the critical buckling load according Timoshenko.
- When a verification method is based on the critical buckling load without this factor π^2 , the same verification is obtained as found in the DIN 18800 for out-of-plane stability of arches.

5.3.3 Comparison Proposed verification - DIN 18800

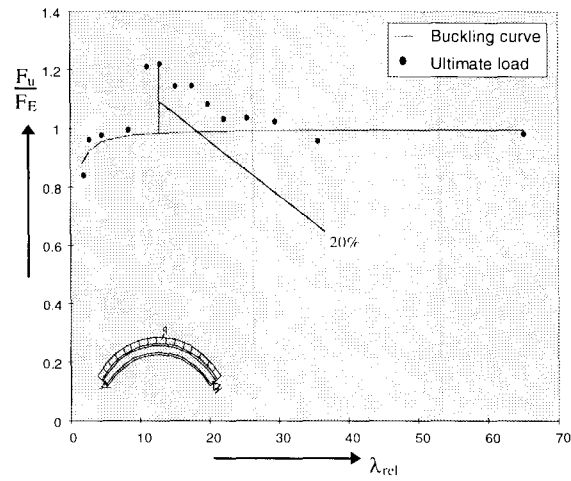
In Figure 5.15 and Figure 5.16 the buckling curves and the ultimate loads are given once again for the proposed verification and the DIN 18800. In these figures they are given related to the Euler buckling load to see the differences more clearly. A comparison with Eurocode 3 makes no sense, because of the mistake in the critical buckling load. When the critical buckling load is corrected, the same verification as the DIN 18800 is obtained.

For the loadcase uniform compression the DIN 18800 is more conservative than the proposed verification in this report. The influence of the warping effect is clear to see when Figure 5.15a is compared to Figure 5.15b. For arches with a relative slenderness of about 15, the DIN is the most conservative. The highest relative difference between the ultimate load and the maximum load allowed by the stability check is twenty percent. For the proposed verification the highest relative difference is just four percent.

For the loadcase uniform bending the proposed verification is more conservative than the DIN 18800 but, DIN 18800 is not always safe. The use of another buckling curve than the standard column buckling curve leads to the differences from the fourth ultimate load. The highest relative difference between the ultimate load and the verification is for the proposed verification twelve percent. For the DIN 18800 this is sixteen percent but the verification overestimate the ultimate load. Due to the positive buckling behaviour of these arches this is not that critical as it seems.

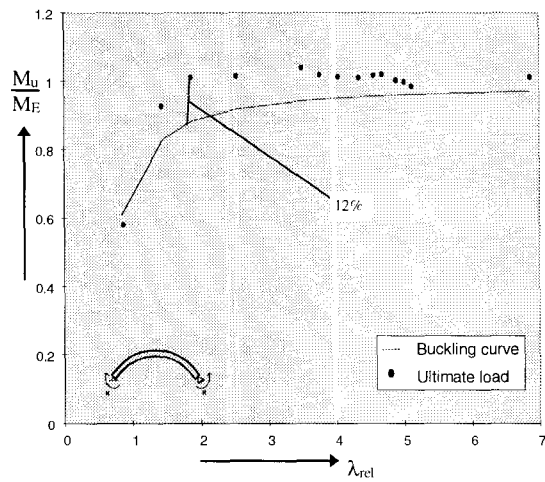


a) Proposed method

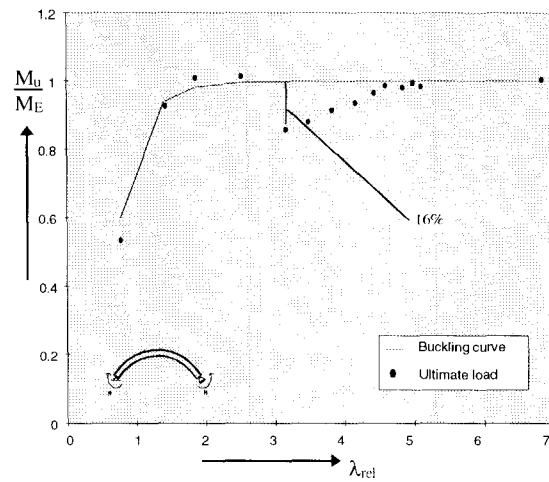


b) DIN 18800

Figure 5.15 Verification methods for arches under uniform compression



a) Proposed method



b) DIN 18800

Figure 5.16 Verification methods for arches under uniform bending

6. CONCLUSIONS AND RECOMMENDATIONS

6.1 Conclusions

6.1.1 Literature and Euler buckling load

From the literature studied it can be concluded that not many codes have provisions to verify out-of-plane stability of arches. The German code DIN 18800 is the most detailed on this subject. Literature study also showed that a number of researchers defined an analytical model to determine the Euler buckling load of an arch. The different models are based on straight beam theory or curved beam theory and they are worked out with a direct or indirect calculation method. These varying approaches lead to different Euler buckling loads.

For the models separately, the following conclusions can be made:

- The model of Timoshenko [3] neglects the effect of warping which results in small Euler buckling loads. Especially for stocky arches his model is conservative.
- The model of Vlasov [4] leads to a significantly higher Euler buckling load for arches under uniform compression than the other models. The use of the straight beam theory is a possible explanation for the high Euler buckling loads.
- The model of Yoo [5,6] gives for both loadcases, uniform compression and uniform bending, significantly higher results than other models do. The translation of the straight beam theory to the curved beam theory in his model, is the cause of this overestimation.
- The models of Trahair [7,8,9,10,11], Rajasekaran [12] and Yang [13,14,15,16] give quite corresponding Euler buckling loads which also correspond with numerically determined Euler buckling loads. Different assumptions in strain-displacement relations lead to small differences in the results.

After a study of the analytical models, the model of Rajasekaran seems to be the most appropriate for further use. The model provides in a relatively simple way the Euler buckling load, which can be seen as an upper limit of the ultimate load an arch can carry.

6.1.2 Non-linear FEM analyses

An important finding of the non-linear FEM analyses is the positive post-buckling behaviour of slender arches. These arches can carry a larger load than the Euler buckling load. The non-linear FEM analyses also showed that very slender arches deform extremely before they collapse. In that case the ultimate load is not clearly defined. Five options for the definition of the ultimate load are considered and the most appropriate is determined.

The ultimate load is defined as:

Load belonging to: $\min \left| \frac{d(\text{load})}{d(\text{displacement top-node})} \right|$ of the load-displacement diagram.

For arches with a positive post-buckling behaviour this is the point of contraflexure in the load-displacement diagram. For arches without a positive post-buckling behaviour this is the top in the load-displacement diagram. It can be concluded that this definition for arches with or without positive post-buckling behaviour gives a good estimate of the ultimate load.

6.1.3 Verification method

The proposed verification method for out-of-plane stability of arches provides, in a relatively simple way, a stability check for arches subjected to uniform compression or uniform bending. The method corresponds to the Dutch code concerning stability of columns. The use of the column buckling curves to determine the buckling factor, turned out to be successful.

Like for columns, a relative slenderness has to be determined to obtain the buckling factor. This relative slenderness depends not only on the dimensions of the arch but also strongly on the load distribution. The same arch under uniform compression has a much larger relative slenderness than under uniform bending. From this, it can be concluded that comparing arches on the basis of their relative slenderness is only useful when the loadcase is similar.

The proposed stability check for uniform compression is:
$$\frac{N_{c,s,d}}{\omega_{arch,out} N_{c,u,d}} \leq 1$$

with:

$N_{c,s,d}$ design value of the compressive force

$N_{c,u,d}$ design plastic resistance to compression of the cross section

$\omega_{arch,out}$ buckling factor for out-of-plane buckling of arches

The proposed stability check for uniform bending is:
$$\frac{M_{y,s,max,d}}{\omega_{arch,out} M_{y,u,d}} \leq 1$$

with:

$M_{y,max,s,d}$ design value of the bending moment

$M_{y,u,d}$ design plastic resistance to bending of the cross section

$\omega_{arch,out}$ buckling factor for out-of-plane buckling of arches

The buckling factor for out-of-plane buckling of arches can be obtained from the column buckling curves. The curve to be used is **a**, for rolled sections and circular hollow sections. Only the relative slenderness must be known, in order to obtain the buckling factor.

For uniform compression the relative slenderness is:
$$\lambda_{rel} = \sqrt{\frac{N_{c,u,d}}{F_{y,E}}}$$

For uniform bending the relative slenderness is:
$$\lambda_{rel} = \sqrt{\frac{M_{c,u,d}}{M_E}}$$

in which

$N_{c,u,d}$ is the design plastic resistance to compression of the cross section

$M_{c,u,d}$ is the design plastic resistance to bending of the cross section

$F_{y,E}$ is the Euler buckling load for uniform compression based on the model of Rajasekaran [12]

M_E is the Euler buckling load for uniform bending based on the model of Rajasekaran [12]

$$F_{y,E} = \beta_{\text{red}} \frac{M_0}{R^2} \left(\frac{b/a (a^2 - 1)^2}{a^2 + b^2} \right)$$

$$M_E = \beta_{\text{red}} M_0 \left(-\frac{a}{b} - \frac{ab}{2} + \sqrt{\left(\frac{a}{b} + \frac{ab}{2} \right)^2 + 1 - a^2} \right)$$

with:

L, H, ℓ and R according to figure 5

$$a = \frac{L}{\pi R} \quad b = \frac{\pi M_0}{P_z L} \quad P_z = \frac{\pi^2 EI_z}{L^2} \quad M_0 = \sqrt{P_z \left(GJ + \frac{\pi^2 EI_w}{L^2} \right)}$$

$$\beta_{\text{red}} = 1 \quad \text{for } \frac{H h}{L \ell} \leq 0.25$$

$$= 1.05 - 0.2 \frac{H h}{L \ell} \quad \text{for } \frac{H h}{L \ell} > 0.25$$

The reduction factor β_{red} is added to the original formulae from Rajasekaran yielding Euler buckling loads that comply with numerical results.

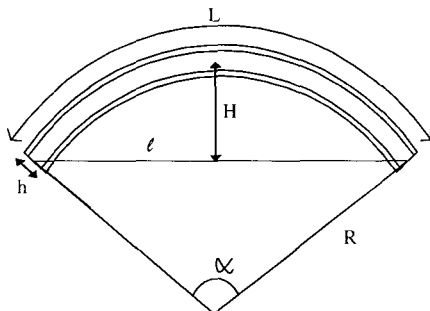


Figure 1 Parameters of the arch

When the verification method in DIN 18800 is compared to the verification method determined in this investigation, it seems to be more conservative for the loadcase uniform compression. For the loadcase uniform bending, the determined verification method is more conservative than DIN 18800. The maximum load allowed by DIN 18800 leads however sometimes to larger deformations than allowed by the ultimate load.

In the prestandard for Eurocode 3 part 2, steel bridges, a critical load for out-of-plane buckling of arch bridges is given. This critical load however is a factor π^2 larger than the Euler buckling load according to Timoshenko's model. It can be concluded that it is much too large. Correction for this leads to the same rule as the one of DIN 18800 and thus the same remarks holds.

6.2 Recommendations

Cross section

The arches, which are used for the investigation on out-of-plane stability, have all an IPE section. Other types of cross sections should also be investigated. Also the influence of an a-symmetric cross section is a topic for further investigation.

Arch shape

Besides circular arches, used in this investigation, there are also parabolic and chain-line arches. Whether these arches can also be verified with the proposed verification method should be investigated.

Euler buckling load

The Euler buckling load is used in the verification method to determine the relative slenderness of an arch. The model of Rajasekaran is used as basis for the Euler buckling load. The model however seems to overestimate the Euler buckling load for arches with a relatively high section depth. Further investigation to the cause of this overestimation is advised.

The reduction factor, β_{red} , introduced to reduce the analytical Euler buckling load, is related to the factor $\frac{H h}{L l}$. More extensive investigation into the accuracy of the reduction factor and to the factor $\frac{H h}{L l}$ is advised.

Verification

The proposed verification method is checked by FEM analyses for a number of arches. Most of these arches have a positive post-buckling behaviour. For arches without a positive post-buckling behaviour, stocky arches, the verification is nevertheless more critical. Therefore it is advised to investigate more arches without a positive post-buckling behaviour. For the loadcase uniform compression these are arches with a relative slenderness smaller than 4. For the loadcase uniform bending arches have to be investigated with a relative slenderness smaller than 2.

The investigation of Verstappen [1] resulted in a proposal for the verification of the in-plane stability of arches. This investigation resulted in a proposal for the verification of the out-of-plane stability of arches. For one special type of in-plane stability there still is no verification available. To cover all stability phenomena for arches, a verification for snap-through buckling should be determined.

Two verification rules are proposed in this investigation; one for uniform compression and one for uniform bending. For the combination of uniform compression and uniform bending a verification method is suggested. This method needs to be worked out or another method should be determined. In practice, uniform compression and uniform bending hardly occur. The influence of non-uniform loading should be investigated and incorporated in the verification.

As shown in this investigation, an arch can deform extremely before it collapses due to buckling. These large deformations can not be allowed in practice. The serviceability limit state should be checked especially for arches.

Load distribution

For the loadcases studied in this investigation, it is obvious which normal force or bending moment should be used in the verification method. For other loadcases it should be defined how to determine the forces in the arch and which force, should be used in the verification method.

Ultimate load

The ultimate load defined in this investigation turned out to be useful for arches with and without positive post-buckling behaviour. The definition of an ultimate load in the case of positive post-buckling yields a problem also for other structures and other stability phenomenons. For example local buckling of thin plated structures is also a stability phenomenon with positive post-buckling behaviour. It is an interesting study to find out whether the ultimate load defined in this investigation also works for this stability problem.

REFERENCES

- [1] Verstappen I. Toetsingsregels voor stalen bogen. TNO rapport 96-CON-RO623/01, 1996.
- [2] Kuranishi S. Stability of metal structures. A World View, 2nd edition, pp 432-445, 1991.
- [3] Timoshenko S.P. and Gere J.M. Theory of elastic stability. McGraw-Hill (US), 2nd ed., 1961
- [4] Vlasov V.Z. Thin-walled elastic beams. National Science Foundation, Washington, 2nd ed., 1961.
- [5] Yoo C.H. Flexural-torsional stability of curved beams. Journal of the Engineering Mechanics Division, vol. 108 No. 6 p. 1351-1369, 1982.
- [6] Yoo C.H. & Pfeiffer P.A. Elastic stability of curved beams. Journal of Structural Engineering, vol. 109 No. 12 p.2922-2940, 1983.
- [7] Papangelis J.P. & Trahair N.S. Flexural-torsional buckling of arches. Research Report R492, School of Civil and Mining Engineering, University of Sydney, Australia, 1985.
- [8] Papangelis J.P. & Trahair N.S. Flexural-torsional buckling of arches. Journal of Structural Engineering, vol. 113 No. 4 p. 889-905, 1987.
- [9] Papangelis J.P. & Trahair N.S. Flexural-torsional buckling tests on arches. Journal of Structural Engineering, vol. 113 No. 7 p. 1433-1443, 1987.
- [10] Trahair N.S. & Papangelis J.P. Flexural-torsional buckling of monosymmetric arches. Journal of Structural Engineering, vol. 113 No. 10 p. 2271-2288, 1987.
- [11] Trahair N.S. Flexural-torsional buckling of structures. CRC Press Inc. ,Florida, 1st ed.,1993.
- [12] Rajasekaran S. & Padmanabhan S. Equations of curved beams. Journal of Engineering Mechanics, vol. 115 No. 5 p. 1095-1110, 1989.
- [13] Yang Y.B. & Kuo S.R. Static stability of curved thin-walled beams. Journal of Engineering Mechanics, vol. 112 No. 8 p. 821-841, 1986.
- [14] Yang Y.B. & Kuo R.S. Effect of curvature on stability of curved beams. Journal of Structural Engineering, vol. 113 No. 6 p. 1185-1202, 1987.
- [15] Yang Y.B & Kuo S.R. & Yau J.D. Use of straight-beam approach to study buckling of curved beams. Journal of Structural Engineering, vol. 117 No. 7 p. 1963-1987, 1991.
- [16] Kuo S.R. & Yang Y.B. New theory on buckling of curved beams. Journal of Engineering Mechanics, vol. 117 No. 8 p. 1698-1717, 1991.

- [17] Dawe D.J. Numerical studies using circular arch finite elements. *Computers and Structures*, vol. 4 pp 729-740, 1974. 12 p. 2922-3000, 1983.
- [18] Sakimoto T. & Sakata T. The out-of-plane buckling strength of through-out arch bridges. *Journal of Construction Steel Research (GB)*, vol. 16 No. 4 p. 307-318, 1991.

APPENDICES

A. CODES

A.1. Code DIN 18 800

In this appendix, the verification rules for out-of-plane stability of arches are given according to DIN 18 800.

Article 6.1.2 Arches under compression

All rules for the out-of-plane stability of arches under compression, are based on the next verification:

$$\frac{N}{\kappa N_{pl,d}} \leq 1$$

where:

N is the normal compression force in the crown of the arch.

$N_{pl,d}$ is the maximum allowable compression force.

κ is a factor based on the slenderness of the arch.

The slenderness of the arch depends on the dimensions, the restraints and the loading of the arch. In the next subarticles is written how the slenderness for different arches can be obtained. With the slenderness λ_k , the factor κ can be determined in the following way:

When $\lambda_k \leq 0.2$: $\kappa = 1$

$$\text{When } \lambda_k > 0.2 : \kappa = \frac{1}{k + \sqrt{k^2 - \lambda_k^2}}$$

with

$$k = 0.5(1 + \alpha(\lambda_k - 0.2) + \lambda_k^2)$$

When $\lambda_k > 0.3$: κ can be simplified to $\frac{1}{\lambda_k(\lambda_k + \alpha)}$

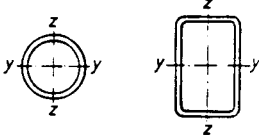
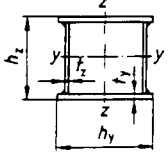
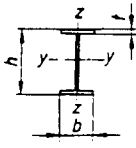
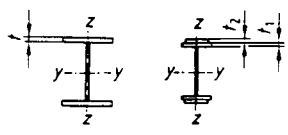
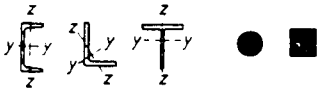
The value of α can be obtained from Table A.1.

The selection of the buckling curve for a cross section is given in Table A.2.

Table A.1 Parameter α to determine reduction factor κ

Buckling curve	a	b	c	d
α	0.21	0.34	0.49	0.76

Table A.2 Selection of buckling curve for a cross section

1		warm gefertigt	y-y	a
		kalt gefertigt	z-z	b
2			y-y	b
		$h_y/t_y < 30$ $h_z/t_z < 30$	z-z	c
3		$h/b > 1,2; t \leq 40 \text{ mm}$	y-y	a
			z-z	b
		$h/b > 1,2; 40 < t \leq 80 \text{ mm}$ $h/b \leq 1,2; t \leq 80 \text{ mm}$	y-y	b
			z-z	c
		$t > 80 \text{ mm}$	y-y	d
			z-z	d
4		$t_f \leq 40 \text{ mm}$	y-y	b
			z-z	c
		$t_f > 40 \text{ mm}$	y-y	c
			z-z	d
5			y-y	c
		z-z		

• Article 6.1.2.1 Arches without bracing

For a parabolic arch, the slenderness is: $\lambda_k = \frac{\beta_1 \beta_2 l}{i_z \lambda_a}$

For a circular arch, the slenderness is: $\lambda_k = \sqrt{\frac{N_{pl}}{N_{ki,Kr}}}$

with $N_{ki,Kr} = \frac{E I_z}{R^2} \frac{(\pi^2 - \alpha^2)^2}{\alpha^2(\pi^2 + \alpha^2 K)}$

β_1 Reduction factor with respect to the effective length out-of the plane of the arch according to Table A.3

β_2 Reduction factor with respect to the effective length according to Table A.4

i_z Radius of gyration with respect to the z-axis

λ_a Limit value for the slenderness

$N_{ki,Kr}$ Buckling value of an arch under uniform compression, with a double invariable symmetric cross section and pin-ended supports

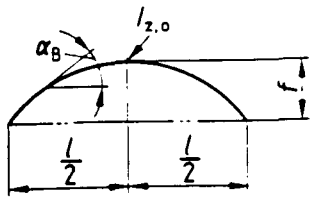
R Radius of the arch

α Included angle of the arch

K Ratio between the bending stiffness and the torsional stiffness

Table A.3 Buckling factor β_1

β_1	1	2	3	4	5	6
1	f/L	0.05	0.10	0.20	0.30	0.40
2	I_z constant	0.05	0.54	0.65	0.82	1.07
3	I_z variable	0.05	0.52	0.59	0.71	0.86



$$I_z(\alpha_B) = \frac{I_{z,0}}{\cos\alpha_B}$$

Table A.4 Buckling factor β_2

	Loading	β_2	explanation
1	conservative	1	q total load
2	by hangers	$1 - 0.35 q_h/q$	q_h load part transmitted by hangers
3	by posts	$1 + 0.45 q_{st}/q$	q_{st} load part transmitted by posts

- Article 6.1.2.2 Arches with braces and end frame

For this type of arches, the slenderness is: $\lambda_k = \frac{\beta h}{i_z \lambda_{cr}}$

β Reduction factor according to Table A.5

h Height of the end frame, see Figure A.1

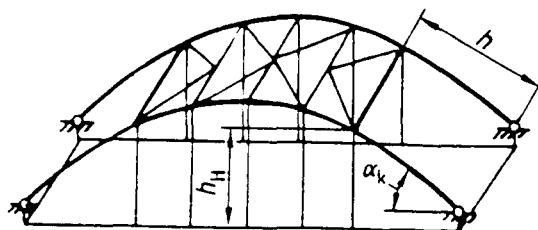
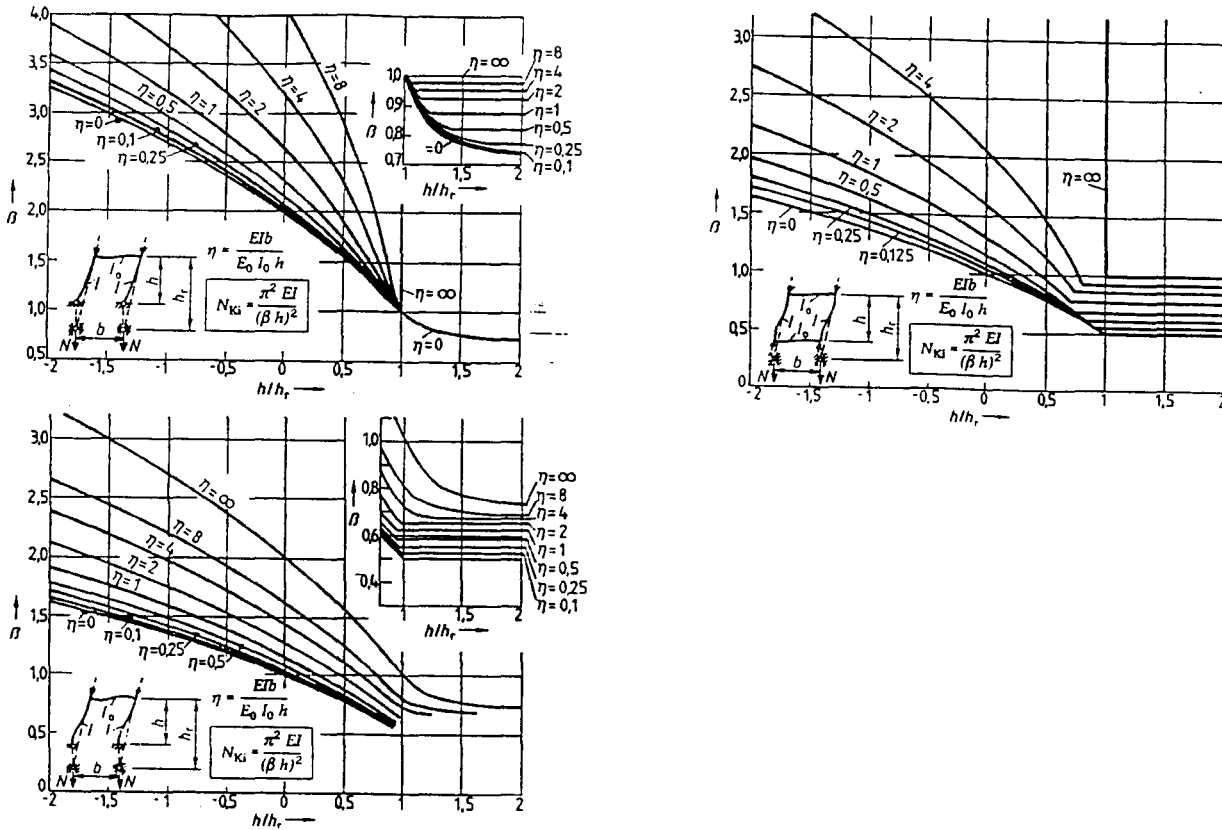


Figure A.1 Arch with wind bracing and end portals

Table A.5 Diagram to obtain β



Article 6.2.2 Arches under compression and bending

- Article 6.2.2.1 General

In general the slenderness λ_k , for arches under uniform compression and uniform bending is the same as in article 6.1.2.

- Article 6.2.2.2 Arches loaded in the crown of the arch, with invariable rectangular or I-shaped cross section.

For this type of arches, the slenderness is: $\lambda_k = \frac{\beta s}{i_z \lambda_{cl}}$ with $\beta = \frac{\pi}{\sqrt{K_1}}$

for arches under compression: $K_1 = 2.47 - (3 + 0.21 K) \frac{\alpha}{100} + (700 - 6 K + 0.08 K^2) \left(\frac{\alpha}{100}\right)^2$

for arches under tension : $K_1 = -0.036 + \frac{9.58}{10 + K} + \frac{7.58}{(10 + K)^2} + \frac{1}{\alpha} \left(0.134 - \frac{36.2}{5 + K} - \frac{62.5}{(5 + K)^2} \right) - \left(0.226 + \frac{13.4}{K} + \frac{1.94}{K^2} \right) \left(\frac{1}{\alpha}\right)^2$

β	Reduction factor
s	Half of the arch length
α	Included angle of the arch
K	Ratio between the bending stiffness and the torsional stiffness

- Article 6.2.2.3 Circular arch with I-shaped cross section and pin-ended

The verification rule for this type of arches is:

$$\frac{N}{\kappa_z N_{pl,d}} + \frac{M_y}{\kappa_m M_{pl,y,d}} \kappa_y \leq 1$$

κ_z	Buckling factor with respect to the z-axis
κ_m	Flexural-torsional buckling factor
κ_y	Factor which introduces the influence of the moment distribution and the slenderness gradient

$$\kappa_z : \quad \begin{array}{ll} \lambda_k \leq 0.2 & \kappa_z = 1 \\ \lambda_k > 0.2 & \kappa_z = \frac{1}{k + \sqrt{k^2 - \lambda_k^2}} \end{array} \quad \text{with } k = 0.5(1 + \alpha(\lambda_k - 0.2) + \lambda_k^2)$$

$$\lambda_k = \frac{\beta s}{i_z \lambda_a} \quad \text{with } \beta = \frac{2\pi}{\sqrt{K_1}} \quad \text{and} \quad K_1 = \frac{(\pi^2 - \alpha^2)^2}{\pi^2 + \alpha^2 K}$$

$$\kappa_m : \quad \begin{array}{ll} \lambda_m \leq 0.4 & \kappa_m = 1 \\ \lambda_m > 0.4 & \kappa_m = \left(\frac{1}{1 + \lambda_m^{2n}} \right)^{\frac{1}{n}} \end{array} \quad \text{with } n \text{ from Table A.7}$$

$$\lambda_m = \sqrt{\frac{M_{pl,y}}{M_{ki,y}}} \quad \text{with} \quad M_{ki,y} = -\frac{EI_z + C}{2R} \pm \sqrt{\left(\frac{EI_z - C}{2R} \right)^2 + \frac{EI_z C \pi^2}{R^2 \alpha^2}}$$

$$C = \frac{EI_0 \pi^2}{R^2 \alpha^2} + GJ$$

$$\kappa_y : \quad \kappa_y = 1 - \frac{N}{\kappa_z N_{pl,d}} a_y \leq 1 \quad \text{with } a_y = 0.15 \lambda_{k,z} \beta_{m,z} - 0.15 \leq 0.90$$

$\beta_{m,z}$ Factor with respect to flexural-torsional buckling according to Table A.6

Table A.6 factor $\beta_{m,z}$


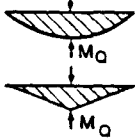
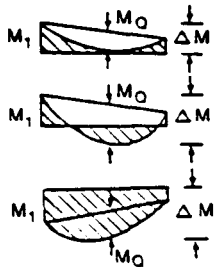


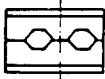
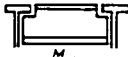
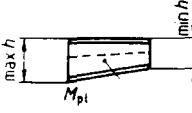
Moment distribution	$\beta_{m,z}$
<p>and moments</p>  <p>M_1 ψM_1 $-1 \leq \psi \leq 1$</p>	$\beta_{m,z,\psi} = 1.8 - 0.7\psi$
<p>moments due to in-plane lateral loads</p>  <p>M_Q M_Q</p>	$\beta_{m,z,q} = 1.3$ $\beta_{m,z,q} = 1.4$
<p>moments due to in-plane lateral loads plus end moments</p>  <p>M_1 M_Q ΔM M_1 M_Q ΔM M_1 M_Q ΔM</p>	$\beta_{m,z} = \beta_{m,z,\psi} + \frac{M_q}{\Delta M} (\beta_{m,z,q} - \beta_{m,\psi})$ $M_q = I_{max} M_l$ $\Delta M = I_{max} M_l \text{ or } I_{max} M_l + I_{min} M_l$

Table A.7 Factor n

	Profil	n
1		2.5
2		2.0
3	 M_{pl}	1.5
4	 M_{01}	2.0
5	 M_{pl} $\frac{\min h}{\max h} \geq 0.25$	$0.7 + 1.8 \frac{\min h}{\max h}$

Article 6.2.3 Spatial loaded arches

For the verification of the loading capacity of an arch, usually an elastic theory is used. When this calculation method used to determine the forces in the arch, an imperfection must be introduced. In Table A.8 and Table A.9, values are given for the imperfection. Only one imperfection has to be applied on the arch: in-the-plane or perpendicular to the plane of the arch. The most unfavourable imperfection should be applied.

Table A.8 In-plane imperfection

	w_0 for different buckling stress lines			
	a	b	c	d
Arch with symmetric deformations	$\frac{s}{300}$	$\frac{s}{250}$	$\frac{s}{200}$	$\frac{s}{150}$
Arch with anti-symmetric deformations	$\frac{L}{600}$	$\frac{L}{500}$	$\frac{L}{400}$	$\frac{L}{300}$

Table A.9 Out-of-plane imperfection

	v_0 for different buckling stresslines			
	a	b	c	d
$L \leq 20$ m	$\frac{L}{300}$	$\frac{L}{250}$	$\frac{L}{200}$	$\frac{L}{150}$
$L \geq 20$ m $L_1 = \sqrt{20L}$	$\frac{L_1}{300}$	$\frac{L_1}{250}$	$\frac{L_1}{200}$	$\frac{L_1}{150}$

A.2 Buckling curves

In the Dutch code NEN 6770, the buckling factor for columns is given a.o. in curves (Figure A.2). When the relative slenderness is known, the buckling factor can be determined with these curves. Which buckling curve should be used is given in Table A.10.

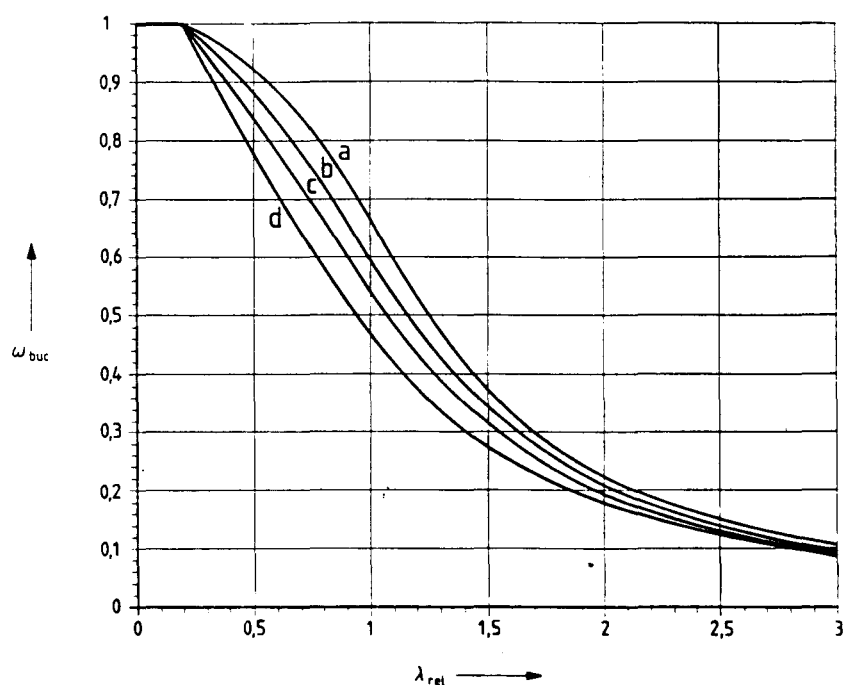
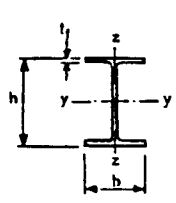
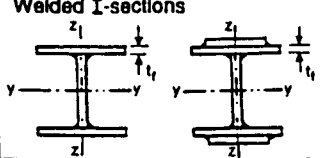

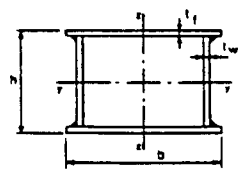
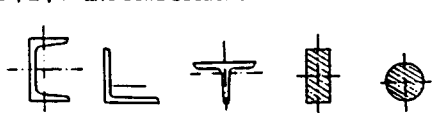


Figure A.2 Column buckling curves

Table A.10 Selection of buckling curve for a cross section

Table 5.5.3 Selection of buckling curve for a cross-section			
Cross section	Limits	Buckling about axis	Buckling curve
<p>Rolled I-sections</p> 	$h/b > 1,2:$ $t_f \leq 40\text{mm}$	y - y z - z	a b
	$40\text{mm} < t_f \leq 100\text{mm}$	y - y z - z	b c
	$h/b \leq 1,2:$ $t_f \leq 100\text{mm}$ $t_f > 100\text{mm}$	y - y z - z y - y z - z	b c d d
<p>Welded I-sections</p> 	$t_f \leq 40\text{mm}$ $t_f > 40\text{mm}$	y - y z - z y - y z - z	b c c d
<p>Hollow sections</p> 	hot rolled	any	a
	cold formed - using f_{yb})	any	b
	cold formed - using f_{ya})	any	c
<p>Welded box sections</p> 	generally (except as below)	any	b
	thick welds and $b/t_f < 30$ $h/t_w < 30$	y - y z - z	c c
<p>U-, L-, T- and solid sections</p> 		any	c

) See 5.5.1.4(4) and figure 5.5.2

B. EULER BUCKLING LOAD

B.1 Calculation methods

The different analytical models to obtain the Euler buckling load, result all in solving differential equations. To determine these equations several methods are available. A division can be in two main methods: The direct method and indirect method.

Direct method

The direct method consists of defining the equilibrium of a piece of the arch directly. Timoshenko and Vlasov used this method. For simple structures this is the easiest way to obtain the equilibrium equations.

Indirect method

For complex structures it is difficult to derive the equilibrium equations directly. In that case it is more convenient to use an energy or virtual displacement approach. The equilibrium equations are obtained indirectly from the total energy (U_T) respectively the total work (W).

Energy and work are related in the following way: $W' = U_T$.

A structure is in equilibrium when it is in the state of minimal potential energy. This is the case when the first variation of the total energy, is equal to zero. For a stable equilibrium the second variation must be greater than zero. The critical value for buckling can be obtained by putting the second variation of the total energy to zero. For the virtual displacement method only the first variation should be greater than zero.

A short review of the energy method will follow, applied for an arch element with double symmetric cross-section. The execution of the virtual displacement method is more or less the same, because of their relation. Therefore the explanation of this method is omitted.

The total energy contains the strain energy and the potential energy. For an arch element with linear elastic behaviour it can be expressed as:

$$U_T = \frac{1}{2} \int_v (E\varepsilon^2 + G\gamma^2) dV - \int_0^L (pw + qv) ds + \sum_{i \rightarrow 2} \{ -Pw - Vv - M\theta \}$$

The strain-displacement relations are used to substitute the strain terms in the energy functional. This energy functional will contain several functions of one independent variable x . This can be expressed as: $\pi = \int F(u, v, \phi, w', u', \phi', v'', u'', \phi'') dx$

Four differential equations for the stability of a curved beam are obtained from this functional by differentiating twice with respect to the different degrees of freedom. Two equations are dependent

on w , v and their derivatives, which describes the in-plane-stability. The other two are dependent on u , ϕ and their derivatives. They describe the out-of-plane-stability.

By assuming a buckling displacement for ϕ and u with the form:

$$u = B_1 \sin(n\pi s/L) \quad \text{and} \quad \phi = B_2 \sin(n\pi s/L)$$

The two differential equations for out-of-plane buckling can be written in the next form:

$$\{B_1 \ B_2\} \begin{bmatrix} k_{11} & k_{12} \\ k_{21} & k_{22} \end{bmatrix} \begin{Bmatrix} B_1 \\ B_2 \end{Bmatrix} = 0$$

The critical moment or compression q -load for buckling can be obtained by putting the determinant to zero. In the following appendices different executions by different persons of this method are discussed.

B.2 Timoshenko & Gere

In [3] Timoshenko and Gere determine the equilibrium equations directly by solving the equilibrium for a straight beam. These are adapted for a curved beam by using the curvature and twist for a curved beam.

The equations for calculating the curvatures and twist are:

$$M_z = \frac{EI_z}{\rho_1}$$

$$M_y = EI_y \left(\frac{1}{\rho_2} - \frac{1}{R} \right)$$

$$M_x = GJ\theta$$

$\frac{1}{R}$ is the initial curvature of the centre line of the bar.

θ is the angle of twist per unit length.

For small displacements the components of displacements can be considered separately and summed up to get the final change in curvature.

Curvatures and twist of a curved bar after deformation are:

$$\frac{1}{\rho_1} = \frac{\phi}{R} - u''$$

$$\frac{1}{\rho_2} = \frac{1}{R} + \frac{v}{R^2} + v''$$

$$\theta = \phi' + \frac{u'}{R}$$

For the case of bending two equal end moments M_0 are applied. The directions x' , y' , z' are the local directions of the axes. The projection of M_0 to these axes:

$$M_{z'} = M_0 \phi \quad M_{y'} = M_0 \quad M_{x'} = M_0 u'$$

Combining these equations the differential equations for bending are obtained:

$$\phi M_0 = EI_z \left(\frac{\phi}{R} - u'' \right)$$

$$M_0 = EI_y \left(\frac{v}{R^2} + v'' \right)$$

$$M_0 u' = GJ \left(\phi' + \frac{u'}{R} \right)$$

M_{cr} can be obtained by eliminating u from the first and the third equation and solving the differential equation for ϕ .

For the case of uniform compression the Euler buckling load can be determined in a similar way.

B.3 Vlasov

Vlasov uses like Timoshenko the method of equilibrium. As can be seen in [4] he starts with six equilibrium equations and reduces them till three by eliminating the forces.

$$\frac{dQ_z}{dx} + \frac{N}{R} + q_z = 0 \quad \frac{dM_z}{dx} + Q_y + \frac{H}{R} = 0 \quad M_y''' + \frac{M_y'}{R^2} + q_z' + \frac{q_x}{R} = 0$$

$$\frac{dQ_y}{dx} + q_y = 0 \quad \frac{-dM_y}{dx} + Q_z = 0 \quad \text{leads to:} \quad M_z'' + \frac{H'}{R} - q_y = 0$$

$$\frac{dN}{dx} - \frac{Q_z}{R} - q_x = 0 \quad \frac{dH}{dx} - \frac{M_z}{R} + m = 0 \quad \frac{-M_z}{R} + H' + m = 0$$

with :

- $Q_{x,y,z}$ are the forces in the directions of the axes
- $q_{x,y,z}$ are the projections of the external loads per unit length
- $M_{x,y,z}$ are the bending moments in the cross section
- N is the normal force in the cross section
- H is the torsional moment in the cross section
- m is the externally applied torsional moment

Replacing the following terms:

$$M_y = EI_y v'' \quad q_y = -Pu'' + M_y \phi''$$

$$M_z = -EI_z u'' \quad q_z = -Pv''$$

$$H = -EI_w \phi''' + GJ\phi' \quad q_x = 0$$

$$m = M_y u'' - r^2 P \phi''$$

Leads to the general stability equations for a part of a circular beam with a double symmetric section:

$$-EI_y \left(v'''' + \frac{v''}{R^2} \right) + P v'' = 0$$

$$-EI_z u'''' - P u'' - EI_w \frac{\phi''''}{R} + GJ \frac{\phi''}{R} + M_y \phi'' = 0$$

$$-EI_z \frac{u''}{R} - M_y u'' + EI_w \phi'''' + r^2 P \phi'' - GJ \phi'' = 0$$

When a displacement field for ϕ and u is assumed in the last two equations, the critical bending moment and critical compression force can be determined.

B.4 Yoo

Yoo uses the energy method [5,6]. His starting point is the total potential energy for a straight beam. The curvatures and twist of a straight beam are replaced by those of a curved beam, to get the total potential energy for an arch. In Figure B.1 the translation of the axes is shown from Yoo's model to the standard arch.

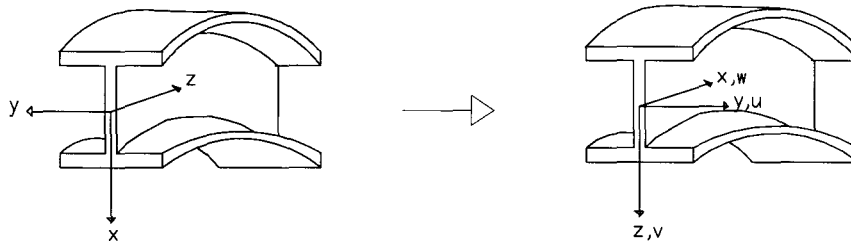


Figure B.1 Translation of the main axes

Curvatures and twist for a straight beam replaced by those for a curved beam:

$$P_x = EA w' \Rightarrow EA \left(w' + \frac{v}{R} \right)$$

$$M_y = EI_y v'' \Rightarrow EI_y \left(v'' + \frac{v}{R^2} \right)$$

$$M_z = EI_z u'' \Rightarrow EI_z \left(u'' + \frac{\phi}{R} \right)$$

$$T_s = GJ \phi' \Rightarrow GJ \left(\phi' - \frac{u'}{R} \right)$$

$$M_\omega = EI_w \phi'' \Rightarrow EI_w \left(\phi'' - \frac{u''}{R} \right)$$

After adapting the directions of the axes to the standard directions (see Figure B.1 Translation of the main axes), the total potential energy for a straight beam with double symmetric cross-section according to Yoo becomes:

$$\pi = U + V$$

$$U = \frac{1}{2} \int_0^L \{ EA(w')^2 + EI_y(v'')^2 + EI_z(u'')^2 + EI_w(\phi'')^2 + GJ(\phi')^2 \} dx$$

$$V = \frac{1}{2} \int_0^L \{ P_x(v'^2 + u'^2 + r^2\phi'^2) + 2M_y u''\phi \} dx$$

$$\text{with } P_x = q_x \cdot R$$

The terms u'' , ϕ' and ϕ'' are replaced by the terms according to the equations above. For u' there is no good substitute. Yoo rewrites this to:

$$(u')^2 = uu'' = u \left(u'' + \frac{\phi}{R} \right)$$

The total potential energy for a curved beam according to Yoo:

$$\begin{aligned} \pi = & \frac{1}{2} \int_0^L \left\{ EA \left(w' - \frac{v}{R} \right)^2 + EI_y \left(v'' + \frac{v}{R^2} \right)^2 + EI_z \left(u'' + \frac{\phi}{R} \right)^2 + EI_w \left(\phi'' - \frac{u''}{R} \right)^2 + GJ \left(\phi' - \frac{u'}{R} \right)^2 \right\} dx \\ & + \frac{1}{2} \int_0^L \left\{ P_x \left[v \left(v'' + \frac{v}{R^2} \right) + u \left(u'' + \frac{\phi}{R} \right) + r^2 \left(\phi' - \frac{u'}{R} \right)^2 \right] + 2M_y \left(u'' + \frac{\phi}{R} \right) \phi + 2M_z \left(v'' + \frac{v}{R^2} \right) \right\} dx \end{aligned}$$

The two differential equations for out-of-plane buckling are:

$$EI_z \left(u'' + \frac{\phi}{R} \right)'' - \frac{EI_w}{R} \left(\phi'' - \frac{u''}{R} \right)'' + \frac{GJ}{R} \left(\phi' - \frac{u'}{R} \right)' + P \left(u'' + \frac{\phi}{2R} - \frac{r^2}{R} \left(\frac{u''}{R} - \phi'' \right) \right) + (M\phi)'' = 0$$

$$\frac{EI_z}{R} \left(u'' + \frac{\phi}{R} \right) + EI_w \left(\phi'' - \frac{u''}{R} \right)'' - GJ \left(\phi' - \frac{u'}{R} \right)' + \frac{Pu}{2R} - Pr^2 \left(\phi'' - \frac{u''}{R} \right) + M \left(\frac{2\phi}{R} + u'' \right) = 0$$

When $(u')^2$ is not substituted for $u \left(u'' + \frac{\phi}{R} \right)$, the differential equations for out-of-plane buckling are:

$$EI_z \left(u'' + \frac{\phi}{R} \right)'' - \frac{EI_w}{R} \left(\phi'' - \frac{u''}{R} \right)'' + \frac{GJ}{R} \left(\phi' - \frac{u'}{R} \right)' + P \left(-u'' - \frac{r^2}{R} \left(\frac{u''}{R} - \phi'' \right) \right) + (M\phi)'' = 0$$

$$\frac{EI_z}{R} \left(u'' + \frac{\phi}{R} \right) + EI_w \left(\phi'' - \frac{u''}{R} \right)'' - GJ \left(\phi' - \frac{u'}{R} \right)' - Pr^2 \left(\phi'' - \frac{u''}{R} \right) + M \left(\frac{2\phi}{R} + u'' \right) = 0$$

For the arch under uniform bending, the Euler buckling load does not change.

For u and ϕ , a sinus-shape displacementfield is assumed. The differential equations for an arch under uniform compression could be rewritten to:

$$A \left[EI_z \frac{\pi^2}{L^2} + \frac{EI_w \pi^2}{R^2 L^2} + \frac{GJ}{R^2} + P \left(1 + \frac{r^2}{R^2} \right) \right] + B \left[-\frac{EI_z}{R} - \frac{EI_w \pi^2}{R L^2} - \frac{GJ}{R} - P \frac{r^2}{R} \right] = 0$$

$$A \left[-\frac{EI_z}{R} - \frac{EI_w \pi^2}{R L^2} - \frac{GJ}{R} - P \frac{r^2}{R} \right] + B \left[\frac{EI_z L^2}{R^2 \pi^2} + EI_w \frac{\pi^2}{L^2} + GJ + P r^2 \right] = 0$$

To solve P_E :

$$\left[P_z + \frac{P_\phi}{R^2} + P \left(1 + \frac{r^2}{R^2} \right) \right] \left[\frac{P_z L^4}{R^2 \pi^4} + P_\phi + P r^2 \right] - \left[-\frac{P_z L^2}{R \pi^2} - \frac{P_\phi}{R} - P \frac{r^2}{R} \right]^2 = 0$$

$$P = \frac{-B \pm \sqrt{B^2 - 4C}}{2} \quad \text{with} \quad B = -P_\phi - P_z \left(a^4 \frac{R^2}{r^2} + (a^2 - 1)^2 \right) \quad \text{and} \quad C = \frac{M_0^2}{r^2} (a^2 - 1)^2$$

B.5 Trahair & Papangelis

Like Yoo, Trahair uses the energy method. In [7,8,9,10,11] the normal and shear strains for a curved beam are first determined. With these strains the total potential energy is formed. See Figure B.2 for the translation of the main axes from Trahair's model to the standard arch.

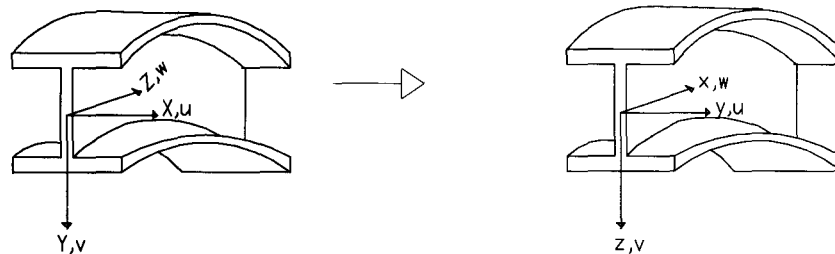


Figure B.2 Translation of the main axes

The adapted normal strain and shear strain according to Trahair are:

$$\varepsilon_x = \frac{R}{R-z} \left[\left(w' - \frac{v}{R} \right) - y \left(u'' + \frac{\phi}{R} \right) - z \left(v'' + \frac{w'}{R} \right) + \alpha_w \left(\phi'' - \frac{u''}{R} \right) \right]$$

$$\gamma = 2t \left[\left(\phi' - \frac{u'}{R} \right) - u' \left(v'' + \frac{v}{R^2} \right) \right]$$

Second order terms are neglected to make a better comparison with other theories.

Trahair mentioned in advance that ϕ and u are not related with v and w . For the out-of-plane buckling only the terms with ϕ and u are of influence. For the energy Trahair already neglected v and w . He used, terms of second order of the normal strain, to get the energy equation.

Total energy for a double symmetric cross-section according to Trahair:

$$\begin{aligned} U_T = & \frac{1}{2} \int_0^1 \left\{ EI_z \left(u'' + \frac{\phi}{R} \right)^2 + EI_w \left(\phi'' - \frac{u''}{R} \right)^2 + GJ \left(\phi' - \frac{u'}{R} \right)^2 \right\} ds \\ & + \frac{1}{2} \int_0^1 P \left\{ (u')^2 + r_x^2 (\phi')^2 + r_y^2 \left(\phi' - \frac{u'}{R} \right)^2 \right\} ds \\ & + \frac{1}{2} \int_0^1 \left\{ M \left(2\phi u'' + \frac{\phi^2}{R} \right) \right\} ds = 0 \end{aligned}$$

The two differential equations for out-of-plane buckling are according to Trahair:

$$EI_z \left(u'' + \frac{\phi}{R} \right)'' - \frac{EI_w}{R} \left(\phi'' - \frac{u''}{R} \right)'' + \frac{GJ}{R} \left(\phi' - \frac{u'}{R} \right)' - P u'' - P \frac{r_y^2}{R} \left(\frac{u''}{R} - \phi'' \right) + (M\phi)'' = 0$$

$$\frac{EI_z}{R} \left(u'' + \frac{\phi}{R} \right) + EI_w \left(\phi'' - \frac{u''}{R} \right) - GJ \left(\phi' - \frac{u'}{R} \right)' - P r^2 \phi'' + P r_y^2 \frac{u''}{R} + M \left(\frac{\phi}{R} + u'' \right) = 0$$

To obtain the Euler buckling load, Trahair ignores the terms r^2/R^2 and r_y^2/R^2 , because they are small compared to unity.

B.6 Rajasekaran & Padmanabhan

Rajasekaran uses more or less the same approach as Trahair. Instead of deriving the equation for total potential energy, he works with the principle of virtual displacement [12]. See Figure B.3 for the translation of the main axes.

$$\int_V \sigma \delta \epsilon dv = \int_S t \delta u ds$$

The normal strain and shear strain are according to Rajasekaran are:

$$\epsilon_x = \frac{R}{R-z} \left[\left(w' - \frac{v}{R} \right) - y u'' - z \left(v'' + \frac{w'}{R} \right) + \alpha_w \left(\phi'' - \frac{u''}{R} \right) \right]$$

$$\gamma = 2\eta \left(\phi' - \frac{u'}{R} \right)$$

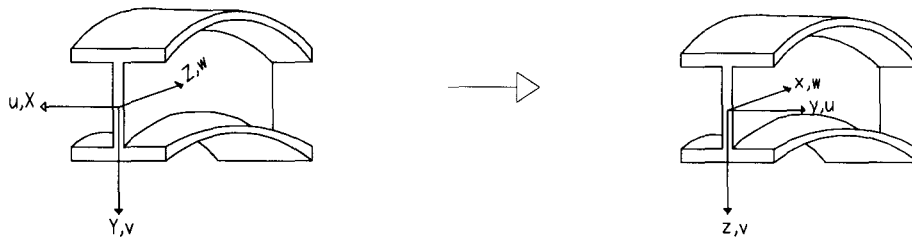


Figure B.3 Translation of the main axes

Integrating leads to four equilibrium equations.

With the boundary conditions of this case:

$$EI_z \left(u'' + \frac{\phi}{R} \right)'' - \frac{EI_w}{R} \left(\phi'' - \frac{u''}{R} \right)'' + \frac{GJ}{R} \left(\phi' - \frac{u'}{R} \right)' - (Pu')' - M \left(\phi'' - \frac{u''}{R} \right) = 0$$

$$EI_y \left(v'' + \frac{w'}{R} \right)'' - \frac{EA}{R} \left(w' - \frac{v}{R} \right)' - (Pv')' - \frac{(Pw)'}{R} - \frac{(Mv)'}{R} - \frac{(Mw)'}{R^2} + \frac{Pv}{R^3} + \frac{M\phi}{R^2} = q_z$$

$$EA \left(w' - \frac{v}{R} \right)' - \frac{EI_y}{R} \left(v'' + \frac{w'}{R} \right)' + \frac{Pv'}{R} + \frac{Pw}{R^2} + \frac{M}{R^2} \left(v' + \frac{w}{R} \right) = 0$$

$$EI_w \left(\phi'' - \frac{u''}{R} \right)'' + \frac{EI_z}{R} \left(u'' + \frac{\phi}{R} \right)'' - GJ \left(\phi' - \frac{u'}{R} \right)' - M \left(\frac{\phi}{R} + u'' \right) = 0$$

From these equations can be seen that the in-plane stability and out-of-plane stability can be look at separately. The second and third equations describe the in-plane stability, because they are only dependent on v and w . The first and last equations describe the out-of-plane stability, they are only dependent on ϕ and u .

In paragraph 3.1.1.5, the critical q -load has been reproduced according to the critical load in the literature of Rajasekaran [12]. When the just mentioned differential equations are solved another solution is found.

Differential equations for out-of-plane stability of an arch under uniform compression:

$$EI_z \left(u'' + \frac{\phi}{R} \right)'' - \frac{EI_w}{R} \left(\phi'' - \frac{u''}{R} \right)'' + \frac{GJ}{R} \left(\phi' - \frac{u'}{R} \right)' - (Pu')' = 0$$

$$\frac{EI_z}{R} \left(u'' + \frac{\phi}{R} \right) + EI_w \left(\phi'' - \frac{u''}{R} \right) - GJ \left(\phi' - \frac{u'}{R} \right) = 0$$

With a sinus-shaped displacementfield for u and ϕ this becomes:

$$A \left[P_z + \frac{P_\phi}{R^2} + P \right] + B \left[-\frac{P_z L^2}{R \pi^2} - \frac{P_\phi}{R} \right] = 0$$

$$A \left[-\frac{P_z L^2}{R \pi^2} - \frac{P_\phi}{R} \right] + B \left[\frac{P_z L^4}{R^2 \pi^4} + P_\phi \right] = 0 \quad \Rightarrow \quad \begin{bmatrix} P_z + \frac{P_\phi}{R^2} + P & -\frac{P_z L^2}{R \pi^2} - \frac{P_\phi}{R} \\ -\frac{P_z L^2}{R \pi^2} - \frac{P_\phi}{R} & \frac{P_z L^4}{R^2 \pi^4} + P_\phi \end{bmatrix} \begin{bmatrix} A \\ B \end{bmatrix} = 0$$

The solution is:

$$P = \frac{P_z P_\phi (a^2 - 1)^2}{P_z a^4 R^2 + P_\phi}$$

This can be rewritten to:

$$q^*_{*E} = \frac{M_0 (a^2 - 1)^2}{\frac{a}{b} R^2 + ab R^2}$$

To compare the results to the ones of Trahair [11], Rajasekaran introduced afterwards the factor r^2 in the solution of the differential equation [12]. Due to this a factor r^2 appears in the solution.

Trahair on the contrary neglect the terms related to the radii of gyration. The solution q^*_{*E} is the same as the solution of Trahair in which the terms related to the radii of gyration are neglected.

Trahair's solution:

$$q_E = \frac{P_z}{R} ab \left(\left(ab + \frac{1}{ab} \right) - \frac{\left(b + \frac{1}{b} \right)^2}{\frac{a}{b} + \frac{b}{a}} \right) = \frac{P_z}{R} ab \left(\frac{\left(ab + \frac{1}{ab} \right) \left(\frac{a}{b} + \frac{b}{a} \right)}{\frac{a}{b} + \frac{b}{a}} - \frac{b^2 + 2 + \frac{1}{b^2}}{\frac{a}{b} + \frac{b}{a}} \right) = \frac{P_z}{R} ab \left(\frac{a^2 - 2 + \frac{1}{a^2}}{\frac{a}{b} + \frac{b}{a}} \right)$$

Rajasekaran:

$$q^*_{*E} = \frac{M_0 (a^2 - 1)^2}{\frac{a}{b} R^2 + ab R^2} = \frac{P_z L b}{\pi} \frac{(a^2 - 1)^2}{R^2 \left(\frac{a}{b} + ab \right)} = \frac{P_z}{R} ab \left(\frac{a^4 - 2a^2 + 1}{a^2 \left(\frac{a}{b} + \frac{b}{a} \right)} \right) = \frac{P_z}{R} ab \left(\frac{a^2 - 2 + \frac{1}{a^2}}{\frac{a}{b} + \frac{b}{a}} \right)$$

B.7 Yang & Kuo

Like Rajasekaran the model of Yang in [13,14,15,16] is based on the principle of virtual work. See Figure B.4 for the translation of the main axes.

The strains Yang uses to get the equilibrium equations are:

$$\varepsilon_x = \frac{R}{R-z} \left[\left(w' - \frac{v}{R} \right) - y \left(u'' + \frac{\phi}{R} \right) - z \left(v'' + \frac{w'}{R} \right) - \alpha_w \left(\phi'' - \frac{u''}{R} \right) \right]$$

$$\gamma = 2\eta \left(\phi' - \frac{u'}{R} \right)$$

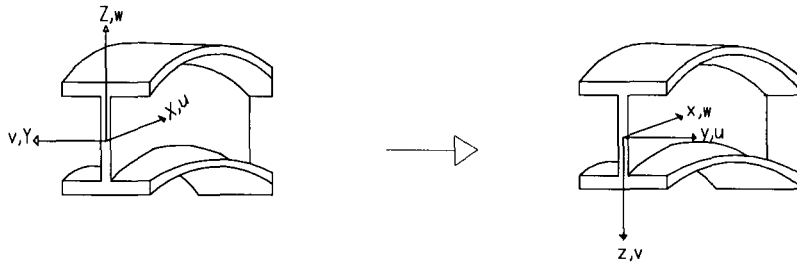


Figure B.4 Translation of the main axes

The equation from which Yang derives his equilibrium equations is:

$$\begin{aligned} & \frac{1}{2} \int_0^1 \left\{ EI_z \delta \left(u'' + \frac{\phi}{R} \right)^2 + EI_w \delta \left(\phi'' + \frac{\phi}{R^2} \right)^2 + GJ \delta \left(\phi' - \frac{u'}{R} \right)^2 \right\} ds \\ & \frac{1}{2} \int_0^1 \left\{ P \delta \left((u')^2 + r^2 \left(\phi' - \frac{u'}{R} \right)^2 \right) \right\} ds \\ & - \frac{1}{2} \int_0^1 \left\{ M \delta \left(2\phi' u' - \frac{(u')^2}{R} + \frac{r^2}{R} \left(\phi' - \frac{u'}{R} \right)^2 \right) + \frac{\phi^2}{R} \right\} ds = 0 \end{aligned}$$

The two differential equations for out-of-plane buckling are according to Yang:

$$EI_z \left(u'' + \frac{\phi}{R} \right)'' + \frac{GJ}{R} \left(\phi' - \frac{u'}{R} \right)' - P u'' - P \frac{r^2}{R} \left(\frac{u''}{R} - \phi'' \right) + M \left(\phi'' - \frac{u''}{R} \right) \left(1 - \frac{r^2}{R^2} \right) = 0$$

$$\frac{EI_z}{R} \left(u'' + \frac{\phi}{R} \right) + EI_w \left(\phi'''' + \frac{2\phi''}{R^2} + \frac{\phi}{R^4} \right) - GJ \left(\phi' - \frac{u'}{R} \right)' - P r^2 \left(\phi'' - \frac{u''}{R} \right) - M \frac{r^2}{R} \left(\frac{u''}{R} - \phi'' \right)$$

$$+ M \left(\frac{\phi}{R} + u'' \right) = 0$$

B.8 Influence of warping

The Euler buckling loads for the loadcases uniform compression and uniform bending are given in Table B.1 and Table B.2 respectively. For each loadcase an analytical and a numerical solution are given. The analytical Euler buckling loads without warping influence are according to Timoshenko's model. The analytical Euler buckling loads with the influence of warping are according the model of Trahair. For the numerical results the beam element model is used to omit the warping influence and the shell element model gives results with warping influence.

It is remarkable that for both calculation methods, the Euler buckling loads without warping influence are very similar. The results with warping influence are not that corresponding, especially for larger cross sections. This is an indication that the effect of warping is differently included in the two calculation methods.

When the cross section of the arch is small the analytical results with warping do not differ much from the numerical results and the influence of warping is small. For the more stocky arches the results of the two calculation methods differ and the influence of the warping rigidity is considerable. A parallel can be seen: for a decreasing slenderness, the warping influence increases and the discrepancy between the results of the two calculation methods increases also.

Table B.1 Euler buckling loads for uniform compression

profile	analytical		numerical	
	without warping	with warping	without warping	with warping
IPE 100*	26.7 N/m	27.0 N/m	26.7 N/m	27.0 N/m
IPE 180*	123 N/m	128 N/m	123 N/m	127 N/m
IPE 500*	2250 N/m	3160 N/m	2257 N/m	2813 N/m
IPE 600*	4110 N/m	6090 N/m	4122 N/m	5313 N/m

Table B.2 Euler buckling loads for uniform bending

profile	analytical		numerical	
	without warping	with warping	without warping	with warping
IPE 100*	344 Nm	347 Nm	-	347 N/m
IPE 180*	1570 Nm	1645 Nm	-	1636 N/m
IPE 500*	28900 Nm	41240 Nm	-	36340 N/m
IPE 600*	52700 Nm	80300 Nm	-	69140 N/m

In Figure B.5 the relative influence of warping is given in a column diagram. The relative influence of warping means the difference between the Euler buckling loads with and without warping, related to the loads without warping. In this figure it is very clear to see that for stocky arches the influence of warping is considerable. For the loadcase uniform bending, the influence of warping is according the analytical models 50%. The influence in the numerical models is smaller but still 28%. Therefore, for stocky arches it is worth the effort to take into account the warping influence.

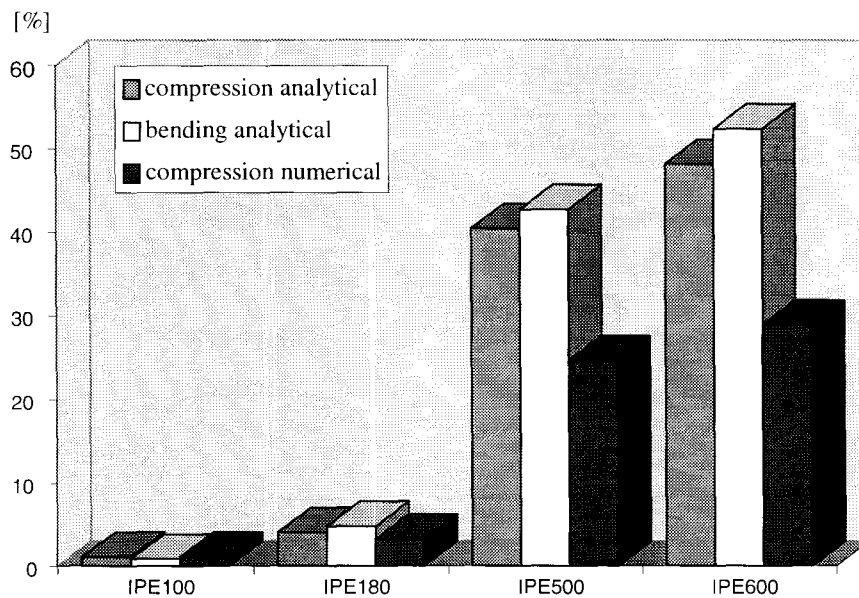


Figure B.5 Relative influence of warping

C. SHELL ELEMENT FEM MODEL

C.1 Cross section properties shell element model

As mentioned in chapter 3 the profile IPE100* created with shell-elements has not the same properties as a common IPE100 profile. In Figure C.1 the difference in cross-section can be seen: For an IPE100 the link between the web and the flange is round. The profile created with shell elements has not these roundings. Another difference is the small overlap of the shell elements at the top and bottom of the web element. The rigidities of the IPE100* profile created with shell elements can be calculated according to the dimensions of the cross-section.

The values of the IPE100* profile are:

$$A = (100 - 5.7) * 4.1 + 2(55 * 5.7) = 1014 \text{ mm}^2$$

$$I_y = \frac{1}{12} * 4.1 * (94.3)^3 + 2 \left(\frac{1}{12} * 55 * (5.7)^3 + 5.7 * 55 * (47.15)^2 \right) = 168,23 \cdot 10^4 \text{ mm}^4$$

$$I_z = \frac{1}{12} * 94.3 * (4.1)^3 + 2 \left(\frac{1}{12} * 5.7 * 55^3 \right) = 15.86 \cdot 10^4 \text{ mm}^4$$

$$J = \frac{1}{3} * 94.3 * (4.1)^3 + 2 \left(\frac{1}{3} * 55 * (5.7)^3 \right) = 8957 \text{ mm}^4$$

$$I_w = \frac{1}{24} * 5.7 * 94.3^2 * 55^3 = 351 \cdot 10^6 \text{ mm}^6$$

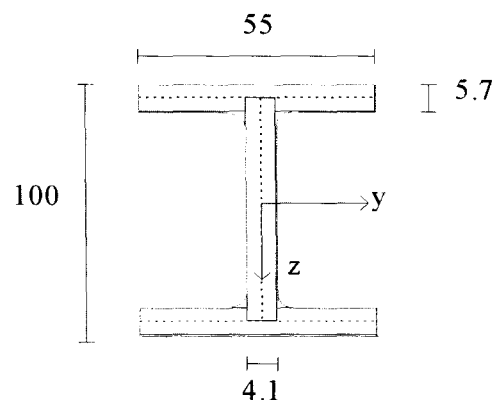
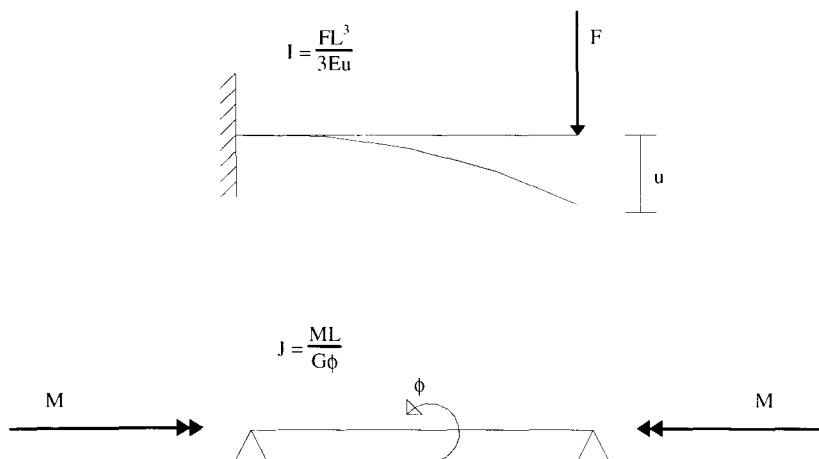


Figure C.1 Created "IPE100" profile

Table C.1 Profile properties

IPE	I_y	I_z	A	J	J_2	I_w
100*	1.68E+06	1.59E+05	1014	8957	8486	3.51E+08
140*	5.39E+06	4.49E+05	1633	20590	19612	1.98E+09
180*	1.30E+07	1.01E+06	2368	39600	37848	7.43E+09
220*	2.71E+07	2.04E+06	3268	71540	68491	2.27E+10
270*	5.61E+07	4.19E+06	4469	120400	115774	7.06E+10
330*	1.14E+08	7.86E+06	6069	207000	199055	1.99E+11
400*	2.23E+08	1.31E+07	8184	377200	361375	4.90E+11
500*	4.71E+08	2.14E+07	11340	717300	687811	1.25E+12
600*	9.02E+08	3.38E+07	15330	1341000	1270610	2.85E+12

When the values determined in this way, are introduced in the analytical calculation method, the results do not correspond with the results from numerical results. A straight beam model with shell elements is made to check the calculated properties. To determine the moment of inertia around the y-axis, I_y , the beam is inclined at one end and a force in the y direction is applied at the other end. From the displacement in the y direction, I_y can be obtained. For I_z the same procedure can be followed with a force in the z-direction. See Figure C.2. For J the beam is not inclined but the rotation in the middle of the beam is prevented. When two equal end moments are applied, the torsion moment of inertia, J can be determined from the rotation around the axis of the beam. For this property different values are found, compared to the values determined from the cross section. In Table C.1 these values are indicated as J_2 . These are the values which should be introduced in the analytical models.

**Figure C.2 Determination of the rigidities**

C.2 Preliminary investigation shell element model

The preliminary investigation of the shell element model concerns two aspects. The number of elements needed is investigated and the conditions are checked.

In Table C.2 and Table C.3 Euler buckling loads are given for models with an increasing number of elements and different conditions. For the first row of results no special conditions are added to prevent the end of the arch to deform. For the next two rows of results, the arches have beam elements on the edges, at the supports. The stiffness of these beam elements is varied to find out the influence of the stiffness on the results. The last row of results represents an arch without beam elements. The deformations of the arch edges are in this case prevented by tyings, prescribed deformations.

Properties beam elements	n = 200	n = 300	n = 400	n = 500
$I_y = I_z = 0 \text{ mm}^4$	26.70 N/m	26.65 N/m	26.61 N/m	26.58 N/m
$I_y = I_z = 10^5 \text{ mm}^4$	26.97 N/m	26.97 N/m	26.97 N/m	26.97 N/m
$I_y = I_z = 10^6 \text{ mm}^4$	26.97 N/m	26.97 N/m	26.97 N/m	26.97 N/m
with tyings	27.12 N/m	27.12 N/m	27.10 N/m	27.09 N/m

Table C.2 Euler buckling loads for varying number of elements and varying conditions, loadcase 1

Properties beam elements	n = 200	n = 300	n = 400	n = 500
$I_y = I_z = 0 \text{ mm}^4$	344 Nm	343 Nm	342 Nm	342 Nm
$I_y = I_z = 10^5 \text{ mm}^4$	347 Nm	347 Nm	347 Nm	347 Nm
$I_y = I_z = 10^6 \text{ mm}^4$	347 Nm	347 Nm	347 Nm	347 Nm
with tyings	349 Nm	349 Nm	349 Nm	349 Nm

Table C.3 Euler buckling loads for varying number of elements and varying conditions, loadcase 2

Conclusions

The model without any measures to prevent the edge of the arch of deforming has smaller buckling loads than the other models have. This shows the necessity of using beam elements or tyings.

The Euler buckling loads of the models with varying stiffness of the elements give similar results.

There the stiffness of the beam elements does not effect the Euler buckling load, the beam elements are a good solution to prevent the unwanted deformations. The last possibility, using tyings leads to slightly larger results. There the tyings not for hundred per cent correspond with the wanted situation, the preference is given to use beam elements.

The influence of the number of elements on the Euler buckling loads is very small. For the models with beam elements there is even no difference in results. From these analyses can be concluded that a model with 200 elements can describe buckling of an arch adequately.

In Figure C.3 and Figure C.4 the influence of the number of elements for the different models is given graphically. In these figures it is clear to see that the influence of the number of elements used in the model is very small and that the tyings lead to a larger result as the beam elements.

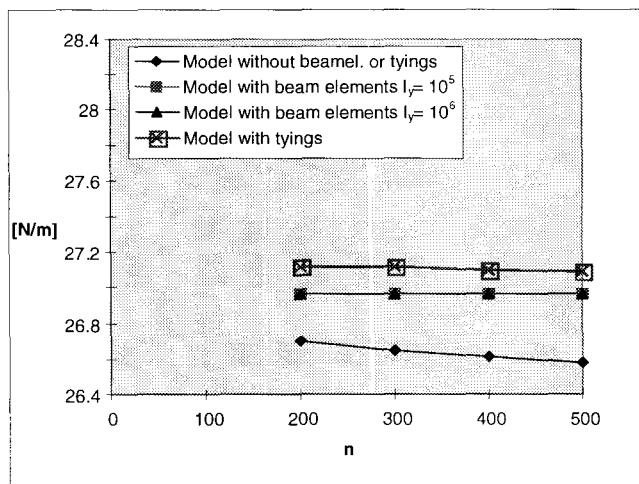


Figure C.3 Influence of number of elements, loadcase 1

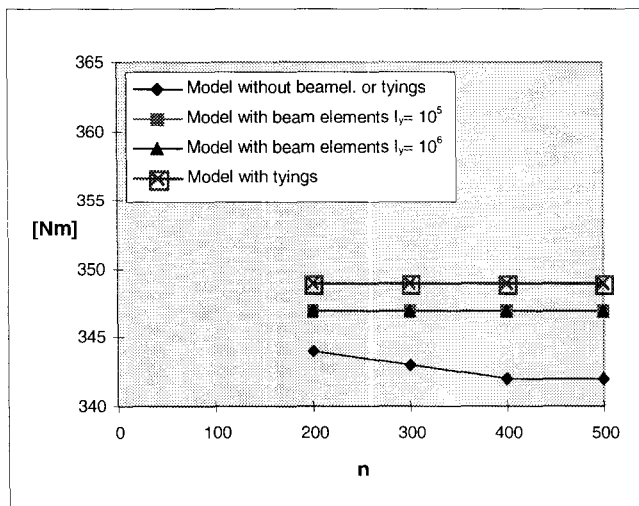


Figure C.4 Influence of number of elements, loadcase 2

C.3 Verifying shell element

It is striking that the results between the analytical and numerical method differ more for larger sections. Also has been shown that the influence of warping is greater for larger sections. It is not for sure that the eight-nodes curved shell elements can describe the warping effect well. Combined these two facts, it is interesting to investigate the capability of shell elements to take into account the influence of warping. For this purpose a straight bar is modelled in DIANA with the same curved shell elements as used for the arch. For a straight beam under uniform bending, the Euler buckling load is known. When the results of DIANA and the analytical load are close to each other, the shell elements probably handle the warping effect well.

In the code NEN 6770 (11.2.5) a factor α_T is defined, which indicates the division of the torsional moment over the twist capacity and the warping capacity of the cross section. α_T lies between one and zero. When α_T is one the influence of the warping is negligible. How closer it gets to zero the bigger is the influence of the warping.

To calculate α_T , first a factor β_T should be calculated.

$$\beta_T = 1 \sqrt{\frac{GJ}{EI_w}}$$

if $\beta_T < 0.7$ then $\alpha_T = 0$

if $\beta_T > 15$ then $\alpha_T = 1$

otherwise $\alpha_T = \frac{\beta_T - 0.7}{14.3}$

The length of the straight beam is 9171 mm and the properties of the cross section are according Table C.1 in appendix D.1.

For the three sections, that will be investigated the α_T values are:

IPE100*¹ $\alpha_T = 1$

IPE330* $\alpha_T = 0.36$

IPE600* $\alpha_T = 0.22$

The first section is not sensible for warping at all. The next two sections show a small value for α_T , the warping plays a part for these sections.

In code NEN 6771 (12.2.5.1) the formula for elastic kip moment is given:

$$M_{ke} = \frac{\pi}{l} \sqrt{E I_z G J \left(1 + \frac{\pi^2 E I_w}{l^2 G J} \right)}$$

¹ IPE100* means a profile with shell elements, which resembles as good as possible a IPE100.

In Table C.4, the results are given for the three sections. As we saw for the arch, the results of DIANA are lower than the results calculated with the analytical determined formula. However the differences for the straight beam are very small. The cause of the differences is not the influence of the warping because the first section is not sensitive for warping and shows the biggest difference. It can be concluded that the shell element used in the FEM model is appropriate to describe warping.

Table C.4 Analytical and numerical results for a straight bar

Section	M_{ke}	DIANA	difference
IPE100*	1649 Nm	1647 Nm	0.12 %
IPE330*	$63.75 \cdot 10^3$ Nm	$63.7 \cdot 10^3$ Nm	0.075 %
IPE600*	$379 \cdot 10^3$ Nm	$378 \cdot 10^3$ Nm	0.00026 %

D. NON-LINEAR ANALYSES

D.1 Numerical results non-linear analyses

In Table D.1 and Table D.2, the ultimate strength of the different arches is given in the first column. The second column represents the Euler buckling value obtained by a DIANA analysis. The relative slenderness can be calculated from the first two columns. In the last column the ultimate load obtained from the non-linear analyses is given.

The shaded rows in Table D.2 indicate that these arches have not a positive post-buckling behaviour. For these arches the characteristic value is also the ultimate load.

Table D.1 Results non-linear analyses, arches with varying cross sections





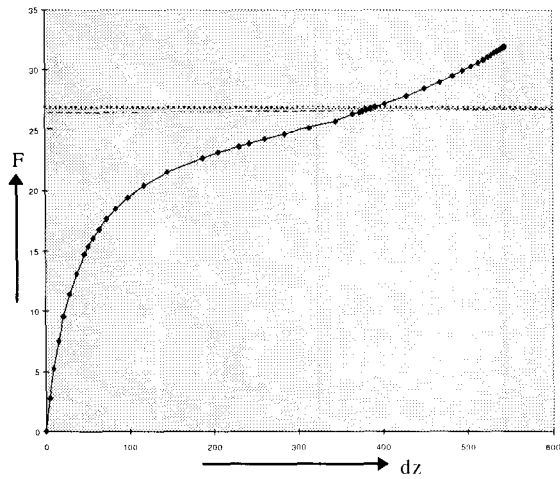
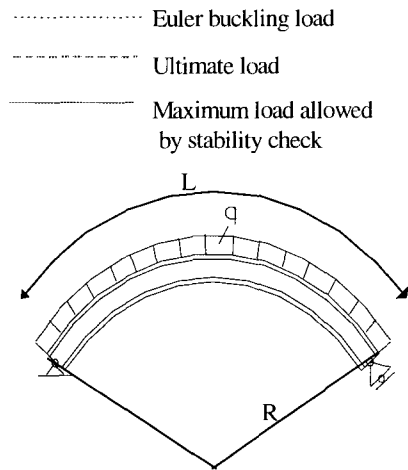
	 Arch length 10m Radius 7m				 Arch length 10m Radius 7m			
IPE	$N_{c,u,d}$	N_{euler}	λ_{rel1}	N_u	$M_{y,u,d}$	M_{euler}	λ_{rel2}	M_u
100	238290	189	35.5	179	9089	347	5.1	342
140	383755	448	29.3	450	20647	824	5.0	822
180	556480	892	24.9	888	38634	1636	4.9	1620
220	767980	1665	21.5	1609	65542	3055	4.6	3051
270	1050215	2971	18.8	2890	110238	5456	4.5	5409
330	1426215	5396	16.2	5284	182400	9921	4.3	9824
400	1923240	10059	13.8	9539	296190	18540	4.0	18460
500	2664900	19691	11.6	19297	504350	36430	3.7	36313
600	3602550	37191	9.8	34887	808700	69140	3.4	69000

Table D.2 Results non-linear analyses, arches with varying dimensions

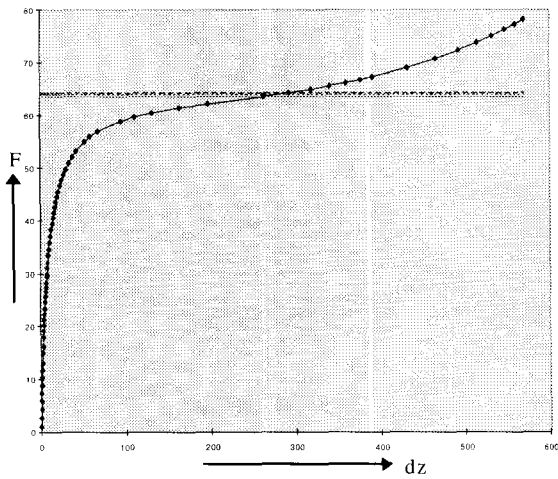
arc-length		Radius	 Profile IPE100				 Profile IPE100			
L	R		$N_{c,u,d}$	N_{euler}	λ_{rel1}	N_u	$M_{y,u,d}$	M_{euler}	λ_{rel2}	M_u
1.25	7.00		238290	182469	1.14	132300	9089	12967	0.84	6430
2.50	7.00		238290	32208	2.72	30306	9089	4436	1.43	4132
3.50	7.00		238290	11725	4.51	11142	9089	2600	1.87	2634
5.00	7.00		238290	3437	8.33	3353	9089	1417	2.53	1440
10.0	5.00		238290	56.7	64.8	55.1	9089	193.3	6.85	195

D.2 Load-displacement diagrams

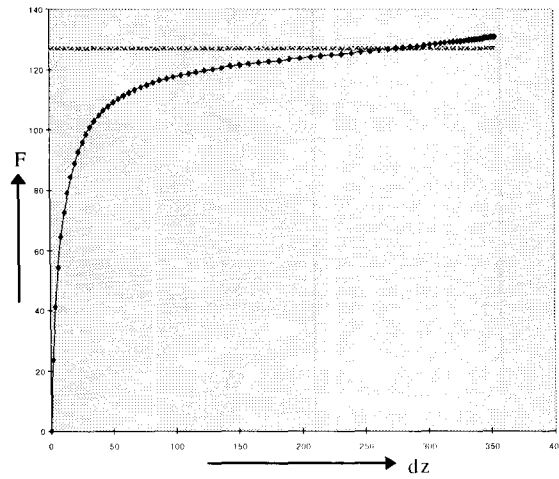
In the next figures the load-displacement diagrams obtained by the non-linear FEM analyses are given. The Euler buckling load, ultimate load and the maximum load allowed by the proposed stability check are also given in these figures. The Euler buckling load given is the numerical Euler buckling load and the stability check is also based on the numerical Euler buckling load.



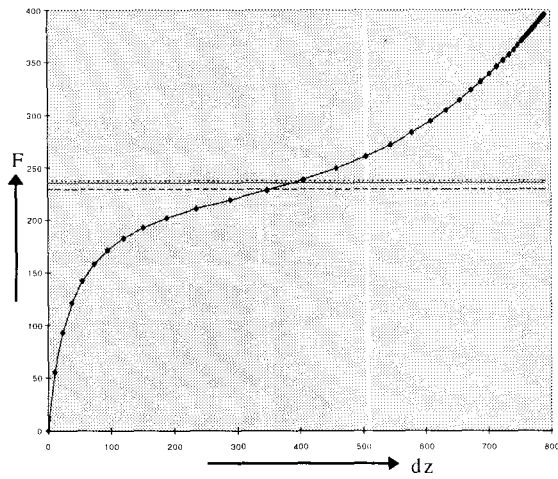
IPE 100 R=7m, L=10m



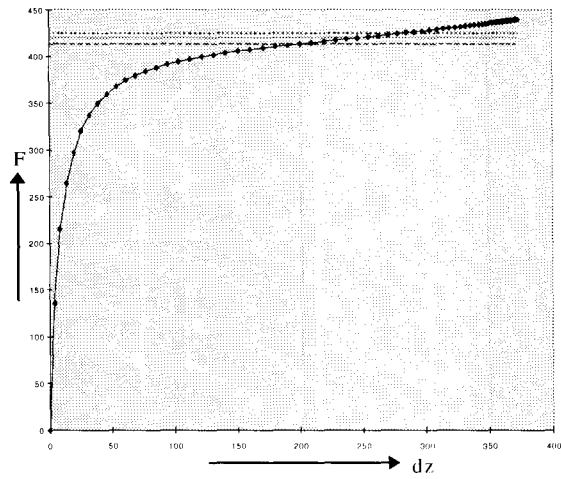
IPE 140 R=7m, L=10m



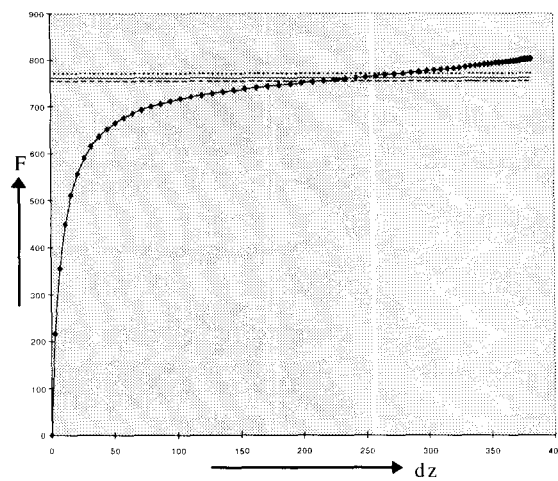
IPE 180 R=7m, L=10m



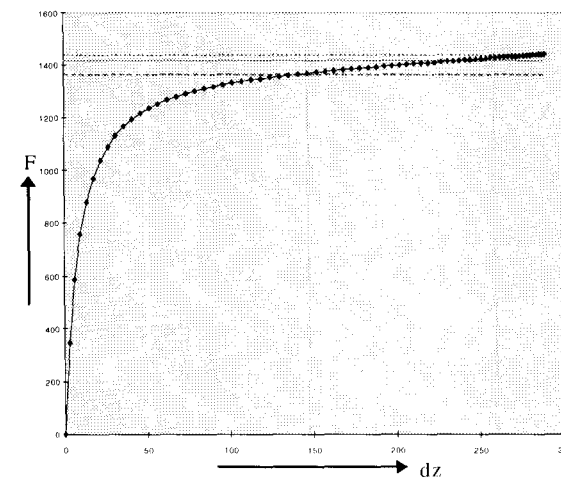
IPE 220 R=7m, L=10



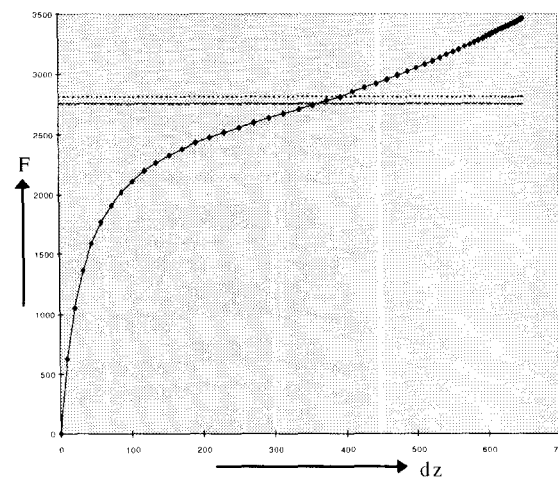
IPE 270 R=7m, L=10m



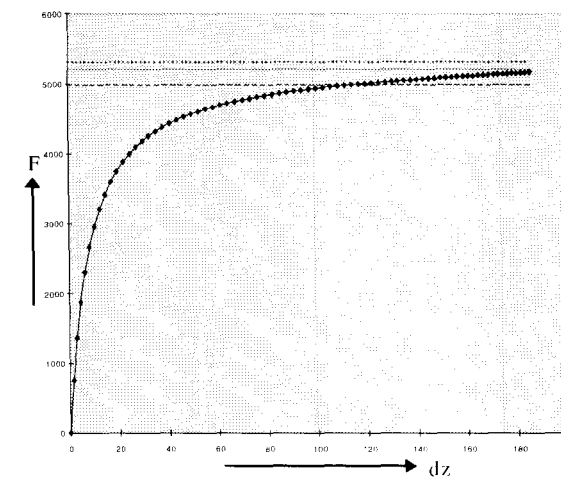
IPE 330 R=7m, L=10m



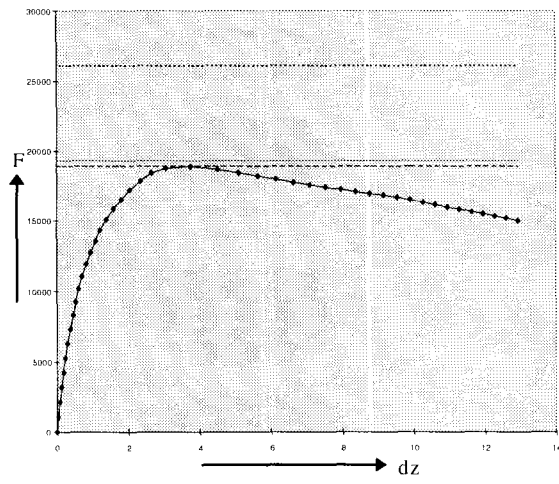
IPE 400 R=7m, L=10



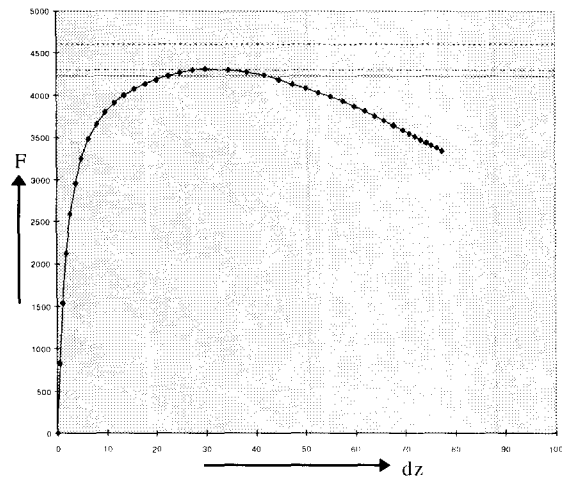
IPE 500 R=7m, L=10m



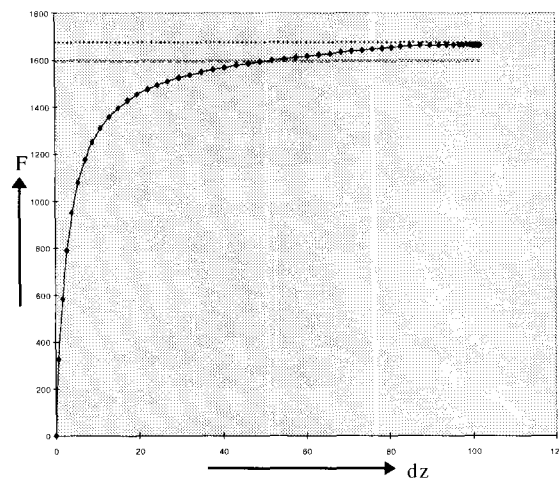
IPE 600 R=7m, L=10m



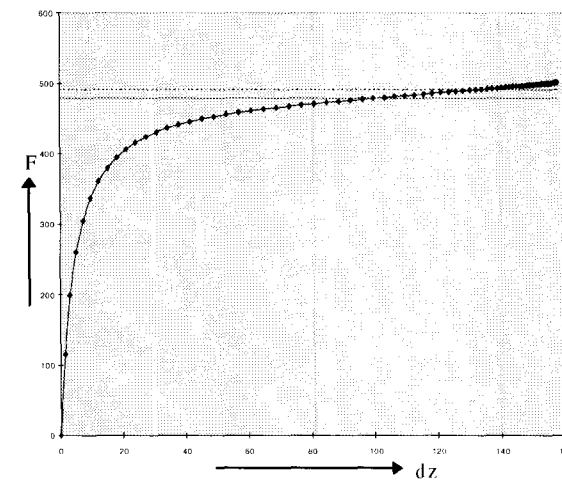
IPE 100 R=7m, L=1.25m



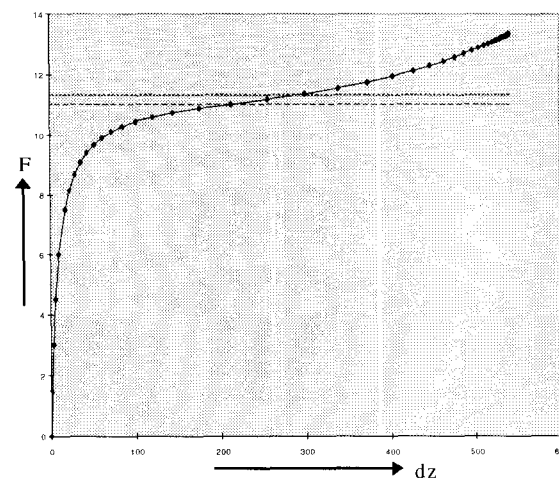
IPE 100 R=7m, L=2.5m



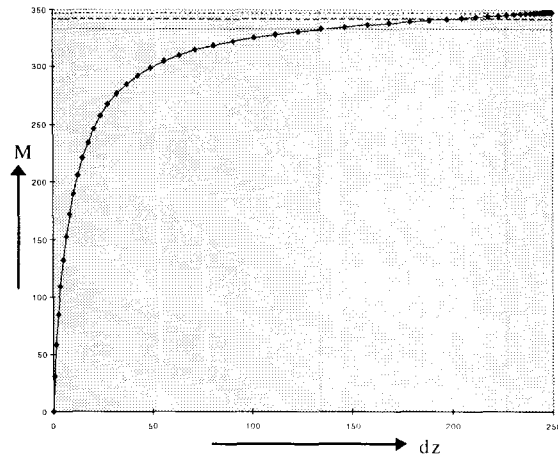
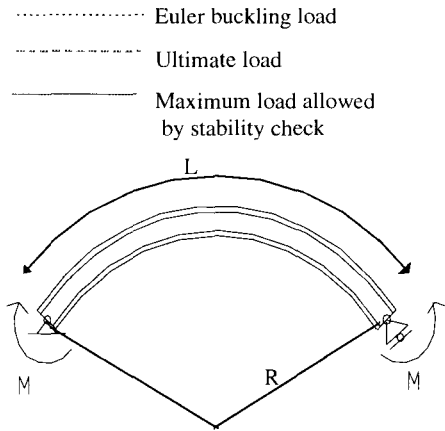
IPE 100 R=7m, L=3.5m



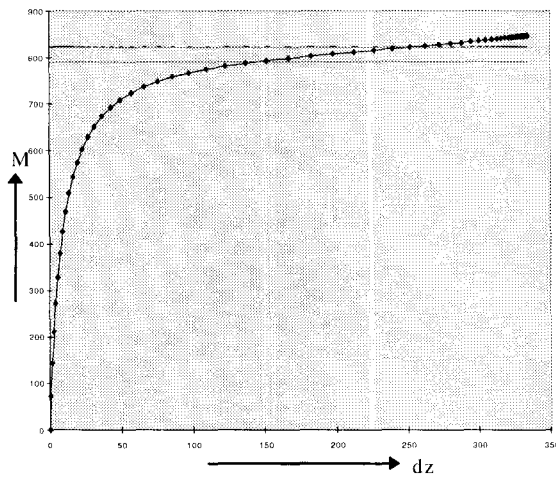
IPE 100 R=7m, L=5m



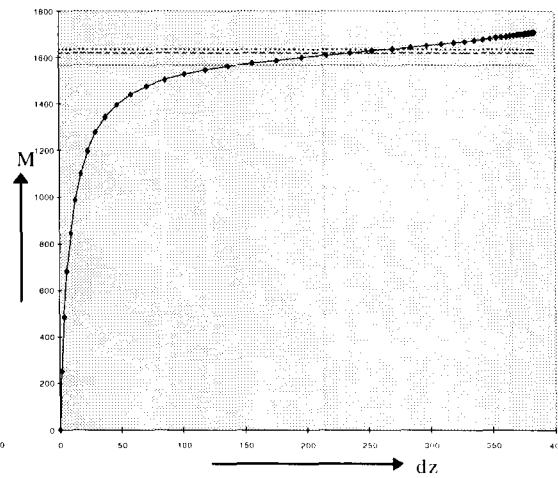
IPE 100 R=5m, L=10m



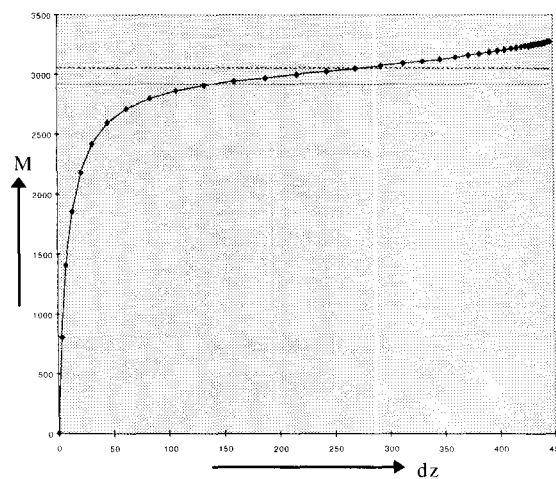
IPE 100 R = 7m, L = 10m



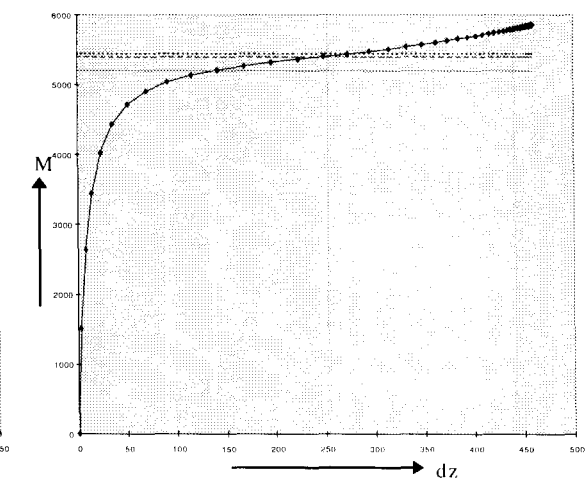
IPE 140 R = 7m, L = 10m



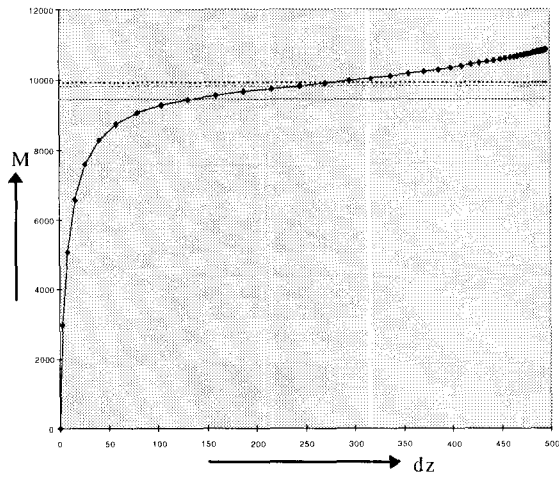
IPE 180 R = 7m, L = 10m



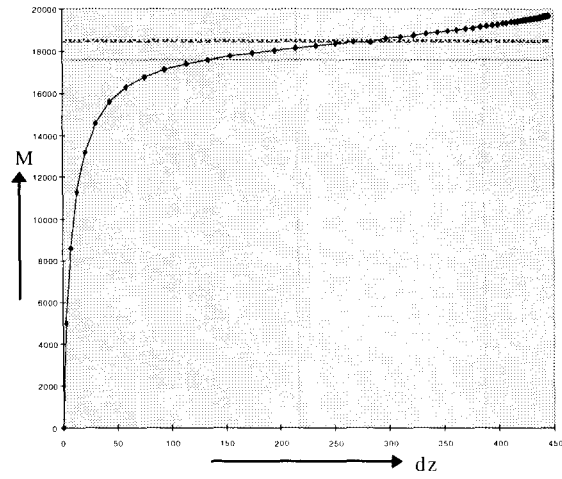
IPE 220 R = 7m, L = 10m



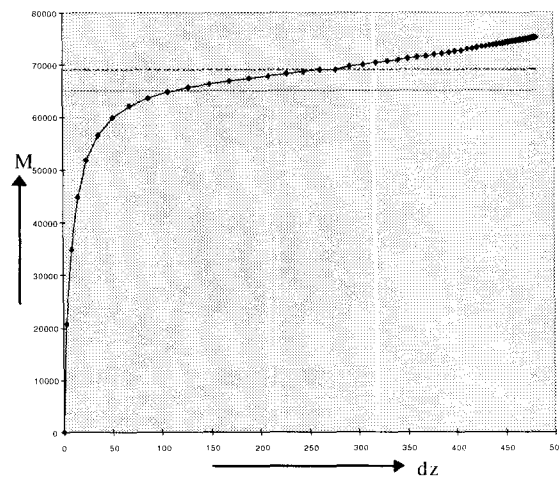
IPE 270 R = 7m, L = 10m



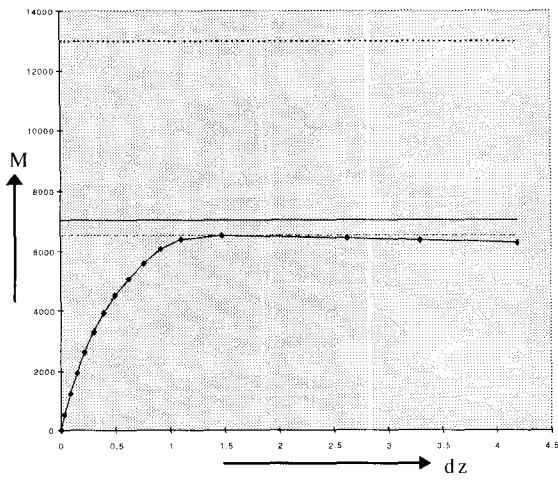
IPE 330 **R =7m, L =10m**



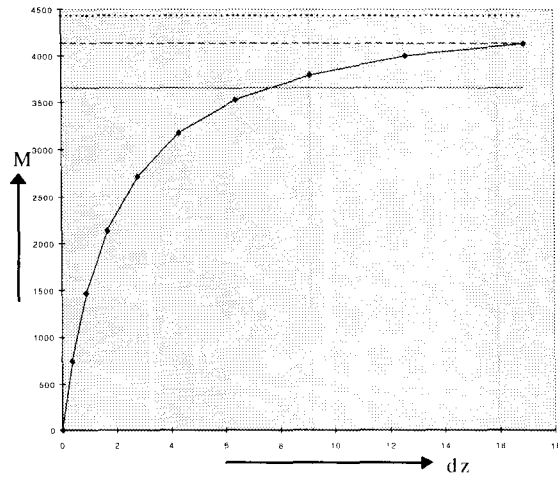
IPE 400 **R =7m, L =10m**



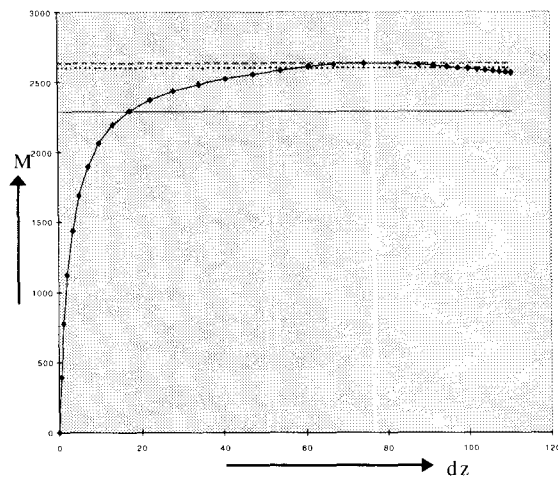
IPE 600 **R =7m, L =10m**



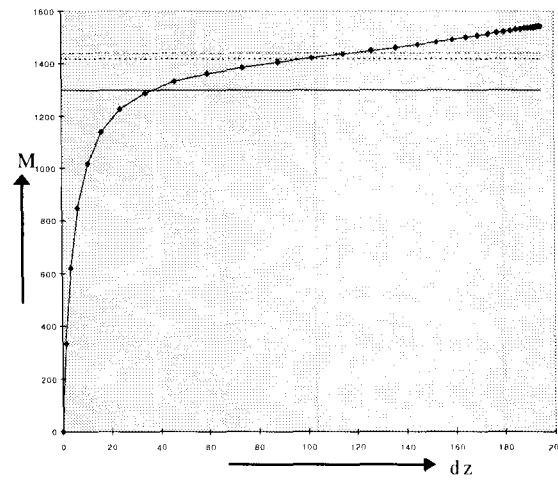
IPE 100 R =7m, L =1.25m



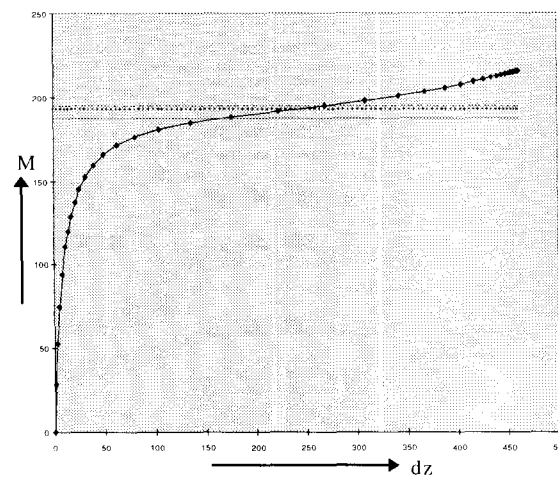
IPE 100 R =7m, L =2.5m



IPE 100 R =7m, L =3.5m



IPE 100 R =7m, L =5m



IPE 100 R =5m, L =10m

E. DIANA FILES

Some DIANA files are given in this appendix. The data file is the file of the standard arch with profile IPE100* and a radius of 7 meters and a length of 10 meters. The linear command files is given and the Euler file for loadcase 1. The last command file is the file with the 5 first steps of the non-linear analysis.

For the three command files the output files are also given. The tabular file of the Euler analysis is given additional to show that the arch buckles out-of-plane.

E.1 Data file

```
FEMGEN MODEL      : IPE100
'COORDINATES'
  1   4.586111E+03  1.758122E+03  .000000E+00
  2   4.083125E+03  1.740193E+03  .000000E+00
  3   3.582700E+03  1.686408E+03  .000000E+00
  4   3.087390E+03  1.597041E+03  .000000E+00
      .
      .
      .
 656  7.248005E+03  1.133988E+03  2.750000E+01
 657  6.782776E+03  1.307646E+03  2.750000E+01
 658  6.306340E+03  1.447654E+03  2.750000E+01
 659  5.821125E+03  1.553298E+03  2.750000E+01
 660  5.329608E+03  1.624040E+03  2.750000E+01
 661  4.834295E+03  1.659521E+03  2.750000E+01
'ELEMENTS'
CONNECTIVITY
  1  CQ40S    1   34    2   45    13   55    12   44
  2  CQ40S    2   35    3   46    14   56    13   45
  3  CQ40S    3   36    4   47    15   57    14   46
  4  CQ40S    4   37    5   48    16   58    15   47
      .
      .
      .
195  CQ40S    606   636   607   647   617   656   616   646
196  CQ40S    607   637   608   648   618   657   617   647
197  CQ40S    608   638   609   649   619   658   618   648
198  CQ40S    609   639   610   650   620   659   619   649
199  CQ40S    610   640   611   651   621   660   620   650
200  CQ40S    611   641   278   321   289   661   621   651
      .
      .
      .
201  L12BE    299   331
202  L12BE    331   288
203  L12BE    288   310
204  L12BE    310   33
205  L12BE    33   246
206  L12BE    246   224
207  L12BE    224   267
208  L12BE    267   235
209  L12BE    171   203
210  L12BE    203   160
211  L12BE    160   182
212  L12BE    182   11
213  L12BE    11   118
214  L12BE    118   96
215  L12BE    96   139
216  L12BE    139   107
217  L12BE    612   642
218  L12BE    642   602
219  L12BE    602   622
```

*]

220 L12BE 622 362
 221 L12BE 362 562
 222 L12BE 562 542
 223 L12BE 542 582
 224 L12BE 582 552
 225 L12BE 492 522
 226 L12BE 522 482
 227 L12BE 482 502
 228 L12BE 502 342
 229 L12BE 342 442
 230 L12BE 442 422
 231 L12BE 422 462
 232 L12BE 462 432
 233 L12BE 11 54
 234 L12BE 54 22
 235 L12BE 22 75
 236 L12BE 75 33
 237 L12BE 342 382
 238 L12BE 382 352
 239 L12BE 352 402
 240 L12BE 402 362

DATA

/ 1-200 / 1

MATERI

/ 1-200 / 1

/ 200-240 / 2

GEOMET

/ 1-20 / 1

/ 101-120 /1

/ 21-100 /2

/ 121-200 /2

/ 201-216 /3

/ 217-232 /4

/ 233-236 /5

/ 237-240 /6

'MATERI'

1 YOUNG 2.1E5
 POISON 0.3
 YIELD VMISES
 YLDVAL 235
 :HARDIA 235. 0.001119 300. 50.
 HARDEN STRAIN
 2 YOUNG 2.1E5
 POISON 0.3

'GEOMET'

1 THICK 4.1
 FLAT
 2 THICK 5.7
 CYLIN 4585.5 -5288.9 0. 0. 0. 1.
 3 ZAXIS -1.1532109 -1.0000 0.0000
 CROSSE 200
 INERTI 1.E6 1.E6 0.1E-7
 4 ZAXIS 1.1532109 -1.0000 0.0000
 CROSSE 200
 INERTI 1.E6 1.E6 0.1E-7
 5 ZAXIS -1.1532109 -1.0000 0.0000
 CROSSE 200
 INERTI 1.E6 1.E6 0.1E-7
 6 ZAXIS -1.1532109 -1.0000 0.0000
 CROSSE 200
 INERTI 1.E6 1.E6 0.1E-7

'DIRECTIONS'

1 1.000000E+00 0.000000E+00 0.000000E+00
 2 0.000000E+00 1.000000E+00 0.000000E+00
 3 0.000000E+00 0.000000E+00 1.000000E+00
 4 1.1532109 1.000000 0.000000
 5 -1.1532109 1.000000 0.000000
 6 0.0000000 0.000000 1.000000

*2

'DATA'

1 NGAUS 2 2 5

*3

'SUPPORTS'

```

/ 352 /      TR  5 6
/ 22 /      TR  1 2 3
/ 11 54 75 33 342 382 402 362 / TR  3

```

*4

'LOADS'

```

CASE 1
ELEMEN

```

*5

```

/ 11-20 /
  EDGE      ETA1
  FORCE      -1E-3
  DIRECT    2

/ 111-120 /
  EDGE      ETA1
  FORCE      -1.5E-3
  DIRECT    2

```

```

CASE 2
NODAL

```

*6

```

11 FORCE 4      10.604454
33 FORCE 4     -10.604454
342 FORCE 5     10.604454
362 FORCE 5     -10.604454

```

```

CASE 3
NODAL

```

```

12 FORCE 3  1
:prestress

```

```

CASE 4
ELEMEN

```

*7

```

/ 1-10 / PRESTR  -20 -20  -20 107 235 235 235 107 0 0 0 0 0 0 0 0
                   0  0  0  0  0  0  0  0  0  0  0  0  0  0  0  0
                   0  0  0  0  0  0  0  0  0  0  0  0  0  0  0  0
                   0  0  0  0  0  0  0  0  0  0  0  0  0  0  0  0
                   0  0  0  0  0  0  0  0  0  0  0  0  0  0  0  0
/ 101-110 /PRESTR -20 -20 -20 107 235 235 235 107 0 0 0 0 0 0 0 0
                   0  0  0  0  0  0  0  0  0  0  0  0  0  0  0  0
                   0  0  0  0  0  0  0  0  0  0  0  0  0  0  0  0
                   0  0  0  0  0  0  0  0  0  0  0  0  0  0  0  0
                   0  0  0  0  0  0  0  0  0  0  0  0  0  0  0  0
/ 11-20 /PRESTR  -235 -235 -235 -107 20 20 20 -107 0 0 0 0 0 0 0 0
                   0  0  0  0  0  0  0  0  0  0  0  0  0  0  0  0
                   0  0  0  0  0  0  0  0  0  0  0  0  0  0  0  0
                   0  0  0  0  0  0  0  0  0  0  0  0  0  0  0  0
                   0  0  0  0  0  0  0  0  0  0  0  0  0  0  0  0
/ 111-120 /PRESTR -235 -235 -235 -107 20 20 20 -107 0 0 0 0 0 0 0 0
                   0  0  0  0  0  0  0  0  0  0  0  0  0  0  0  0
                   0  0  0  0  0  0  0  0  0  0  0  0  0  0  0  0
                   0  0  0  0  0  0  0  0  0  0  0  0  0  0  0  0
                   0  0  0  0  0  0  0  0  0  0  0  0  0  0  0  0
/ 21-60 / PRESTR  -165 -165 -165 -165  0 0 0 -165 0 0 0 0 0 0 0 0
                   0  0  0  0  0  0  0  0  0  0  0  0  0  0  0  0
                   0  0  0  0  0  0  0  0  0  0  0  0  0  0  0  0
                   0  0  0  0  0  0  0  0  0  0  0  0  0  0  0  0
                   0  0  0  0  0  0  0  0  0  0  0  0  0  0  0  0
/ 121-160 /PRESTR -165 -165 -165 -165 -165 -165 -165 -165 00000000
                   0  0  0  0  0  0  0  0  0  0  0  0  0  0  0  0
                   0  0  0  0  0  0  0  0  0  0  0  0  0  0  0  0
                   0  0  0  0  0  0  0  0  0  0  0  0  0  0  0  0
                   0  0  0  0  0  0  0  0  0  0  0  0  0  0  0  0
                   0  0  0  0  0  0  0  0  0  0  0  0  0  0  0  0
/ 61-100 / PRESTR 165 165 165 165 165 165 165 165 00000000
                   0  0  0  0  0  0  0  0  0  0  0  0  0  0  0  0
                   0  0  0  0  0  0  0  0  0  0  0  0  0  0  0  0
                   0  0  0  0  0  0  0  0  0  0  0  0  0  0  0  0
                   0  0  0  0  0  0  0  0  0  0  0  0  0  0  0  0
                   0  0  0  0  0  0  0  0  0  0  0  0  0  0  0  0

```



```

/ 161-200 /PRESTR 165 165 165 165 165 165 165 165 165 00000000
      0 0 0 0 0 0 0 0 0 0 0 0 0 0 0
      0 0 0 0 0 0 0 0 0 0 0 0 0 0 0
      0 0 0 0 0 0 0 0 0 0 0 0 0 0 0
      0 0 0 0 0 0 0 0 0 0 0 0 0 0 0
      0 0 0 0 0 0 0 0 0 0 0 0 0 0 0
/ 21-60 / PRESTR -20 0
      0 0
      0 0
      0 0
      0 0
      0 0
/ 121-160 /
  PRESTR -20 0
      0 0
      0 0
      0 0
      0 0
/ 61-100 /PRESTR 20 0
      0 0
      0 0
      0 0
      0 0
      0 0
/ 161-200 /
  PRESTR 20 0
      0 0
      0 0
      0 0
      0 0
'END'

```

COMMENT

- *1 Beam elements to prevent deformation of the cross section at the end of the arch.
- *2 Direction tangent to the arch in the left support.
- *3 Number of integration points in in the two directions in the plane of the shell and over the depth of the shell.
- *4 Support conditions
- *5 Loadcase uniform compression
- *6 Loadcase uniform bending
- *7 Residual stresses

E.2 Command files

Command file for linear analysis

```

*FILOS
  INITIA MA=100000
*INPUT
*ELASSE
*ELMAT
*LOADS
*ORDER
*SOLVE
*POST
LAYOUT
  CHARAC SI=15
  MODEL.O

```

*]

```

END LAYOUT
:
SELECT
  ELEMENTS ALL /
  END ELEMENTS
END SELECT
:
OUTPUT GRAPHI FI="FRA" *2
  DISPLA GLOBAL
END OUTPUT
:
:SELECT
: NODES / 12-22 55-64 352-361 392-401 /
:END SELECT
:OUTPUT TABULAR *3
: DISPLA TOTAL TRANSLA GLOBAL Z
: DISPLA TOTAL ROTATI GLOBAL X
:END OUTPUT
*END

```

COMMENT

- 1* Specifies the layout of the output graph.
- 2* Generates an output graph with the global displacements of the arch.
- 3* Generates an output file with the global translations and the global rotations

Command file stability analysis

```

*EULER
OUTPUT TABULA
  DISPLA TRANSLA
END OUTPUT
:
EXECUTE
  STRESS ELASTI CA=1 *1
  MODES NM=1 *2
  NODISP *3
  IMPERF.B (1) 9.171 *4
  PERFOR SUBSPA NT=5 MI=30 *5
END EXECUTE
OUTPUT GRAPHI FI="eul" *6
  DISPLA GLOBAL
END OUTPUT
*END

```

COMMENT

- 1* Loadcase 1 from the linear analyses is considered.
- 2* Number of eigenvalues to be calculated.
- 3* No influence of displacements.
- 4* The imperfection for the non-linear analysis is defined here. The maximum deformation is scaled to 9.171.
- 5* Specifies the subspace iteration: 5 trial vectors and a maximum of thirty iterations
- 6* Generates an output graph with the buckling shape of the arch.

Command file non-linear analysis

```

*NONLIN
INITIA
  ANALYS PHYSIC GEOMET *1
USE
END USE
OPTION TANGEN *2
START STRESS.I (4) 1. / *3
END INITIA
LOADING
  LOAD(1): (1) 1. /
END LOADING
:
  SELECT *4
  NODES 12 6 17 /
:   NODES 12 17 21 357 353 /
: ELEMEN 10 20 30 40 50 60 70 80 90 100 101 111
:   121 131 141 151 161 171 181 191 /
: INTPT ALL /
: NODES ALL /
: END ELEMEN
END SELECT
  OUTPUT NEUTRA
  DISPLAY GLOBAL
: STRESS TOTAL CAUCHY INTPT
END OUTPUT
:
  SELECT *5
  NODES 12 6 17 /
END SELECT
  OUTPUT TABULA
  DISPLAY GLOBAL
  END OUTPUT
:
SAVE STEPS 5 / *6
EXECUTE LOAD(1) STEPS
  SIZE 3.A (5) / *7
: SIZE 4. (2) 2. (4) /
  PERFOR.A NEWTON REGULA MI=30 *8
  NORM ENERGY CONTIN CO=1.E-4 *9
END EXECUTE
*post
model eye=1000000 1000000 1000000
end model
output graphi nonlin FI="plot"
displa global SC=1
end output
*END

```

COMMENT

- *1 Indicates that the analysis is geometrical and physical non-linear.
- *2 Use a tangent stiffness method.
- *3 Indicates that the analysis starts with initial stresses, the loadcase is defined in the dat file.
- *4 Selection for output for a neutral file.
- *5 Selection for output for a tabular.
- *6 Save step 5, from which the analysis can be continued.
- *7 Defination of the number of steps and the step size.
- *8 Use a Newton-Raphson iteration.

*9 Specifies the convergence criterion

E.3 Output files

linear analysis output file

```

1:*FILOS
  2: INITIA MA=100000
  FILOS FILE INITIALIZED
  MA= 100000  DI= 300  BF= 1024  2048  8192  16384  32768
  3:*INPUT
  /DIANA/DC/ST33  13:23:06  .00-CPU  .00-IO  20.-FA  BEGIN
  4:*ELASSE
  5:*ELMAT
  6:*LOADS
  7:*ORDER
  8:*SOLVE
  9:*POST
 10: LAYOUT
 11: CHARAC SI=15
 12: MODEL.O
 13: END LAYOUT
 14:SELECT
 15: ELEMENTS ALL /
 16: END ELEMENTS
 17:END SELECT
 18: OUTPUT TABULAR
 19: DISPLA GLOBAL
 20: STRESS TOTAL CAUCHY
 21: END OUTPUT
 22:OUTPUT GRAPHI FI="FRA"
 23: DISPLA GLOBAL
 24:END OUTPUT
 36:*END
    
```

0

```

$$$$$$$  $$$$$$$$  $$  $$$  $$  $$
$$$$$$$$$  $$$$$$$$  $$  $$$  $$  $$
$$  $$  $$  $$$  $$$  $$  $$$
$$  $$  $$  $$$  $$$  $$  $$$
$$  $$  $$  $$$  $$$  $$  $$$
$$  $$  $$  $$$  $$$  $$  $$$
$$  $$  $$  $$$  $$$  $$  $$$
$$$$$$$$$  $$$$$$$$  $$  $$$  $$  $$$
$$$$$$$$$  $$$$$$$$  $$  $$$  $$  $$$
    
```

```

*****
*****
***
*** FEMGEN MODEL      : IPE100
***
*****
*****
*** DIANA RELEASE 6.2  LATEST UPDATE: Tue Oct 15 07:09:35 MDT 1996
*****
    
```

1

```

/DIANA/IN/CO30  13:23:13  .57-CPU  .93-IO  375.-FA  BEGIN
/DIANA/IN/MA30  13:23:14  1.26-CPU  1.04-IO  419.-FA  BEGIN
/DIANA/IN/GE30  13:23:14  1.28-CPU  1.13-IO  463.-FA  BEGIN
/DIANA/IN/DA30  13:23:15  1.32-CPU  1.26-IO  507.-FA  BEGIN
/DIANA/IN/DI30  13:23:15  1.34-CPU  1.35-IO  551.-FA  BEGIN
/DIANA/IN/EL30  13:23:16  1.37-CPU  1.49-IO  595.-FA  BEGIN
/DIANA/IN/LO30  13:23:17  1.81-CPU  1.65-IO  641.-FA  BEGIN
/DIANA/IN/SU30  13:23:18  1.92-CPU  1.77-IO  687.-FA  BEGIN
/DIANA/IN/CF30  13:23:18  1.94-CPU  1.89-IO  732.-FA  BEGIN
/DIANA/EA/IT30  13:23:19  1.96-CPU  2.00-IO  773.-FA  BEGIN
  ELEMENT-TYPE DATA READY: HE= 240 NE= 240 MD= 40
    
```

```

/DIANA/EA/ID30 13:23:20 2.15-CPU 2.10-IO 821.-FA BEGIN
  ELEMENT DATA EVALUATED : HE= 240
  NODE-ELEMENT CONNECTION TABLE EVALUATED
/DIANA/EA/BC30 13:23:36 8.06-CPU 3.08-IO 916.-FA BEGIN
  SYSTEM BASES GENERATED : NB= 1322 NN= 661 MT= 2
  BOUND. COND. EVALUATED : NS= 13 NT= -1 ND= 13
/DIANA/EA/AT30 13:23:37 8.47-CPU 3.35-IO 1002.-FA BEGIN
  SYSTEM D.O.F. GENERATED: ND= 3425
  ELEM.TRANSF.MAT. STORED: HE= 240 MC= 43 MV= 55
/DIANA/EM/ST30 13:23:41 9.83-CPU 3.99-IO 1160.-FA BEGIN
  ELEM. STIFFNESS STORED : HE= 240 SF.ELSTIF
/DIANA/EM/RE30 13:23:51 17.41-CPU 4.92-IO 1296.-FA BEGIN
/DIANA/LO/LV30 13:23:51 17.45-CPU 4.98-IO 1337.-FA BEGIN
  RHS-VECTORS INITIALIZED: ML= 4 ND= 3425 SF.RHSIDE
  EXTER. LOAD INITIALIZED: ML= 4 ND= 3425 SF.EXTLOD
  CONST.DISP. INITIALIZED: ML= 4 ND= 3425 SF.DISCON
  STRESS LOAD INITIALIZED: ML= 4 ND= 3425 SF.SIGLOD
/DIANA/LO/FI30 13:23:52 17.47-CPU 5.11-IO 1403.-FA BEGIN
  ELM. FORCES TO RHS-VECT: NV= 4 ML= 240 SF.RHSIDE
/DIANA/LO/NO30 13:23:54 17.95-CPU 5.80-IO 1806.-FA BEGIN
  NODAL LOADS TO RHS-VECT: NV= 4 NL= 0 SF.RHSIDE
  NODAL LOADS TO EXT.LOAD: NV= 4 NL= 0 SF.EXTLOD
/DIANA/LO/EL30 13:23:54 17.98-CPU 6.01-IO 1879.-FA BEGIN
  ELEMENTLOAD TO RHS-VECT: NV= 4 SF.RHSIDE
  ELEMENTLOAD TO EXT.LOAD: NV= 4 SF.EXTLOD
/DIANA/LO/WE30 13:23:56 18.37-CPU 6.56-IO 2025.-FA BEGIN
/DIANA/LO/DF30 13:23:57 18.41-CPU 6.64-IO 2067.-FA BEGIN
/DIANA/LO/RL30 13:23:57 18.43-CPU 6.76-IO 2114.-FA BEGIN
  INC. INITIAL STRAIN/STRESS LOAD ADDED TO RHS-VECT: NV= 4 SF.RHSIDE
/DIANA/LO/LV30 13:24:04 22.83-CPU 7.65-IO 2497.-FA BEGIN

```

SUM OF EXT.LOAD TO CALC: ML= 4 ND= 3425 SF.EXTLOD

SUM OF EXTERNAL LOADS:

```

=====
LOAD SET  TR  X      TR  Y      TR  Z      RO  X      RO  Y      RO  Z
1  -.7314D-03  -.9172D+01  .0000D+00  .0000D+00  .0000D+00  -.4206D+05
2  .0000D+00  .0000D+00  .0000D+00  .0000D+00  .0000D+00  .1283D-02
3  .0000D+00  .0000D+00  .1000D+01  .1711D+04  -.4586D+04  .0000D+00
4  .0000D+00  .0000D+00  .0000D+00  .0000D+00  .0000D+00  .0000D+00
/DIANA/OR/NR30 13:24:05 22.97-CPU 7.84-IO 2611.-FA BEGIN
  NESTED DISSECTION: MBAND= 644 PROFILE= 65686
/DIANA/SO/GE31 13:24:06 23.26-CPU 8.02-IO 2667.-FA BEGIN
  DECOMPOSITION SIMULATED: MB= 360 NQ= 3412 ND= 3425 NG= 180
  FLOPS= 38064029. PROFIL= 422599.( 776854.)
  RMS= 149.
  DECOMPOSITION EXECUTED : SD= .61405D+00 HD= .24499D+12
/DIANA/PO/WR30 13:24:31 32.88-CPU 10.65-IO 3499.-FA BEGIN
  TABULA file lin.tb OPENED
  PICT.COORD. STORED..... NN= 661
  GRAPHI file FRA012.pic OPENED FOR: DISPLA TOTAL TRANSL
  GRAPHI file FRA013.pic OPENED FOR: DISPLA TOTAL TRANSL
  GRAPHI file FRA014.pic OPENED FOR: DISPLA TOTAL TRANSL
  GRAPHI file FRA015.pic OPENED FOR: DISPLA TOTAL TRANSL
/DIANA/DC/END 13:25:50 99.47-CPU 16.19-IO 4838.-FA STOP

```

Euler analysis outfile

```

1: *EULER
/DIANA/DC/ST33 13:26:00 .00-CPU .00-IO 27.-FA BEGIN
2: OUTPUT TABULA
3: DISPLA TRANSLA
4: END OUTPUT
5: EXECUTE
6: STRESS ELASTI CA=1
7: MODES NM=1
8: NODISP
9: IMPERF.B (1) 9.171
11: END EXECUTE

```

```

12:OUTPUT GRAPHI FI="eul"
13: DISPLA GLOBAL
14:END OUTPUT
15:*END

```

0

```

$$$$$$ $$$$$$ $$ $$$ $$ $$
$$$$$$$$ $$$$$$$ $ $ $$$ $ $
$$ $ $ $ $$$$ $$$ $ $$$
$$ $ $ $ $$$ $ $ $ $$$
$$ $ $ $ $ $ $ $ $ $ $
$$ $ $ $ $ $ $ $ $ $ $
$$$$$$$$ $$$$$$$ $ $ $ $$$ $ $
$$$$$$$$ $$$$$$$ $ $ $ $ $ $

```

```

*****
*****
*** FEMGEN MODEL : IPE100 ***
***
*****
*****
*** DIANA RELEASE 6.2 LATEST UPDATE: Tue Oct 15 07:09:35 MDT 1996 ***
*****

```

1

```

/DIANA/EM/KG30 13:26:01 .06-CPU .31-IO 155.-FA BEGIN
STRESS STIFFNESS STORED: HE= 240 SF.KGSTIF
/DIANA/EI/EV30 13:26:14 10.83-CPU 1.29-IO 543.-FA BEGIN
0 1 EIGENVALUES FOUND AFTER 4 ITERATIONS
0 BUCKLING-VALUES:
.26968D+02( 1)
0 GENERALIZED MASS :
.32562D-02( 1)
0 RELATIVE ERROR ||R|| / ||Kx||:
.41434D-04( 1)
EIG-VAL,FREQ,VEC STORED: ND= 3425 NV= 1
EIG-VAL,FREQ,VEC STORED: ND= 3425 NV= 1
/DIANA/NL/IV30 13:26:42 34.91-CPU 3.27-IO 2362.-FA BEGIN
DISP.-FIELD INITIALIZED
ELEMENT-DATA INITIALIZED
/DIANA/SO/GE31 13:27:03 50.63-CPU 4.79-IO 2975.-FA BEGIN
DECOMPOSITION SIMULATED: MB= 360 NQ= 3412 ND= 3425 NG= 180
FLOPS= 38064029. PROFIL= 422599.( 776854.)
RMS= 149.
DECOMPOSITION EXECUTED : SD= .61408D+00 HD= .24498D+12
/DIANA/EM/KG30 13:27:25 59.48-CPU 6.97-IO 3418.-FA BEGIN
STRESS STIFFNESS STORED: HE= 240 SF.KGSTIF
/DIANA/EI/EV30 13:27:37 70.16-CPU 8.01-IO 3830.-FA BEGIN
0 1 EIGENVALUES FOUND AFTER 4 ITERATIONS
0 BUCKLING-VALUES:
.26969D+02( 1)
0 GENERALIZED MASS :
.32557D-02( 1)
0 RELATIVE ERROR ||R|| / ||Kx||:
.46863D-04( 1)
EIG-VAL,FREQ,VEC STORED: ND= 3425 NV= 1
EIG-VAL,FREQ,VEC STORED: ND= 3425 NV= 1
/DIANA/PO/WR30 13:28:04 94.32-CPU 9.92-IO 5677.-FA BEGIN
TABULA file euler.tb OPENED
PICT.COORD. STORED..... NN= 661
GRAPHI file eul004.pic OPENED FOR: DISPLA TOTAL TRANSL
/DIANA/DC/END 13:28:09 97.96-CPU 11.04-IO 5786.-FA STOP

```

Part of the Euler tabular file with the global displacements

```

Analysis type EULER
Mode nr. 1
Buckling value 2.697E+01

```

Result Axes	DISPLA TOTAL TRANSL GLOBAL			
Nodnr	DtX	DtY	DtZ	
1	-4.072E-05	5.281E-03	9.999E-01	Point in the middle of the arch
2	-4.106E-05	5.213E-03	9.876E-01	
3	-4.236E-05	4.997E-03	9.509E-01	
4	-4.492E-05	4.641E-03	8.908E-01	
5	-4.899E-05	4.161E-03	8.088E-01	
6	-5.459E-05	3.579E-03	7.069E-01	
7	-6.123E-05	2.918E-03	5.876E-01	
8	-6.736E-05	2.202E-03	4.539E-01	
9	-6.990E-05	1.456E-03	3.089E-01	
10	-6.357E-05	7.036E-04	1.564E-01	
11	-4.043E-05	-3.500E-05	.000E+00	
12	-4.161E-05	5.114E-03	9.706E-01	Point in the middle of the arch
13	-4.199E-05	5.050E-03	9.587E-01	
14	-4.323E-05	4.844E-03	9.231E-01	
15	-4.548E-05	4.505E-03	8.648E-01	
16	-4.875E-05	4.048E-03	7.852E-01	
17	-5.270E-05	3.491E-03	6.862E-01	
18	-5.633E-05	2.856E-03	5.704E-01	
19	-5.759E-05	2.168E-03	4.406E-01	
20	-5.283E-05	1.448E-03	2.999E-01	
21	-3.636E-05	7.189E-04	1.518E-01	
22	.000E+00	.000E+00	.000E+00	
23	-4.251E-05	4.947E-03	9.414E-01	
24	-4.291E-05	4.887E-03	9.298E-01	
25	-4.408E-05	4.692E-03	8.953E-01	
26	-4.603E-05	4.369E-03	8.387E-01	
27	-4.850E-05	3.934E-03	7.615E-01	
28	-5.079E-05	3.403E-03	6.656E-01	
29	-5.142E-05	2.795E-03	5.532E-01	
30	-4.780E-05	2.134E-03	4.273E-01	
31	-3.575E-05	1.440E-03	2.908E-01	
32	-9.141E-06	7.342E-04	1.472E-01	
33	4.043E-05	3.499E-05	.000E+00	
34	-4.079E-05	5.266E-03	9.968E-01	
35	-4.157E-05	5.123E-03	9.722E-01	
36	-4.346E-05	4.835E-03	9.237E-01	
37	-4.676E-05	4.415E-03	8.525E-01	
38	-5.162E-05	3.882E-03	7.602E-01	
39	-5.786E-05	3.257E-03	6.493E-01	
40	-6.452E-05	2.565E-03	5.224E-01	
41	-6.937E-05	1.831E-03	3.826E-01	
42	-6.830E-05	1.079E-03	2.334E-01	
43	-5.474E-05	3.315E-04	7.843E-02	
44	-4.117E-05	5.197E-03	9.853E-01	
45	-4.152E-05	5.132E-03	9.731E-01	
46	-4.279E-05	4.920E-03	9.370E-01	
47	-4.520E-05	4.573E-03	8.778E-01	
48	-4.887E-05	4.105E-03	7.970E-01	
49	-5.365E-05	3.535E-03	6.966E-01	
50	-5.878E-05	2.887E-03	5.790E-01	
51	-6.248E-05	2.185E-03	4.472E-01	
52	-6.137E-05	1.452E-03	3.044E-01	
53	-4.997E-05	7.113E-04	1.541E-01	
54	-2.022E-05	-1.750E-05	.000E+00	
		:		
634	1.502E-03	-3.087E-03	3.604E-01	
635	1.057E-03	-3.202E-03	4.920E-01	
636	6.957E-04	-3.311E-03	6.115E-01	
637	4.192E-04	-3.407E-03	7.160E-01	
638	2.223E-04	-3.487E-03	8.028E-01	
639	9.367E-05	-3.547E-03	8.698E-01	
640	1.707E-05	-3.584E-03	9.155E-01	
641	-2.715E-05	-3.599E-03	9.385E-01	
642	4.447E-03	-4.163E-03	1.676E-05	
643	3.521E-03	-4.667E-03	1.473E-01	
644	2.676E-03	-5.194E-03	2.910E-01	
645	1.939E-03	-5.723E-03	4.275E-01	
646	1.327E-03	-6.231E-03	5.535E-01	

647	8.460E-04	-6.698E-03	6.658E-01
648	4.907E-04	-7.106E-03	7.617E-01
649	2.481E-04	-7.437E-03	8.389E-01
650	9.686E-05	-7.681E-03	8.954E-01
651	9.755E-06	-7.826E-03	9.299E-01
652	5.353E-03	-5.955E-03	7.391E-02
653	4.151E-03	-6.886E-03	2.198E-01
654	3.083E-03	-7.833E-03	3.604E-01
655	2.177E-03	-8.760E-03	4.920E-01
656	1.445E-03	-9.632E-03	6.115E-01
657	8.872E-04	-1.041E-02	7.160E-01
658	4.907E-04	-1.108E-02	8.028E-01
659	2.316E-04	-1.159E-02	8.699E-01
660	7.729E-05	-1.195E-02	9.155E-01
661	-1.173E-05	-1.212E-02	9.386E-01

Output file of step 1 and step 5, of the non-linear analysis

```

1:*NONLIN
/DIANA/DC/ST33 13:28:10 .01-CPU .00-IO 27.-FA BEGIN
2: INITIA
3: ANALYS PHYSIC GEOMET
4: USE
5: END USE
6: OPTION TANGEN
10: END INITIA
11: LOADING
12: LOAD(1): (1) 1. /
13: END LOADING
15: SELECT
16:  NODES 12 6 17 /
23: END SELECT
24: OUTPUT NEUTRA
25: DISPLAY GLOBAL
27: END OUTPUT
29: SELECT
30:  NODES 12 6 17 /
31: END SELECT
32: OUTPUT TABULA
33: DISPLAY GLOBAL
34: END OUTPUT
36:SAVE STEPS 5 /
37: EXECUTE LOAD(1) STEPS
38: SIZE 3 (5) /
40: PERFOR NEWTON REGULA M1=30
41: NORM ENERGY CONTIN CO=1.E-4
42: END EXECUTE
43:*POST
44:MODEL EYE=1000000 1000000 1000000
45:END MODEL
46:OUTPUT GRAPHI NONLIN FI="plot"
47:DISPLA GLOBAL SC=1
48:END OUTPUT
49:*END
0

```

```

$$$$$$ $$$$$$ $$ $$$ $$ $$
$$$$$$$$ $$$$$$ $$ $$$$ $$ $$
$$ $$ $$ $$$$ $$$$ $$ $$$$
$$ $$ $$ $$$$ $$ $$ $$ $$$$
$$ $$ $$ $$ $$ $$ $$$ $ $ $ $
$$ $$ $$ $$$$$$ $$ $$ $$$$$$
$$ $$ $$ $$$$$$ $$ $$$ $$$$$$
$$$$$$$$ $$$$$$ $$ $$ $$$$ $ $ $
$$$$$$ $$$$$$ $$ $$ $$$$ $ $

```



```

*****
*****
***
*** FEMGEN MODEL : IPE100 ***
***
*****
*****
*** DIANA RELEASE 6.2 LATEST UPDATE: Tue Oct 15 07:09:35 MDT 1996 ***
*****

```

```

1
/DIANA/NL/IN30 13:28:12 .13-CPU .49-IO 221.-FA BEGIN

```

ANALYSIS INCLUDES:
(QUALIFIERS AND PARAMETERS CAN BE OVERRULED PER EXECUTION BLOCK)

PHYSICALLY NONLINEAR BEHAVIOR:
PLASTI NS= 10 TY= 1.000E-04
GEOMETRICALLY NONLINEAR ALGORITHM:
TOTAL LAGRANGE

```

/DIANA/NL/LO30 13:28:36 7.51-CPU 3.09-IO 555.-FA BEGIN
/DIANA/NL/XQ31 13:28:36 7.57-CPU 3.21-IO 630.-FA BEGIN

```

```

STEP 1 INITIATED:
LOAD INCREMENT: LOADING( 1) * 3.000E+00
DECOMPOSITION SIMULATED: MB= 360 NQ= 3412 ND= 3425 NG= 180
FLOPS= 38064029. PROFIL= 422599.( 776854.)
RMS= 149.
DECOMPOSITION EXECUTED : SD= .61408D+00 HD= .24498D+12
IN SEGMENT EXECUT:= NPLAST= 0

```

STEP 1 : ENERGY NORM = 9.869E-02 TOLERANCE = 1.000E-04

```

DECOMPOSITION SIMULATED: MB= 360 NQ= 3412 ND= 3425 NG= 180
FLOPS= 38064029. PROFIL= 422599.( 776854.)
RMS= 149.
DECOMPOSITION EXECUTED : SD= .66138D+00 HD= .24498D+12
IN SEGMENT EXECUT:= NPLAST= 0

```

RELATIVE ENERGY VARIATION = 7.502E-01 CHECK = FALSE

```

DECOMPOSITION SIMULATED: MB= 360 NQ= 3412 ND= 3425 NG= 180
FLOPS= 38064029. PROFIL= 422599.( 776854.)
RMS= 149.
DECOMPOSITION EXECUTED : SD= .60230D+00 HD= .24498D+12
IN SEGMENT EXECUT:= NPLAST= 0

```

RELATIVE ENERGY VARIATION = 6.734E-02 CHECK = FALSE

```

DECOMPOSITION SIMULATED: MB= 360 NQ= 3412 ND= 3425 NG= 180
FLOPS= 38064029. PROFIL= 422599.( 776854.)
RMS= 149.
DECOMPOSITION EXECUTED : SD= .60239D+00 HD= .24498D+12
IN SEGMENT EXECUT:= NPLAST= 0

```

RELATIVE ENERGY VARIATION = 3.569E-05 CHECK = TRUE

STEP 1 TERMINATED, CONVERGENCE AFTER 3 ITERATIONS
TOTAL LOAD FACTOR: LOADING(1) * 3.000E+00

```

/DIANA/PO/WR30 13:31:45 165.85-CPU 18.50-IO 3814.-FA BEGIN
SEVERITY : WARNING
TRACE BACK: POUTBL
ERROR CODE: /DIANA/PO/WR30/0001

```

ERRORMSG.W: The serial number of the neutral file in which the model of the first phase of the analysis is stored is 018 and not 000.

```
NEUTRA file nlq018.nf OPENED
NEUTRA file nlq019.nf OPENED
TABULA file nlq.tb OPENED
/DIANA/FL/MA30 13:31:49 166.74-CPU 20.11-IO 4000.-FA BEGIN
/DIANA/NL/XQ31 13:31:50 166.76-CPU 20.20-IO 4047.-FA BEGIN
```

```
STEP 5 INITIATED:
LOAD INCREMENT: LOADING( 1) * 3.000E+00
DECOMPOSITION SIMULATED: MB= 360 NQ= 3412 ND= 3425 NG= 180
FLOPS= 38064029. PROFIL= 422599.( 776854.)
RMS= 149.
DECOMPOSITION EXECUTED : SD= .56850D+00 HD= .24498D+12
IN SEGMENT EXECUT:= NPLAST= 0
```

```
STEP 5 : ENERGY NORM = 8.093E+00 TOLERANCE = 1.000E-04
```

```
DECOMPOSITION SIMULATED: MB= 360 NQ= 3412 ND= 3425 NG= 180
FLOPS= 38064029. PROFIL= 422599.( 776854.)
RMS= 149.
DECOMPOSITION EXECUTED : SD= .10535D+01 HD= .24498D+12
IN SEGMENT EXECUT:= NPLAST= 0
```

```
RELATIVE ENERGY VARIATION = 3.099E-01 CHECK = FALSE
```

```
DECOMPOSITION SIMULATED: MB= 360 NQ= 3412 ND= 3425 NG= 180
FLOPS= 38064029. PROFIL= 422599.( 776854.)
RMS= 149.
DECOMPOSITION EXECUTED : SD= .55736D+00 HD= .24498D+12
IN SEGMENT EXECUT:= NPLAST= 0
```

```
RELATIVE ENERGY VARIATION = 9.141E-02 CHECK = FALSE
```

```
DECOMPOSITION SIMULATED: MB= 360 NQ= 3412 ND= 3425 NG= 180
FLOPS= 38064029. PROFIL= 422599.( 776854.)
RMS= 149.
DECOMPOSITION EXECUTED : SD= .59086D+00 HD= .24498D+12
IN SEGMENT EXECUT:= NPLAST= 0
```

```
RELATIVE ENERGY VARIATION = 1.884E-04 CHECK = FALSE
```

```
DECOMPOSITION SIMULATED: MB= 360 NQ= 3412 ND= 3425 NG= 180
FLOPS= 38064029. PROFIL= 422599.( 776854.)
RMS= 149.
DECOMPOSITION EXECUTED : SD= .55731D+00 HD= .24498D+12
IN SEGMENT EXECUT:= NPLAST= 0
```

```
RELATIVE ENERGY VARIATION = 7.397E-04 CHECK = FALSE
```

```
DECOMPOSITION SIMULATED: MB= 360 NQ= 3412 ND= 3425 NG= 180
FLOPS= 38064029. PROFIL= 422599.( 776854.)
RMS= 149.
DECOMPOSITION EXECUTED : SD= .55731D+00 HD= .24498D+12
IN SEGMENT EXECUT:= NPLAST= 0
```

```
RELATIVE ENERGY VARIATION = 1.193E-05 CHECK = TRUE
```

```
STEP 5 TERMINATED, CONVERGENCE AFTER 5 ITERATIONS
TOTAL LOAD FACTOR: LOADING( 1) * 1.500E+01
```

```
/DIANA/PO/WR30 13:46:40 973.36-CPU 96.24-IO 19920.-FA BEGIN
NEUTRA file nlq023.nf OPENED
TABULA file nlq.tb OPENED
```

```
/DIANA/FL/MA30 13:46:43 973.67-CPU 97.76-IO 20086.-FA BEGIN
CPITMS : WARNING : TTIME : NOT FOUND
CPITMS : WARNING : TIME : NOT FOUND
NONLIN STEP 5: SAVED ON /usr4/user/desx/desx5.ff
/DIANA/PO/WR30 13:48:45 973.70-CPU 110.06-IO 20393.-FA BEGIN
  TABULA file nlq.tb OPENED
/DIANA/PO/WR30 13:48:53 973.88-CPU 111.02-IO 20505.-FA BEGIN
  PICT.COORD. STORED..... NN= 661
  GRAPHI file plot005.pic OPENED FOR: DISPLA TOTAL TRANSL
/DIANA/DC/END 13:49:07 977.86-CPU 112.48-IO 20657.-FA STOP
```